Using water isotopes, geochemistry, and Unmanned Aerial Vehicles to investigate the origin of the Shu-Shu thermal springs and their role in affecting surface water/groundwater heat and chemical exchange: uThukela River

by

GUGU H BUTHELEZI

Submitted in partial fulfilment of the academic requirements of

Master of Science

in Hydrology

School of Agricultural, Earth and Environmental Sciences
College of Agriculture, Engineering and Science
University of KwaZulu-Natal
Pietermaritzburg
South Africa

25 March 2025

PREFACE

The research contained in this thesis was completed by the candidate while based in the Discipline of Hydrology, School of Agricultural, Earth and Environmental Sciences of the College of Agriculture, Engineering and Science, University of KwaZulu-Natal, Pietermaritzburg, South Africa. The research was financially supported by the Water Research Commission.

The contents of this work have not been submitted in any form to another university and, except where the work of others is acknowledged in the text, the results reported are due to investigations by the candidate.

Signed: Professor Seifu Kebede Gurmessa

Date: April 2025

DECLARATION 1: PLAGIARISM

I, Gugu Happiness Buthelezi, declare that:

(i) the research reported in this thesis, except where otherwise indicated or acknowledged, is my original work;

(ii) this thesis has not been submitted in full or in part for any degree or examination to any other university;

(iii) this thesis does not contain other persons' data, pictures, graphs or other information, unless specifically acknowledged as being sourced from other persons;

(iv) this thesis does not contain other persons' writing, unless specifically acknowledged as being sourced from other researchers. Where other written sources have been quoted, then:

a) their words have been re-written but the general information attributed to them has been referenced;

b) where their exact words have been used, their writing has been placed inside quotation marks, and referenced;

(v) where I have used material for which publications followed, I have indicated in detail my role in the work;

(vi) this thesis is primarily a collection of material, prepared by myself, published as journal articles or presented as a poster and oral presentations at conferences. In some cases, additional material has been included;

(vii) this thesis does not contain text, graphics or tables copied and pasted from the Internet, unless specifically acknowledged, and the source being detailed in the thesis and in the References sections.

Signed: Gugu Buthelezi

Date: April 2025

ABSTRACT

The Shu-Shu thermal springs are located in Nkandla, KwaZulu-Natal, emerging underneath and at the margin of the uThukela River. This work aimed to determine the geothermal energy potential of the Shu-Shu thermal springs, their origin, and their role in heat and chemical exchange with the uThukela River. The specific objectives of the investigation included determining the origin, the extent of discharge, the depth of circulation of the thermal springs, and assessing the impact the Shu-Shu thermal springs have on the surrounding surface water of the uThukela River. The Shu-Shu thermal springs were investigated using; isotopic, physio-chemical, and Unmanned Aerial Vehicles (UAV) methods. Water samples were collected from the thermal springs, surrounding surface waters, and rainfalls across different altitudes during wet and dry seasons.

The stable isotope ($\delta^{18}O$, $\delta^{2}H$) analysis confirms the meteoric origin of the thermal waters with a positive ^{18}O shift. The Shu-Shu thermal springs are regionally sourced as they have a similar isotopic signature to the rainfall in the Drakensberg Mountains. A hydrochemistry analysis performed indicates that the Shu-Shu thermal springs are Na-Cl waters that are dominated by ions such as SO_4^{2-}, Na^{+}, Cl^{-}, $Ca^{+,}$ and SiO_2. The major ions signify a rock-water interaction and the leaching of amphibolites, gneiss, and pyrite. From the numerous geothermometers used, only the Silica (quartz and chalcedony) geothermometers provide a reliable estimation (76-80 °C) of the reservoir temperature, and the estimated depth of 1.8-2 km.

Mineral saturation states calculated from GWB 11 software indicate that thermal waters are supersaturated (SI>0) with respect to quartz, tridymite, chalcedony, cristobalite, and undersaturated (SI<0) with respect to amorphous silica, anhydrite, gypsum, bassanite, halite and many more. The thermal map produced from the UAV images shows that the Shu-Shu thermal springs discharge zone extends to an area of 3100 m^2 along the faultline that strikes at N 63° E. The metamorphic rocks underlying the thermal springs have a low hydraulic conductivity, causing a low discharge rate.

Based on the reservoir temperature estimations using geothermometry, it can be concluded that the Shu-Shu thermal springs have a low-enthalpy (temperature) energy potential. The origin of the springs is controlled by faults and fractures. The use of geophysics is recommended to further investigate the subsurface extent of the springs. The association of the springs with dykes/fractures indicates the need to investigate the geothermal energy potential associated with the other dense network of fractures and dykes in South Africa.

ACKNOWLEDGMENTS

I want to acknowledge the following people:

Professor Seifu Kebede Gurmessa of the University of KwaZulu-Natal (UKZN) for his supervision, guidance, and support.

Dr. Shaeden Gokool of UKZN, for his advice and aiding with the Unmanned Aeriel Vehicle and the pre-processing of the thermal images

Hydrology postgraduate students, particularly Mr. Mutondi Tshikororo and Ms. Thobeka Mpungose for helping with sample collection and analyses.

Other Hydrology postgraduate students such as Mr. Thobani Ngwazi, and Mr. Glen Mkhonta for driving me and helping with fieldwork.

The UKZN staff: Mr. Vivek Naiken, Agrometeorology, and Hydrology laboratory technician for aiding in flying the drone

Umngeni-uThukela Water Laboratories staff for aiding in sample analyses.

The soil science laboratory technician, for lending me equipment and reagents that allowed me to conduct my analyses in their laboratory.

My funders; the Water Research Commission.

My friends for their words of encouragement and support.

My sister, Ms. Ntombifikile Buthelezi for her kindness, and the rest of my family for their support and prayers, I love you.

Dr. Ashebir Sewale Belay for reviewing my work and the anonymous reviewers of the abstract of my project that was presented at conferences and symposiums

Last but certainly not least, I would like to thank the Lord Almighty! None of this is possible without God

TABLE OF CONTENTS

Page

LIST OF TABLES

Table **Page**

LIST OF FIGURES

Figure **Page**

LIST OF ABBREVIATIONS

CRP	Calibrated Reflection Panel
DLS-2	Downwelling Light Sensor 2
D-LWIA	Double Liquid Water Isotope Analyser
EC	Electrical conductivity
ENE	East-Northeast
GEOTIFF	Geographic Tagged Image File Format
GIS	Geographic Information System
GMWL	Global Meteoric Water Line
GSD	Ground Sampling Distance
GW	Groundwater
GWB 11	Geochemist Workbook Version 11.0.7
IAP	ion activity product
KML	Keyhole Markup Language
KZN	KwaZulu Natal
LGR	Los Gatos Research
LMWL	Local Meteoric Water Line
LWIR	Thermal Infrared
M-300	DJI Marice 300
NZ	New Zealand
NIR	Near Infrared
pH	Potential of Hydrogen
SA	South Africa
SANAS	South African National Accreditation System
SI	Saturation Index
SMOW	Standard Mean Ocean Water
SW	Surface Water
TDS	Total Dissolved Solids
UAV	Unmanned Aerial Vehicle
UK	United Kingdom
UKZN	University of KwaZulu-Natal
USA	United States of America

USB	Universal Standard Bus
V-SMOW	Vienna-Standard Mean Ocean Water
WC	Western Cape
WNW	West-Northwest

LIST OF SYMBOLS WITH UNITS

δ	Deviation of stable isotope composition from a standard
‰	Parts per thousand (permil)
Ca	Calcium (mg/L)
Cl	Chlorine (mg/L)
CO_3	Carbonates (mg/L)
G	Geothermal Gradient (°C/km)
HCO3	Bicarbonates (mg/L)
D/ δ^2H	Deuterium/Hydrogen (‰)
K	Potassium (mg/L)
Mg	Magnesium (mg/L)
Na	Sodium (mg/L)
NaCl	Sodium Chloride
$\delta^{18}O$	Oxygen-18 (‰)
Si	Silicon (mg/L)
SiO_2	Silica (mg/L)
SO_4	Sulphates (mg/L)
Temp	Temperature (°C)
To	Local Annual Average Temperature (°C)
Tz	Average reservoir temperature calculated by the geothermometers (°C)
Z	Reservoir Depth (km)

CHAPTER 1: INTRODUCTION

1.1 Rationale for the research (nature and scope)

Thermal springs, also known as hot springs, can be described as a body of water that has a temperature that exceeds 25°C all year round (Kent, 1949). Hot springs are groundwater (GW) resources that have temperatures remarkably higher than the mean annual air temperature of the surrounding area (LaMoreaux & Tanner, 2001). They can be found on every continent, from Antarctica to North America (Olivier & Jonker, 2013; Olivier, et al., 2011). Most thermal springs that are commonly recognised usually emerge as a combination of boiling water and steam or just as pure steam (Olivier & Jonker, 2013), and humans have been fascinated with the boiling water flowing from the Earth's crust since the dawn of time (Olivier & Jonker, 2013). Thermal springs can be volcanic/magmatic or meteoric in origin (Kent, 1949; LaMoreaux & Tanner, 2001; Olivier, et al., 2008; Olivier, et al., 2011).

South Africa (SA) has numerous thermal springs, with about 6% of these springs found in the KwaZulu-Natal (KZN) Province, while most of them are found in the Limpopo Province (Kent, 1949; Olivier & Jonker, 2013; Durowoju, et al., 2019). In the last few decades, an interest in thermal springs has been on the rise, owing largely to a diversification in their use (Olivier & Jonker, 2013). The generation of geothermal energy is the most significant of these (Bahati, et al., 2003). The usage of thermal spring waters in industrial processing, farming, and the extraction of rare elements has grown in the last decades (Petraccia, et al., 2006). Although South Africa has over 80 thermal springs, none of these have been explored to produce geothermal energy (Dhansay, et al., 2017). The optimum usage of thermal springs is typically dependent on their chemical and physical characteristics in addition to the depth of the geological formation (Durowoju, et al., 2019).

Thermal springs are a natural resource with the potential to significantly impact the local and regional economy if appropriately made use of (Olivier, et al., 2008). For efficient resource usage and development choices, it is essential to have access to the most recent scientific knowledge on thermal springs and their characteristics. Numerous authors (Rindl, 1916; Kent, 1949; Hoole, 2001; Olivier, et al., 2008; Olivier, et al., 2011; Olivier & Jonker, 2013; Durowoju, et al., 2019; Diamond, 2022) have conducted studies on South African thermal springs. More recently, several works (Tshibalo, et al., 2010; Tshibalo, et al., 2015; Dhansay, et al., 2017;

Martin & Croukamp, 2021) have been done to investigate the geothermal potential of South African thermal springs. Given the increased variety of thermal spring uses and the expansion of thermal spring resources in other world regions, it is likely that soon there will be a surge of interest in South African thermal springs and their uses (Olivier & Jonker, 2013). Majorities of the authors that research thermal springs mostly look at the springs located in Limpopo (Olivier, et al., 2008; Olivier, et al., 2011; Durowoju, et al., 2019) and Western Cape (WC) (Diamond & Harris, 2000; Martin & Croukamp, 2021) provinces as they contain more thermal springs than other provinces (Kent, 1949; Olivier & Jonker, 2013).

There is a lack of research conducted on the thermal springs found in KZN, particularly when it comes to their potential to produce geothermal energy and their connections to surface water (SW) and GW interactions. SW and GW interactions are becoming more complex under the effects of climate change and human activity (Chai, et al., 2021). To improve the rational distribution of water resources, particularly in dry and semi-arid regions, it is crucial to completely comprehend the features of regional SW-GW circulation to unveil the water circulation system and the impact of its evolution mechanism (Chai, et al., 2021).

This project adds to the body of knowledge on South African thermal springs, particularly those found in KZN.

1.2 Research Questions

What geological control governs the occurrence of the Shu-Shu thermal springs, and what is their connection to the SW-GW interactions in the uThukela Catchment?

1.3 Aims

The main aim of this project was to understand the origin of the Shu-Shu thermal waters and their role in affecting SW/GW heat and chemical exchange in the uThukela Catchment.

1.4 Objectives

These five objectives were used to achieve the aims mentioned above:

1. Performing a literature review on thermal springs.
2. Determination of thermal waters' origin (regional or local/intermediate) by using isotopic tracers.
3. Identification of the extent of the discharge zone and volume of the water by using an Unnamed Ariel Vehicle (drone).
4. Evaluation of the depth of circulation of the thermal springs by using geothermometry.
5. Assessment of the impact of Shu-Shu thermal waters on the water quality of uThukela River.

CHAPTER 2: LITERATURE REVIEW

2.1 Introduction

In this chapter, the literature on thermal springs is reviewed. The basic review emphasizes the origin, physical and chemical properties, and history of thermal springs in South Africa and the world. The review also discusses the theories underlying the methods used to investigate and map thermal springs and the energy potential of thermal springs globally and in South Africa. Previous studies that have been done on the Shu-Shu thermal springs are also reviewed.

2.2 The origin and age of thermal springs

The origin of thermal waters has long been discussed, with numerous explanations suggested by various researchers (Rindl, 1916; Kent, 1949; Craig, et al., 1963; Ashton & Schoeman, 1986; Giggenbach, 1992; Nicholson, 1993; LaMoreaux & Tanner, 2001; Barbier, 2002). Thermal springs can be volcanic/magmatic in origin or meteoric in origin (LaMoreaux & Tanner, 2001). The difference between volcanic and meteoric springs is demonstrated in **Table 2.1** below.

Table 2.1 Differences between volcanic and meteoric thermal springs

Aspect	Volcanic Springs	Meteoric Springs
Primary heat source	A shallow magmatic body (Nicholson, 1993; Arnórsson, 2000)	Geothermal gradient (Nicholson, 1993)
Geological setting	Within or adjacent to Quaternary/active volcanic centres (Giggenbach, 1992)	Tectonic fault zones, basin margins, or mountainous regions (Olivier & Jonker, 2013)
Water source	Largely meteoric water with minor magmatic fluid/vapour contribution (Giggenbach, 1992)	Dominantly meteoric water with negligible magmatic input (Nicholson, 1993)
Temperature range	Typically, ~75–100 °C, but may exceed 250 °C in high-enthalpy volcanic fields (Nicholson, 1993)	~25–71 °C, reflecting lower enthalpy conditions (Olivier & Jonker, 2013)

Geochemical signature	Enriched in volatiles (Cl^-, SO_4^{2-}) and often acidic (pH < 5) (Arnórsson, 2000; Giggenbach, 1992)	Near-neutral pH; chemistry dominated by Ca^{2+}, Mg^{2+}, HCO_3^-, and SO_4^{2-} (Nicholson, 1993; Olivier & Jonker, 2013)
Examples	Yellowstone hot springs (USA); El Tatio geyser field (Chile); Rotorua springs (NZ) (Nicholson, 1993; Garcia-Valles et al., 2008)	All South African thermal springs; City of Bath springs (UK); Baden-Baden (Germany) (Olivier & Jonker, 2013)

The water that is heated, whether by a volcano or geothermal gradient, expands and upsurges, causing convection currents to form in the groundwater (Grasby & Hutcheon, 2001). When the hot, circulating groundwater comes across a dyke or a fracture zone, it might rise quite rapidly and emerge as a thermal spring (Grasby & Hutcheon, 2001). Every hot spring in SA is meteoric in origin because the evidence of recent volcanic activity is non-existent (Rindl, 1916; Kent, 1949; Ashton & Schoeman, 1986).

The origin, recharge mechanism, and age of spring waters are determined using stable isotope chemistry (Craig, 1961; Craig, et al., 1963). Isotope chemistry make-up of water molecule isotopes ratios, deuterium/hydrogen (D/H) and $^{16}O/^{18}O$ have been investigated in the past (Craig, 1961; Craig, et al., 1963). These ratios were calculated for the thermal waters from many remote sites, and the results were compared to the isotopic make-up of the meteoric (rainfall) waters from the comparable sites. These sites included Yellowstone, Iceland, New Zealand, Italy, and Kenya (Craig, 1961).

The study found that the D/H ratios of thermal waters closely matched those of local meteoric waters at all sites, demonstrating that those thermal waters did not have a volcanic origin (Craig, 1961). In contrast to the D/H ratio, the $^{16}O/^{18}O$ ratio was different (Craig, 1961). The $^{16}O/^{18}O$ ratios in many thermal waters were found to be enriched in ^{18}O relative to local meteoric water. The difference was attributed to the interchange of oxygen isotopes in thermal water with oxygen isotopes in the rocks where the thermal water cycled (Craig, 1961; Abbey, et al., 2024). The process has come to be known as a positive oxygen shift (Kebede, 2024). Together, these findings demonstrated that most of the studied thermal waters had a meteoric origin, having infiltrated from precipitation, circulated to depth where they were heated and isotopically

altered through water–rock interaction, and then re-emerged at the surface as hot springs (Craig, 1961).

Thermal springs were therefore expected to be situated in places with moderate to high rainfall if they drew their water from meteoric sources (Kent, 1949). However, the catchment area is not required to be physically near the thermal spring (Olivier & Jonker, 2013) and thermal springs in SA are only found in zones with an average annual rainfall of more than 254 mm (Kent, 1949). Additionally, the catchment area needs to be higher in elevation than the spring itself (Kent, 1968). Thus, it should not come as a surprise that most thermal springs are found in valleys or low-lying regions (Kent, 1949). Even though most thermal waters in the study by Craig (1961) were meteoric in origin, uncertainties in isotopic ratios and chemical considerations suggested that a small (5-10%) but considerable volcanic component may exist in a few cases (Nicholson, 1993; Barbier, 2002). The discovery of thermal waters with a mainly meteoric origin caused a significant modification in investigation techniques, with greater stress placed on hydrological processes as well as geological processes (Gupta & Roy, 2006).

In contrast to most thermal waters, which have a meteoric origin, the thermal waters produced from thermal systems in volcanic islands have a significant volcanic element (Gupta & Roy, 2006). Based on abundant research on such thermal systems, it was concluded by (Giggenbach, 1992) that ^{18}O changes, formerly regarded as related to the interaction between rocks and water by (Craig, et al., 1963), are more the “exception than the rule”. Giggenbach (1992) found significant hydrogen changes from the local meteoric water values in the thermal water discharge from island volcanoes and proposed that these systems shared a common magmatic genesis, meaning they were volcanic in origin.

2.3 Characteristics of thermal springs

Thermal springs are classified in a variety of ways. Some are founded on their origin, while others are based on physical qualities like temperature and rate of flow. Others are categorised based on their chemical or geological make-up, or both (LaMoreaux & Tanner, 2001).

2.3.1 Physical characteristics

A 25°C temperature is typically utilised to separate thermal springs from non-thermal springs due to the generally warm climate that prevails throughout SA (Kent, 1968). Kent's 1949

categorisation, which is the one used for SA, is as follows: Warm is defined as 25–37°C; hot or hyperthermic is defined as 38–50°C; and scalding is defined as >50°C. Thermal waters that are between the mean air temperature and 25°C are referred to as "tepid". Kent (1949) used these threshold temperatures to categorize 39 springs in SA as warm, hot, and scalding(>50°C).The WC's Brandvlei was generally believed to be SA's hottest spring (64°C), until in 2004, Siloam in Limpopo was confirmed to reach 67.5°C (Olivier, et al., 2008). As a result, according to (Hartnady & Jones, 2007), temperature could be utilised as a "tracer" for hydrogeological processes.

Thermal spring temperatures are impacted by the magma's temperature (for volcanic origins), the characteristics of water channels leading to the surface, the depth of penetration (Kent, 1949), and the pace of ascent to the surface (Grasby & Hutcheon, 2001). It is widely assumed that the temperature of meteoric water rises at a rate of 2-3°C per 100 m (Press & Siever, 1986). According to Limberger et al. (2018), the mean aquifer geothermal gradient is 32 °C/1000 m.

The temperature of flowing GW is also influenced by the heat flow characteristics of rocks (Olivier & Jonker, 2013). The amount of rain, the aquifer's size and storage capacity, the transmissivity and aquifers' discharge capacity, and the discharge capacity of the channel through which water rises to the surface all influence the flow rate of a thermal spring (LaMoreaux & Tanner, 2001). The WC's Brandvlei has the highest flow rate in SA and is situated in an area with an average annual rainfall of 450-600 mm. The thermal springs of SA have the maximum flow rates in the range of 40 000 m^3/d (Kent, 1968).

Thermal springs in SA typically have low flow rates (Kent, 1968) when compared to those in volcanic terrains, where fumaroles and geyser-type thermal springs are found. Even though it was traditionally believed that the springs with the largest flow rates are also the hottest, this is not essentially true (Hartnady & Jones, 2007). The main determinant of spring water emergence temperatures is aquifer permeability, which interacts with conductive and advective heat transport in the host aquifer systems (Hartnady & Jones, 2007). Where GW flow rates are low and rock permeability is low, heat transfer is predominantly conductive, resulting in low spring temperatures (Hartnady & Jones, 2007). High flow rates and advective heat transport are the predominant processes in rocks with high permeability. Spring temperatures, however, continue to be low since high permeability also leads to enormous amounts of flowing water. In general, springs with a moderate range of permeability are the hottest (Hartnady & Jones, 2007).

2.3.2. Chemical characteristics

Thermal water experiences a variety of chemical reactions, most of which are linked to interactions that occur between the water and the rocks where it is found (Olivier & Jonker, 2013). Regional variations in climate and geology influence the chemical composition of thermal springs and of the two, geology plays a dominant role (Nyabeze & Gwavava, 2013). Solute concentrations in the waters circulating vary depending on rock type, heat source, permeability, the fluid supply, and the age of the thermal system (Barbier, 2002).

Mineral solubility is also affected by the pH of the solvent (Olivier, et al., 2011). As a result, the chemical composition of spring water will be heavily influenced by the composition of precipitation, its temperature, and pH (Olivier, et al., 2011). Other chemical reactions take place in the water, and they usually involve anions and cations (Olivier & Jonker, 2013; Olivier, et al., 2008). The most common species found in water are cations, anions, and neutral species such as noble gases, and many more (Olivier, et al., 2008; Olivier & Jonker, 2013). Less common species include dissolved silica species (H_4SiO_4), trace metals such as lithium, strontium, and arsenic, as well as volatile elements like radon and other gases released during geothermal circulation (Arnórsson, 1985; Giggenbach, 1991; Nicholson, 1993). These minor constituents play a critical role in geochemical equilibria and often dictate whether waters reach saturation or oversaturation with respect to specific minerals (Fournier, 1981; Giggenbach, 1991).

When geothermal fluids ascend to the surface and experience cooling, pressure drops, and degassing, conditions frequently shift towards silica and carbonate oversaturation, leading to mineral precipitation. For instance, El Tatio is a thermal site in the Andes of northern Chile where minerals like quartz, tridymite, cristobalite, and chalcedony are supersaturated (Garcia-Valles et al., 2008). El Tatio is a geothermal field located near the Atacama Desert (Garcia-Valles et al., 2008).

The processes of mineral saturation and precipitation are closely related to the ionic composition of geothermal waters, as the dissolution or precipitation of minerals modifies the concentration of dissolved salts and thereby directly influences water chemistry (Ellis & Mahon, 1977; Giggenbach, 1988; Arnórsson, 2000). Salts break down into electrically conducting positively or negatively charged ions (Hayashi, 2004). Electrical conductivity (EC) is a measurement of water's ability to conduct electrical current, and it is directly related to the

concentration of total dissolved solids (TDS) (Hayashi, 2004). TDS refers to the small quantity of organic materials and inorganic salts that are present in a solution (Hayashi, 2004). EC is an indicator of TDS and is based on the presence of ions (Hayashi, 2004). The principal constituents are usually Silicon (Si^{+}), Potassium (K^{+}), Sodium (Na^{+}), Calcium (Ca^{+}), and Magnesium (Mg^{2+}) as the cations and the anions, such as Chlorine (Cl^{-}), Sulphates (SO_4^{2-}), Carbonates (CO_3^{2-}) and Bicarbonates (HCO_3^{-}). If the EC is high, it denotes a high ion concentration, which subsequently dictates whether the water is fit for human consumption (Hayashi, 2004).

The chemical composition of thermal springs can be used to determine the types of waters present (Olivier, et al., 2011). Different types of waters are found in thermal springs, which are acid sulphate chloride water, sodium chloride water, calcium bicarbonate water, and acid sulphate water (Henley, et al., 1984; Giggenbach, 1988). The temperature of water affects the EC, the greater the temperature, the higher the EC (Hayashi, 2004). In thermal springs, high temperature implies high EC values, which are indicators of dissolved minerals in water (Olivier, et al., 2011).

In the past, several authors (Rindl, 1916; Kent, 1949; Kent, 1968; Olivier & Jonker, 2013; Bond, 1946) have studied the chemistry of thermal springs in South Africa. Many others (Olivier, et al., 2008; Olivier, et al., 2011; Nyabeze & Gwavava, 2013; Durowoju, et al., 2019) have performed additional chemical investigations on a small number of springs. South African thermal springs have been categorized using a variety of categories based on their chemical properties (Olivier & Jonker, 2013). The most common classification scheme for thermal springs in South Africa is that developed by Bond in 1946. The classification scheme, as devised by Bond is shown in **Table 2.2.**

Table 2.2 Classes of thermal water in South Africa according to (Bond, 1946)

Class	Water	Chemical Composition
A	Highly mineralised chloride-sulphate water	TDS > 1 000 mg/l; Cl- >27%; SO_4 = >5%
B	Slightly saline chloride water	TDS 300-500 mg/l; Cl- >27%; SO4 = <3%
C	Temporary hard carbonate water	TDS <800 mg/l; pH >7.6
D	Alkaline sodium carbonate water	TDS <1000 mg/l; Na2CO3 or NaHCO3 >15%. No permanent hardness
E	'Pure' waters	TDS <150 mg/l; pH <7.1

The majority of thermal spring waters in SA are categorised as temporary hard carbonate waters under category C (Nyabeze & Gwavava, 2013). This supports the conclusions reached by (Kent, 1968) and (Ashton & Schoeman, 1986) both of which claim that the waters may be a little bit excessively mineralised. Thermal springs are frequently richer in trace elements because minerals are more soluble in hot water (Hayashi, 2004). Some minerals dissolve more easily than others, and certain rocks are more mineral-rich than others (Olivier, et al., 2011). Multiple types of thermal waters can be frequently found at the same thermal system (Gupta & Roy, 2006). That is why it is crucial to create a logical link between the different types of fluids to understand their chemistry (Gupta & Roy, 2006).

2.4 The geothermal energy potential of thermal springs

2.4.1 Global assessment

Globally, the burning of fossil fuels, which contributes to climate change, is a major energy concern (Adebayo, et al., 2021). The need for alternative energy sources has arisen as a result of these fuels' depletion, unpredictability, and their environmental effects (Abubakar Jumare, et al., 2019; Dhansay, et al., 2017). Renewable energy sources such as wind, solar, and hydro have been employed to mitigate the energy crisis (Abubakar Jumare, et al., 2019; Adebayo, et al., 2021). Geothermal energy, which in simple terms is the heat energy from the Earth, is

another form of renewable energy that offers a reliable source of energy (Abubakar Jumare, et al., 2019).

Europe was the first continent to explore geothermal systems as a source of renewable energy (DiPippo, 1999). In the Italian town of Larderello in the Tuscan region, electricity was first produced from a thermal spring more than a century ago (DiPippo, 1999). By the year 2000, 21 countries around the world were producing geothermal energy, only two of those were African countries which are Kenya and Ethiopia (Huttrer, 2001). According to (Omenda, et al., 2020) Kenya ranks first in Africa for geothermal energy production and sixth globally for geothermal energy production. Geothermal energy is used in over 60 countries throughout the world as a source of power production or in direct-use applications (Omenda, et al., 2020). Geothermal electricity generation is utilized in 32 countries, whereas geothermal heating is implemented in 70 countries (Gutiérrez-Negrín, 2024).

Even though the Earth's geothermal energy is vast, only a small portion of it can be used (Olivier & Jonker, 2013). Thus far, only a few places can use this energy (Olivier & Jonker, 2013). These are areas where geological circumstances allow water in the liquid or vapour phases to be transported from hot deep zones to or close to the surface, thus producing geothermal resources (Abubakar Jumare, et al., 2019). Geothermal development is still growing, albeit slowly, with encouraging advancements in the works. The total installed geothermal power generation capacity at year-end 2023 stood at about 16,335 MW (Gutiérrez-Negrín, 2024). The top 10 countries **(Figure 2.1)** using geothermal systems for energy production as of 2024 are the United States of America, Indonesia, Philippines, Turkey, New Zealand, Kenya, Mexico, Italy, Iceland and Japan in that order (Gutiérrez-Negrín, 2024).

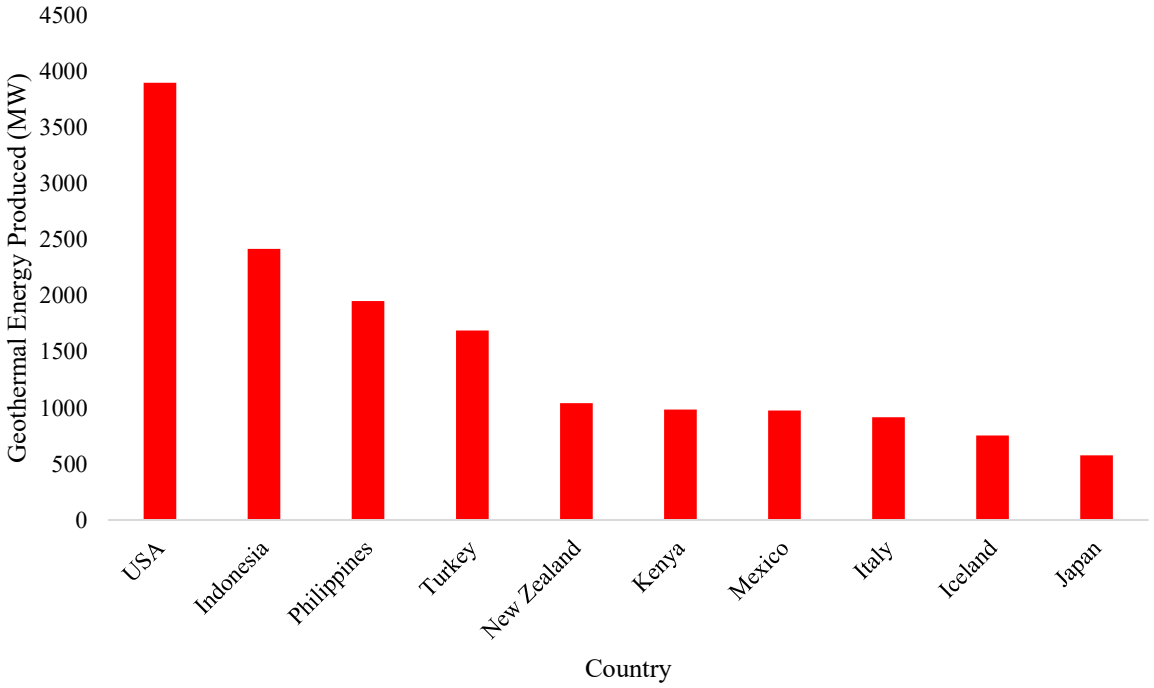

Figure 2.1: Top 10 countries with the highest geothermal energy production in 2024 (Source: World Energy Council, 2023)

Geothermal energy has the potential to provide up to 8.3% of the world's electrical needs, which would serve 17% of the global population. According to the WEC (2023), 39 countries, predominantly in South America, the Pacific, and Africa, can generate entirely their own power from geothermal sources.

2.4.2 South Africa

In comparison to other nations, the thermal springs in SA are among the least studied and least utilized of all natural resources (Olivier & Jonker, 2013). In recent years, there has been significant interest in the potential development of geothermal energy exploitation through thermal springs (Dhansay, et al., 2017; Martin & Croukamp, 2021). Regardless of this interest, not much work has been published on the energy potential of thermal springs in SA, except for the work of (Tshibalo, et al., 2010; Tshibalo, et al., 2015; Dhansay, et al., 2017; Martin & Croukamp, 2021). By contrast, several developing countries, such as Kenya, Ethiopia, and Indonesia, have actively investigated and developed their geothermal resources for energy

production and tourism, highlighting a disparity in research focus and utilisation between South Africa and its developing-country peers.

In 2010, it was stated that no effort had been made to develop geothermal resources to produce electric power due to the low temperatures of thermal springs (Tshibalo, et al., 2010). Thermal springs in SA were therefore limited to direct uses (Olivier & Jonker, 2013). According to (Tshibalo, et al., 2010) there were initiatives underway to persuade the government of the value of investigating the potential for geothermal energy production and other developments. In 2017, Dhansay et al. produced results that suggested that the country does have some potential for harnessing low-enthalpy geothermal energy in five locations **(Figure 2.2)**. Recommendations were made for SA to seriously consider geothermal energy as another renewable option.

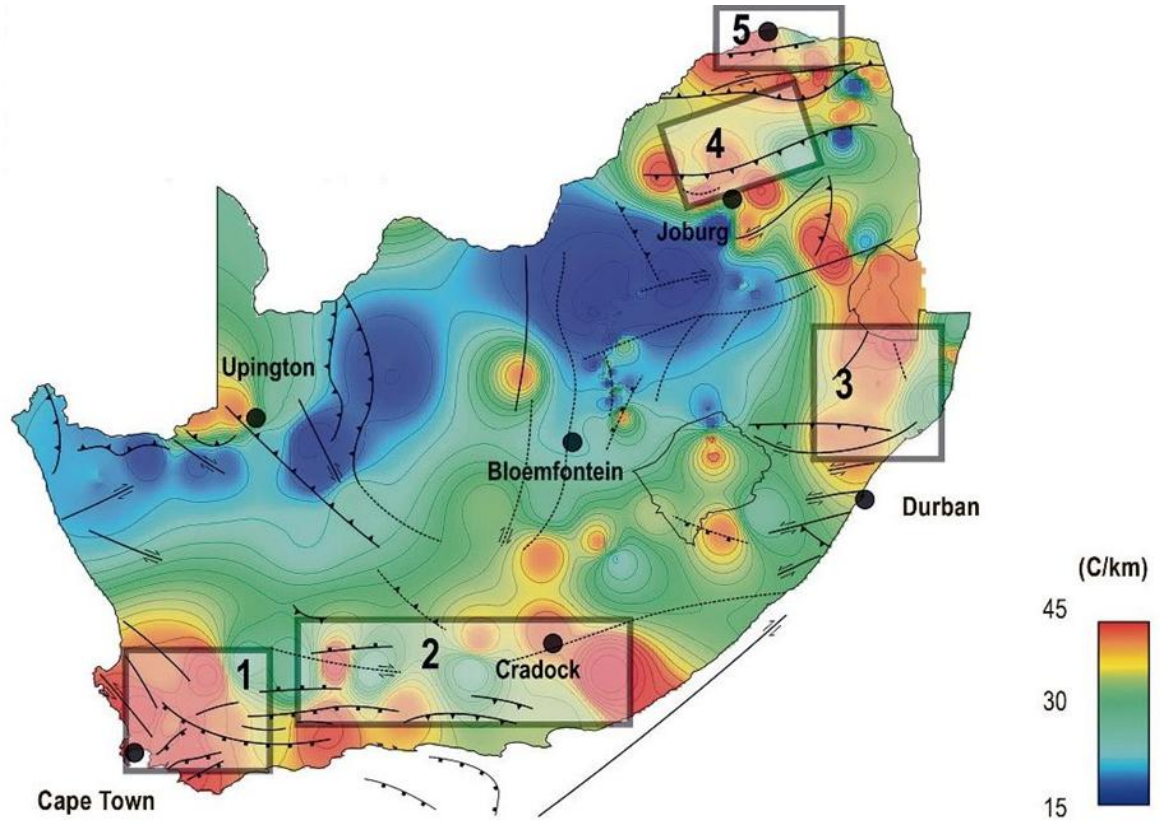

Figure 2.2: Regions with low-enthalpy energy potential (Source: Dhansay et al., 2017)

Martin and Croukamp (2021) investigated the geothermal energy potential in the Cape Fold Belt. Results showed two places; Calitzdorp and Caledon to have high geothermal energy potential warranting further investigation, that was validated by the temperature measurements

of water from the springs and the temperature estimations derived from geothermometry calculations. There was also compelling evidence of a sizable reservoir at the Calitzdorp hot spring, at a suitable depth beneath the Oudtshoorn basin, which, if it existed, would supply enough heat energy for a low-enthalpy geothermal power plant. Low-enthalpy geothermal energy refers to geothermal resources with relatively low temperatures, typically below 150°C (DiPippo, 2012).

According to Dhansay et al. (2017), before geothermal energy can be harvested, a few important conditions must be resolved in South Africa. Significant research and data collection are still needed, including deep hydrogeological and isotope hydrochemical investigations, comprehensive downhole temperature measurements, high-resolution ground-based geophysics, and structural mapping. A more accurate assessment of South Africa's geothermal energy potential will be achievable thanks to these data, which will also show any potential drawbacks, particularly regarding GW quality (Dhansay, et al., 2017).

2.5 Techniques used for examining and mapping thermal springs.

2.5.1 Remote sensing and thermal imagery

The first step in the exploitation of thermal springs requires the identification of appropriate locations for their development (Abubakar, et al., 2019). Exploring thermal springs proves to be a challenging endeavour; however, it is possible to establish the location of geothermal potential by determining the temperature of groundwater reservoirs from observations of surface temperature (Favier, et al., 2021). Traditional survey methods rely on spot measurements or sampling (Abubakar, et al., 2019). However, the application of remote sensing and thermal infrared methods' potential has been demonstrated (Abubakar, et al., 2019) because of their flexibility, the clarification of the results, and the benefits of not being invasive as imaging techniques (Glaser, et al., 2018). Remote sensing can help with the feasibility stages of geothermal research since it provides a synoptic capability of covering broad areas in real-time and can cost-effectively explore prospective geothermal locations that are difficult to locate using traditional survey methods (Abubakar, et al., 2019).

At first, thermal images from satellites were utilised for applications like hydrological modelling, fire detection, or the exploration of mineral resources (Wan, et al., 2021). Recently,

latest technologies, like the manned aerial aircrafts (Lin & Lai, 2018) or more of late, unmanned aerial vehicles (UAVs) (Kim, et al., 2021) have been gaining more attraction in the hydrology community. UAVs have recently been implemented in SW–GW research (Vélez-Nicolás, et al., 2021).

UAVs also known as drones are aircraft that carry no human pilot or passengers which are used to capture images (Kim and Sung, 2024; Rand, 2024). UAVs can be fully or partially autonomous but are more often controlled remotely by a human pilot on the ground (Kim and Sung, 2024; Rand, 2024). UAVs can be used to acquire images at any time and from any location. They operate at low altitudes, leading to their images having higher resolutions than those taken by manned aircraft (Kim and Sung, 2024). Due to their great efficiency and low cost, UAVs are becoming a popular way to quickly acquire high-precision spatial information and data (Kim and Sung, 2024).

When compared to the metric accuracy of satellite photography, UAVs can achieve accuracy of the order of a centimetre while offering more flexibility, portability, and affordability than manned aircraft (Chen, et al., 2019). In addition to all of this, it is important to consider their already established potential for use in the field of hydrogeology for tasks like wetland restoration, groundwater discharge analysis, determining the size of water bodies, and mapping thermal springs (Sedano-Cibrián, et al., 2022). UAVs provide useful information on the size and extent of GW emerging from springs (Vélez-Nicolás, et al., 2021)

2.5.2 Geochemistry

Since the early 1960s, geochemical techniques have been crucial in the first exploration of geothermal systems (Gupta and Roy, 2006). Thermal springs' chemical data on hot water and stream discharges give important information on subsurface water flow patterns (Gupta and Roy, 2006). Due to the low cost, geochemical techniques were often employed throughout a whole geothermal exploration (Giggenbach, 1991). Geochemical investigations are carried out on samples from thermal springs, fumaroles, and hot pools (Gupta and Roy, 2006).

To have a better understanding of the geochemical evolution of GW, water samples collected are plotted on diagrams **(Figure 2.3)** known as the Piper diagram (Piper, 1944), Durov diagram (Durov, 1948), Gibbs plot (Gibbs, 1970), and many others. The Piper diagram is a multi-dimensional plot that shows the milliequivalent percentage concentrations of the principal

anions (HCO_3^-, SO_4^{2-}, and Cl^-) and cations ($Ca^{2+,}$ Mg^{2+}, Na^+, and K^+) in two triangle fields that are then projected farther into the central diamond field. On the other hand, the Durov diagram is a composite plot made up of two ternary diagrams with the milliequivalent percentages of the cations of interest plotted against those of the anions of interest; the sides of the diagram form a rectangular, binary plot of the concentrations of all the cations and all the anion (Ravikumar, et al., 2015).

Both diagrams are used to understand the chemical processes involved along with the water type of GW and thermal springs (Piper, 1944 and Durov, 1948). The Gibbs diagram plots total dissolved solids against Na/(Na+Ca) and Cl/(Cl+HCO3) concentrations of GW. By graphing the TDS, against Na/(Na+Ca) and Cl/(Cl+HCO3) concentration of GW, the Gibbs plot offers crucial information on the mechanisms (evaporation, rock water interaction, or precipitation) governing the chemistry of GW systems (Odiyo et al., 2020).

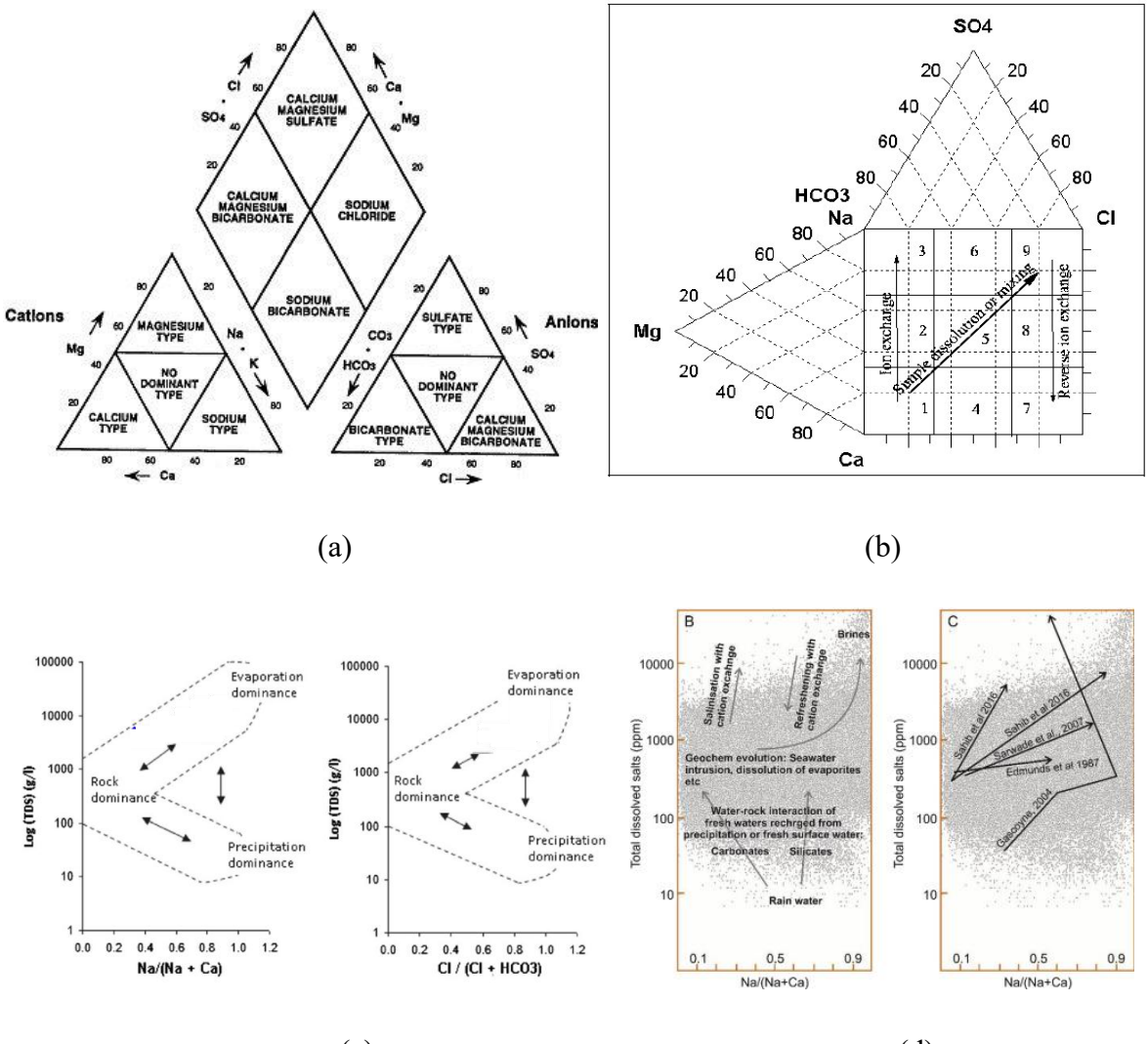

Figure 2.3: Piper (a), Durov (b), and Gibbs (c, d) diagrams used to classify water types and rock-water interaction in thermal springs. Source: (Lonergan & Cange, 1994; Lloyd & Heathcote, 1985)

2.5.3 Geothermics

The use of thermal water's chemical composition to estimate the temperature at which it equilibrated in the subsurface is known as Geothermometry (Cave & Clarke, 2003; Karingithi, 2009). For the research and exploitation of thermal springs, chemical geothermometers are a crucial geochemical tool (Cave & Clarke, 2003; Karingithi, 2009). Subsurface temperatures, or the temperatures that drilling is likely to encounter, are estimated during the exploration phase using geothermometry based on the chemical make-up of the thermal waters (Karingithi, 2009). The reaction between water and minerals approaches equilibrium slowly at low temperatures and considerably more quickly at high temperatures reservoirs (Gupta & Roy, 2006). Additionally, geothermometry can be used to clarify chemical processes that arise in the zone of depressurisation surrounding reservoirs as a result of boiling and/or cooling by refilling cold water (Karingithi,2009).

Geothermometers use certain mineral-solute processes that are slower to re-equilibrate at lower temperatures, particularly when the fluid is successfully isolated from the minerals that regulated the equilibria (Karingithi, 2009). As a result, solute concentration or solute ratios represent the hot equilibrium temperature that is "frozen in" to the fluid (Karingithi, 2009). When using geothermometers, caution is required to avoid significant inaccuracies in the findings and interpretations. Therefore, it is important to consider any geothermometer's limits.

Silica, Na/K, Na-K-Ca, Na-K-Mg, Mg/Li, and Na/Li are the widely used geothermometers that are applied to estimate subsurface temperatures and the depth of the thermal springs by using the geothermometry equations. Some of the first researchers to investigate geothermometry include Fournier and Rowe (1966), who used Silica to estimate underground temperatures of water from hot springs and wet-steam wells. Fournier (1979), Truesdell (1976) and Arnorsson (1983) have all worked on revising the Na/K geothermometer equation. Fournier and Truesdell (1973) worked with the Na-K-Ca geothermometer for natural waters. (Fournier & Potter, 1979) investigated the magnesium correction to the Na-K-Ca chemical geothermometer. Other authors (Kharaka & Mariner, 1989) investigated chemical geothermometers and their application to the formation of waters from sedimentary basins. Fouillac and Michard applied the Na/Li ratio to the geothermometry of geothermal reservoirs in 1981.

Table 2.3: List of geothermometer equations used to estimate subsurface temperatures of thermal springs

Name and reference	Equation	Equation Number
Quartz- Conductive- no steam lost (Fournier, 1977)	$T = \frac{1309}{5.19 - \log(SiO2)} - 273.15$	**(2.1)**
Quartz- Adiabatic- Steam lost (Fournier, 1977)	$T = \frac{1522}{5.75 - \log(SiO2)} - 273.15$	**(2.2)**
Quartz (Truesdell and Fournier, 1976)	$T = \frac{1315}{5.205 - \log(SiO2)} - 273.15$	**(2.3)**
Chalcedony (Arnorsson et al., 1983)	$T = \frac{1112}{4.91 - \log(SiO2)} - 273.15$	**(2.4)**
Chalcedony- C.onductive (Fournier, 1977)	$T = \frac{1032}{5.62 - \log(SiO2)} - 273.15$	**(2.5)**
Amorphous (Fournier, 1977)	$T = \frac{731}{4.52 - \log(SiO2)} - 273.15$	**(2.6)**
Na-K (Truesdell (1976)	$T\left(\frac{Na}{K}\right) = \frac{856}{\log\left(\frac{Na}{K}\right) + 0.875} - 273.15$	**(2.7)**
Na-K (Fournier,1979)	$T\left(\frac{Na}{K}\right) = \frac{1217}{\log\left(\frac{Na}{K}\right) + 1.483} - 273.15$	**(2.8)**
Na-K (Arnorsson *et al.* (1983)	$T\left(\frac{Na}{K}\right) = \frac{933}{\log\left(\frac{Na}{K}\right) + 0.993} - 273.15$	**(2.9)**
Na-K (Giggenbach (1988)	$T\left(\frac{Na}{K}\right) = \frac{1390}{\log\left(\frac{Na}{K}\right) + 1.750} - 273.15$	**(2.10)**
Na-K (Verma and Santoyo (1997)	$T\left(\frac{Na}{K}\right) = \frac{1289}{\log\left(\frac{Na}{K}\right) + 1.615} - 273.15$	**(2.11)**
K-Mg (Giggenbach, 1988)	$T\left(\frac{K}{Mg}\right) = \frac{4410}{\log\left(\frac{K}{\sqrt{Mg}}\right) + 14.00} - 273.15$	**(2.12)**

Na-K-Ca (Fournier and Truesdell, 1973)	$T\left(\frac{Na}{\frac{K}{Ca}}\right) = \frac{1647}{\log\left(\frac{Na}{K}\right) + [\beta \log\left(\frac{\sqrt{Ca}}{Na}\right) + 2.06} - 273.15$	**(2.13)**

Where: T= Temperature in °C

β= 4/3 if $T_{\text{Surfacing}} < 100$°C or β = 1/3 if $T_{\text{Surfacing}} > 100$°C

The temperature of subsurface thermal reservoirs is a critical parameter for assessing the formation mechanisms and utilisation potential of geothermal resources (Gemici & Filiz, 2001; Han et al., 2010; Bozdağ, 2016). Chemical geothermometers, which are employed to evaluate reservoir temperatures, depend on the temperature-dependent chemical equilibria between water and the minerals present in the rock at the temperature of the deep thermal reservoir (Nicholson, 1993; Tarcan, 2005; Bozdağ, 2016). The geothermal energy potential of a thermal spring is often assessed using chemical geothermometers, which establish a correlation between the chemistry of the thermal fluids and the reservoir temperature (Karingithi, 2009).

2.5.4 Stable isotope use

Stable isotopes are used to trace the flow of water (Diamond, 2022). Stable isotopes such as Deuterium and Oxygen-18 offer details on how GW recharges and address inquiries about the origin, factors influencing recharged water, and residence times (Craig, 1949; Olivier et al., 2013; Diamond, 2022). As water passes through the water cycle, the abundances of the various hydrogen and oxygen isotopes change (Diamond, 2022). Reactions and transitions (such as evaporation and condensation) are the source of these fluctuations (Craig, 1961). We can deduce information about the history of the water before it reaches the location where a sample was taken by measuring these changes (Diamond, 2022). To differentiate between new waters and old waters that may circulate in the deeper constricted areas of the aquifer, the isotopic technique is an important tool (Craig, 1949). Climatic variations are indicated by a change in the stable isotope composition of rainfall (Darling, et al., 1997).

Delta notation (δ) is used to indicate the ratio of deuterium and oxygen-18 isotopes to the standard (You, et al., 2021). Values are stated in per mil (‰) (Diamond, 2022). Conventionally, an isotope ratio is the ratio of a heavier isotope to a lighter one (Diamond, 2022). A sample with a relatively high concentration of the heavy isotope will have a δ value greater than zero

(enriched), while a sample with a relatively low concentration of the heavy isotope will have a negative δ value (depleted) (Diamond, 2022).

The standard for both hydrogen and oxygen in water is SMOW, which stands for Standard Mean Ocean Water (Craig, 1961; Diamond, 2022). SMOW was devised by Harmon Craig in 1961 (Craig, 1961) as a virtual reference for measuring hydrogen and oxygen isotope ratios in water. It was intended to represent the average isotopic composition of the Earth's oceans (Craig, 1961). VSMOW was created to provide a reliable and physically defined reference for stable isotope measurements, addressing the limitations of the original (Diamond, 2022).

Stable isotope data performed on rainfall samples are shown on a line known as a meteoric water line (Diamond, 2022). Surface and GW samples can also be used to plot this line, however, data from local, regional, or global precipitation samples are typically used (Diamond, 2022). Craig was the first to recognize the Global Meteoric Water Line (GMWL) in 1961 and a meteoric water line for a region is known as the Local Meteoric Water Line (LMWL). Processes including water-rock interaction, evaporation, recharge, and mixing can be investigated by comparing GW, SW, and specific precipitation events to the LMWL (Jasechko, 2019). This is shown in **Figure 2.4**, the variations in position and slope enable the interpretation of stable isotope data, which allows the formulation of hypotheses regarding water sources, sinks, and interactions within a region (Diamond, 2022).

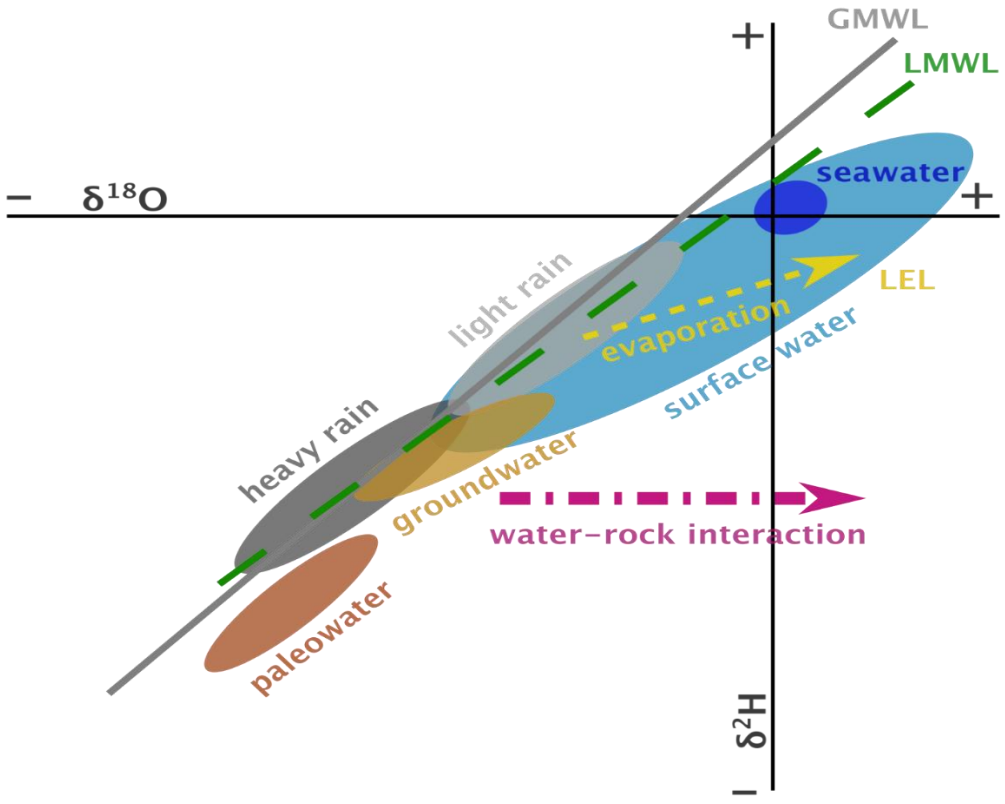

Figure 2.4: "A conceptual diagram showing typical isotope compositions of various water bodies and differences in the LEL (local evaporation line), LMWL (local meteoric water line) and GMWL (global meteoric water line) for a specific region" (Source: Diamond, 2022)

The temperature effect, latitude effect, continental effect, altitude impact, and amount effect are the names given to variables that have an impact on the isotopic composition of precipitation, also referred to as isotope effects (Diamond, 2022). The isotopic composition of precipitation exhibits a trend towards lighter values, characterized by a depletion of deuterium (^{2}H) and oxygen-18 (^{18}O), as influenced by several factors including decreasing temperature, increasing latitude, greater distance from coastal regions, elevated altitudes, and heightened precipitation amounts during specific events (Diamond, 2022).

2.6 Previous work done on the Shu-Shu thermal springs

Gevers (1942) and Kent (1949) were the first researchers to ever conduct investigations on the Shu-Shu thermal springs. Various authors, such as: Gevers (1963); Kent (1969); Mazor and Verhagen (1983) and Olivier et al. (2013) have since referred to their data and interpretations. The majority of information on Shu-Shu, however, comes from indirect sources that describe the region's hydrology and geology (Mazor & Verhagen, 1983; Gravelet-Blondin, 2013). This is due to the limited information present in the literature regarding thermal springs in So uthern Africa, particularly the Shu-Shu thermal springs. The most recent researchers to investigate the Shu-Shu thermal spring were Gravelét-Blondin (2013), who investigated the geological and hydrological characteristics of the springs. And Olivier and Jonker (2013) who travelled across the country investigating all 87 thermal springs in South Africa, including the Shu-Shu springs.

2.6.1 The origin of the Shu-Shu thermal springs

The natural geothermal gradient, which results from rainfall falling to a lower depth and raising groundwater temperatures, is the source of the thermal springs seen throughout southern Africa (Gevers, 1942; Kent, 1949; Hoffmann, 1979; Olivier et al., 2008). The geothermal gradient increases the rainwater turned into groundwater temperature into either the warm (25°C – 37°C), hot (37°C – 50°C) or scalding (>50°C) classes as defined by Kent (1949). Gevers (1942) discovered that rainwater falling and seeping into the sandstone and the underlying rocks on the nearby plateau ultimately reached the temperatures measured in the Shu-Shu thermal springs, because of the natural geothermal gradient.

In 2013, Glevelet-Blondin used isotopes to infer that the Shu-Shu thermal springs are meteoric in origin and most likely receive their water from a 130 km long zone that stretches westward into the Great South African Escarpment, meaning they are regionally sourced. These waters then drop vertically to a depth of between 1827 and 2153 meters, at which point the pressure from the escarpment causes the fissures they travel through to close, effectively trapping the water under pressure (Gravelet-Blondin, 2013). This sealing process contributes to the formation of a confined thermal aquifer, allowing the water to heat up as it equilibrates with the surrounding rock over long residence times. When the water eventually finds pathways back to

the surface, it emerges as the Shu-Shu thermal springs, carrying the thermal signature accumulated during its deep underground circulation (Gravelet-Blondin, 2013).

2.6.2 The hydrochemical characteristics of Shu-Shu thermal springs

The two authors who primarily investigated the Shu-Shu thermal springs: Gevers (1942), and later Kent (1949) reported the surfacing temperature of the Shu-Shu thermal springs to be of 52°C – 53°C and a pH of 8.2, while a more recent investigation by Olivier et al. (2013) found the surfacing temperature to be 50°C. Gravelet-Blondin (2013) stated that because of a slightly increased geothermal gradient of 3.1°C / 100m at depth, the groundwater reaches a temperature of roughly 75°C to 85°C as it flows toward the Shu-Shu thermal springs. Due to the conductive cooling mechanisms, the temperatures of these waters drop to about 67°C before they surface. Nevertheless, the thermal waters are further cooled to a surfacing temperature of around 50°C by intermixing with shallow, cold groundwater.

Gevers (1942) reported that the anions Cl and SO_3 (SO_4), and the cations Na and Ca, are the main constituents of the Shu-Shu thermal spring waters. Moreover, a small amount of H_2S and CO_2 gas bubbles up via the thermal waters' fault zone. Gevers (1942) and Kent (1949) subsequently claim that most of the components dissolved in the Shu-Shu thermal originate from the dissolution of different minerals in the gneisses and amphibolite that the hot waters flow through to the surface. Nonetheless, it is believed that the dispersion of pyrite at depth explains not only the increased SO_4 concentrations in the thermal waters in addition to the presence of gases (Gevers, 1942; Kent, 1949; Gravelet-Blondin, 2013 and Olivier et al., 2013). Gravelet-Blondin (2013) states that the region's shallow groundwater and surfacing thermal water have higher than average amounts of Na, K, Ca, Mg, Fe, Al, Si, F, and Sr, which can be linked to leaching from country rock.

Kent (1949) classified the Shu-Shu thermal waters as "scalding" and described the Shu-Shu thermal springs as belonging to Class A per Bond's (1964) first categorisation (**Table 2.2**). Highly mineralised Cl–SO_4 fluids fall into this class; TDS concentrations must be greater than 1000 mg/l, and Cl and SO_4 concentrations must be greater than 27% and 5%, respectively.

2.6.3 Research gaps from the previous studies

The previous studies (Gevers, 1942; Kent, 1949) of the Shu-Shu thermal springs are out of date, as they were conducted in the early 1900s. The most recent research (Olivier & Jonker, 2013; Gravelet-Blondin, 2013) was conducted more than a decade ago, and while they yielded good results, there are temporal, method, and geographical gaps. The studies done in the early 1900s were primarily concerned with the geological and chemical features of the springs, and the methodologies applied are now out of date, with changes in land use practices and climate occurring since then.

The most recent study by Olivier and Jonker (2013) has a geographical gap, while they investigated all the thermal springs in South Africa, it is more concentrated on the Limpopo and Western Cape thermal springs, largely overlooking the Shu-Shu springs located in KZN. While previous studies (Gravelet-Blondin, 2013) have examined the origin of Shu-Shu springs using isotopes, the sampling techniques used can be improved and provide more evidence to support conclusions. Improvements could include increasing the number of sampling locations along the spring system and its feeder streams, conducting repeated sampling across different seasons to capture temporal variability.

This study will close research gaps by investigating the SW surrounding the Shu-Shu thermal pools to determine whether the thermal springs have an impact on the water quality of the uThukela River. The sampling size will comprise a variety of rainfall samples from various locations/elevations, which will be analysed in comparison to samples collected from thermal springs and surface water nearby. This will provide additional evidence to corroborate the springs' origin. The methodology gap will also be closed by introducing new, innovative technology. The use of UAVs will provide a new viewpoint on what influences the formation of springs, as well as the extent of the discharge zone.

CHAPTER 3: STUDY AREA DESCRIPTION

3.1 Geographical location of the Shu-Shu thermal springs

The Shu-Shu thermal springs are found near Nkandla and Kranskop in KwaZulu-Natal, South Africa, and are located on an island in the middle of the uThukela River, which is the largest river in KwaZulu-Natal. They are situated 250 m above sea level along the Namaqua-Natal Belt. The thermal springs are made up of seven concentrated pools (cf **Figure 8.1** in **APPENDIX A)**. The pools make up an area of 464.82 m^2. The dry season in this region persists from March/April through to September of the same year, resulting in low flow, which substantially impacts the Shu-Shu hot springs and uThukela river water quality. The low flow makes it possible to cross the uThukela River to reach the Shu-Shu thermal springs.

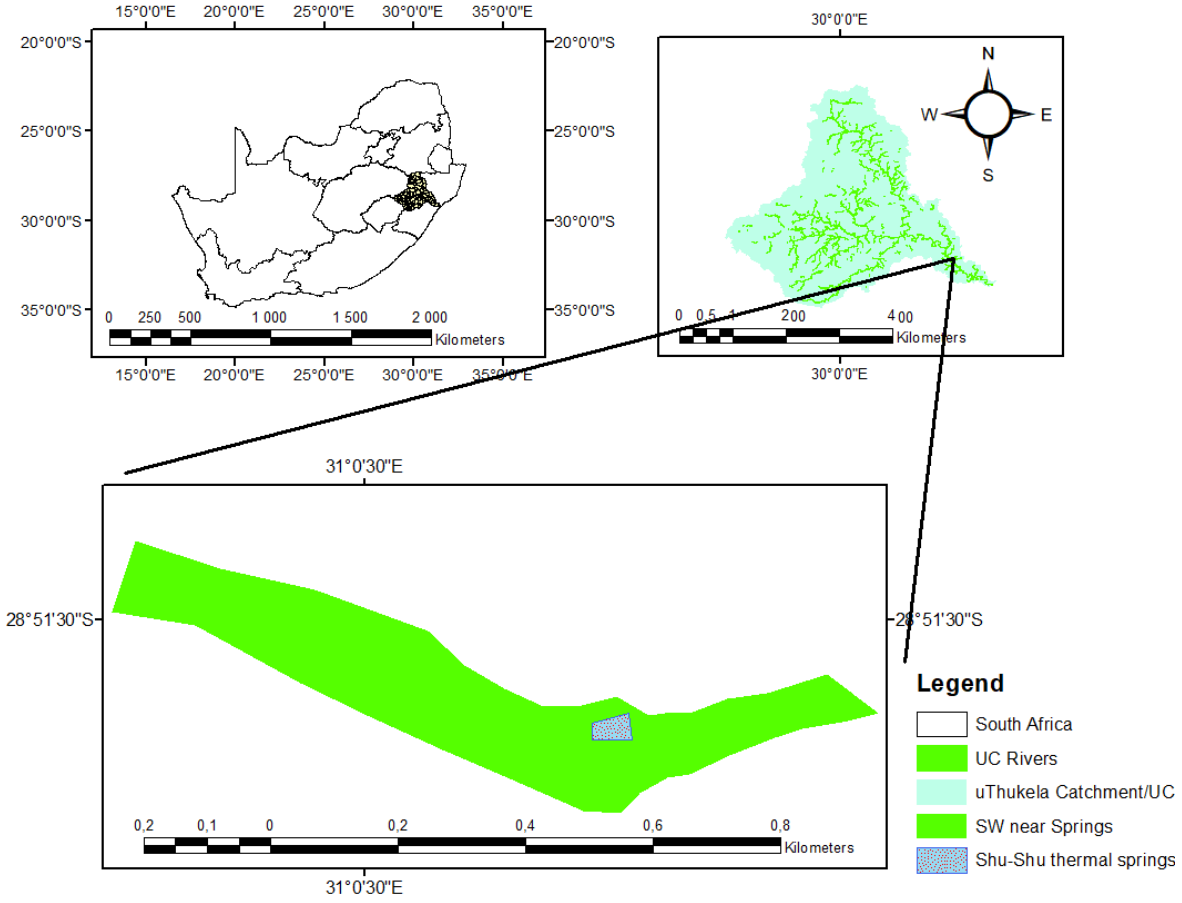

Figure 3.1: Location of the Shu-Shu thermal springs (Coordinates: 28°51'35"S 31°00'42"E)

3.2 Climate of the Area

The studied area is categorised under the semi-arid region (Kottek, et al., 2006). It receives much of its rainfall during summer (October to March). The area normally receives less than 1000 mm of rain per year. It receives the lowest rainfall which is 9mm in July and the highest which is 137mm in January. The area is characterised by high-temperature variations in different seasons of the year with average temperatures ranging from 19 °C to 21 °C in winter, and from 23 °C to 26 °C in summer. The summer months receive almost 80% of the rainfall, while the winter months receive barely 20%.

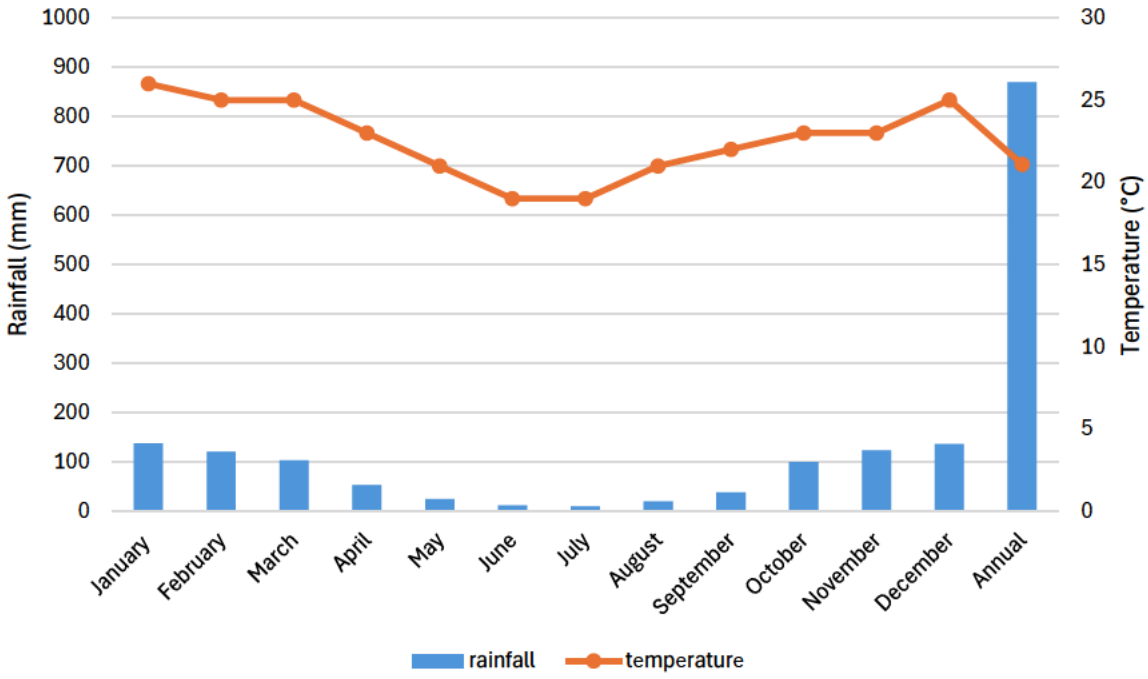

Figure 3.2: The average climate of the area surrounding the Shu-Shu thermal springs. Source: (Spark, 2024)

3.3 Geology of the Area

The Shu-Shu thermal springs are located within the KwaZulu-Natal region on the Kaapvaal Craton, a stable continental block characterized by high-grade metamorphic basement rocks (Charlesworth & Matthews, 1981; Gravelet-Blondin, 2013). These basement rocks are dominated by gneiss and amphibolite (Charlesworth & Matthews, 1981; Gevers, 1942; Gravelet-Blondin, 2013). The area has been shaped by multiple tectonic events, including the Neoarchaean and Namaqua-Natal orogenies, which produced folded, sheared, and foliated gneisses and amphibolites (Gevers, 1942; Charlesworth & Matthews, 1981). These rocks were altered under high temperatures and pressures (amphibolite-to-granulite-grade metamorphism) and were later changed again by retrogressive processes during subsequent tectonic events (Gevers, 1942).

The gneissic rocks are primarily composed of quartz, plagioclase feldspar, and hydrous minerals such as biotite and amphibole (Gevers, 1942). Biotite commonly formed at the expense of hornblende through hydration reactions, a retrograde metamorphic process that has been documented in both the gneiss and amphibolite sequences of the Shu-Shu thermal spring setting (Gevers, 1942; Charlesworth & Matthews, 1981). The hornblende gneiss is dominated by plagioclase and microcline, with smaller amounts of quartz and hornblende, while the biotite-hornblende gneiss contains abundant quartz, feldspar, biotite, hornblende, epidote, and titanite (Gevers, 1942).

The amphibolites, in contrast, are characterised by high concentrations of hornblende, accompanied by plagioclase feldspar, quartz, and accessory phases such as epidote, titanite, and minor garnet (Gevers, 1942). They are typically dark, fine- to medium-grained rocks representing metamorphosed mafic protoliths. They possess low primary porosity, but fractures, foliation, and localised weathering improve secondary permeability (Gevers, 1942; Charlesworth & Matthews, 1981; Gravelet-Blondin, 2013).

The springs are structurally controlled by north-northwest-trending faults and fractures, which act as conduits for deep groundwater flow (Gravelet-Blondin, 2013). Meteoric water infiltrates, circulates to significant depths where it is heated, and then ascends along these structural pathways to discharge at the surface (Gravelet-Blondin, 2013).

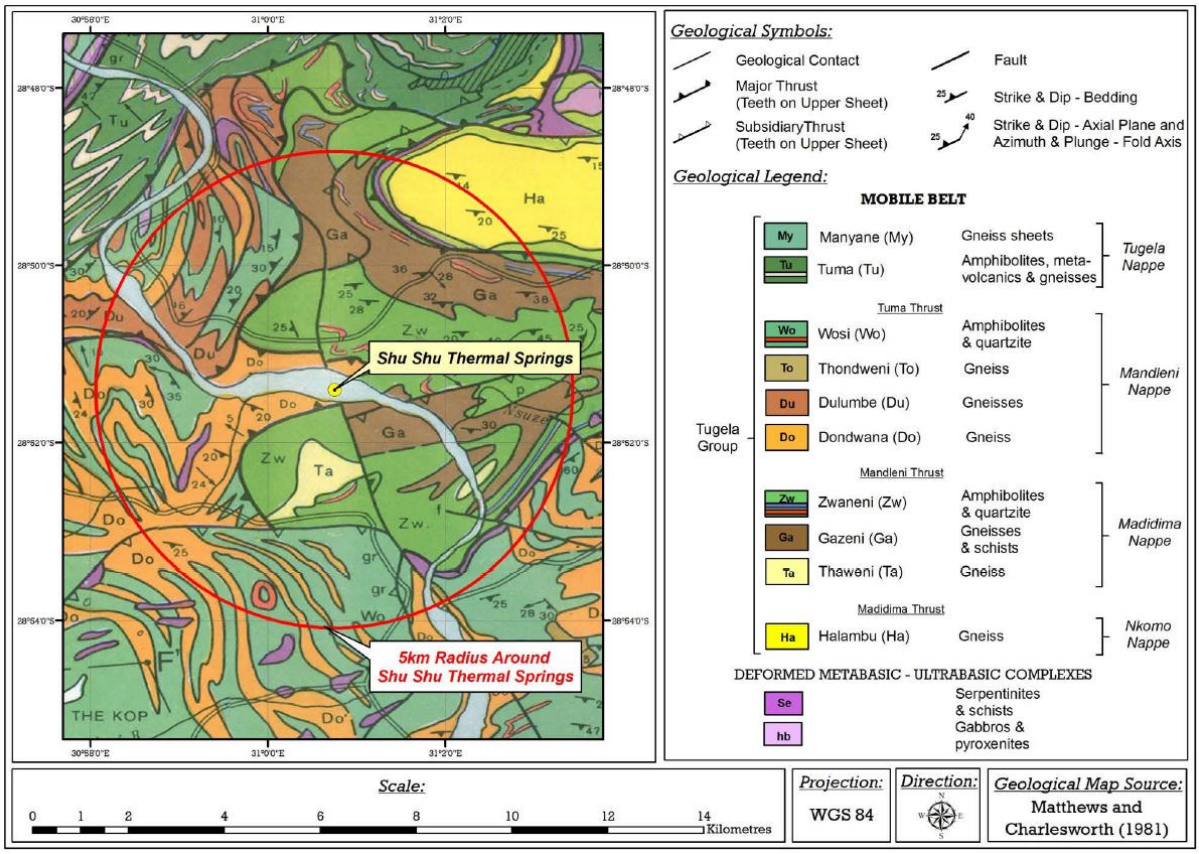

Figure 3.3: The geology of the area surrounding the Shu-Shu thermal springs (Source: Matthews & Charlesworth, 1981)

CHAPTER 4: METHODOLOGY

4.1 Introduction

Three research methods enabled answering the research question and fulfilling the aims and objectives established. The three research methods included the use of Environmental Isotopes, Geochemistry, and UAV.

4.2 In-situ measurements

Sampling occurred at eleven sampling sites. Two sampling points on the surface water, 500 and 250 m upstream of the Shu-Shu thermal springs. Two were on the surface water, 500 and 250 m downstream of the Shu-Shu thermal springs, and seven samples were collected on the seven concentrated pools.

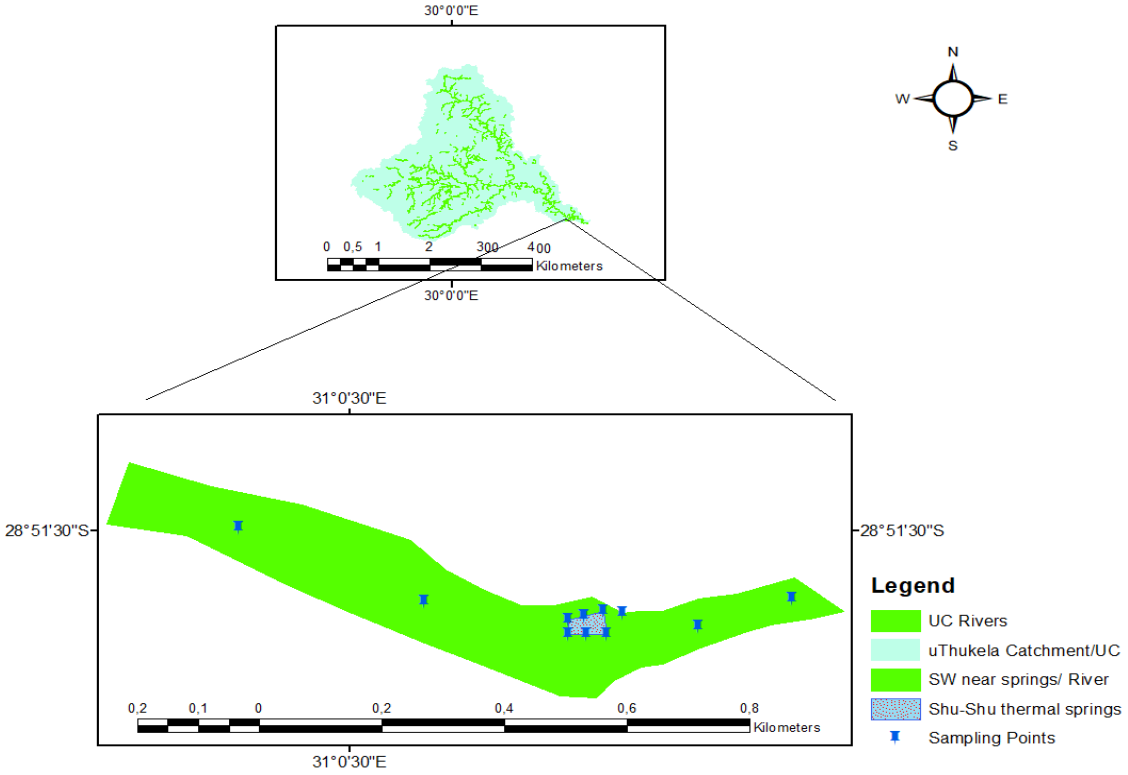

Figure 4.1: Location of the eleven sampling sites across the uThukela River and Shu-Shu thermal springs

Prior to sampling, parameters such as temperature (T), pH and electrical conductivity (EC) were measured at each sampling point using a portable multi-sensor meter.

(a) (b)

Figure 4.2: Portable multi-sensor meter (Hanna, 1996) (a) used to measure T, EC, and pH from water samples collected and pictures taken while sampling the Shu-Shu thermal springs (b)

4.3 Isotope analyses

The two stable isotopes used were: Oxygen 18 and Deuterium ($\delta^{18}O$- $\delta^{2}H$). Sampling for the water isotope analysis was done across the eleven sampling sites during both dry and wet seasons. The samples were collected using 15 mL centrifuge tube containers. The samples were then stored in a cool place while awaiting analysis. The isotope analysis was conducted using a Los Gatos Research (LGR) Double Liquid-Water Isotope Analyzer (D-LWIA) in the isotope laboratory at the University of KwaZulu-Natal, Agricultural campus in Pietermaritzburg. The D-LWIA equipment uses the High-Resolution Laser Absorption Spectroscopy technique and simultaneously measures stable isotope ratios. The isotopic compositions were reported in δ-notation as per mil (‰) relative to the standard isotope ratio of Standard Mean Ocean Water (SMOW).

Figure 4.3: The Los Gatos Research (LGR) Liquid Water Isotope Analyser (LWIA) located at UKZN Agricultural Campus, Pietermaritzburg

Rainfall samples were collected from three rainfall stations located in Eshowe, Winterton, and the Highlands (Mike pass). The rainwaters from the three rainfall stations were analysed for their isotopic make-up using the D-LWIA. Following the isotope analysis of the thermal springs and rainwater samples, the results were plotted against each other on a dual-isotope plot to determine which rainwaters have similar isotopic make-up to the Shu-Shu thermal springs. Knowing the isotopic signature assisted with tracking and tracing the origin of the thermal spring waters.

(a) (b)

Figure 4.4: Location of the comparable rainfall stations situated at Winterton, Eshowe and the Drakensberg Mountain

4.4. Chemistry analyses

4.4.1 Hydrochemistry analyses

Surface water samples were collected at the eleven sampling points during the dry season on the 26th of June 2024. 500 mL sampling bottles were used. Sampling bottles were filled to the top to get rid of air bubbles. The samples were stored in a cool place before the analyses at the uMngeni-uThukela water laboratories at Pietermaritzburg. The analyses were conducted following correct testing methods approved by the South African National Accreditation System (SANAS).

The interpretation was based on the concentration of key cations, such as Si^{+}, K^{+}, Na^{+}, Ca^{+} and Mg^{2+} as well as major anions, such as Cl^{-}, SO_4^{2-}, $CO_3^{2-,}$ and HCO_3^{-}. The cations [Si^{+}, K^{+}, $Na^{+,}$ and $Ca^{2+}Mg^{2+}$] and anions [Cl^{-} and SO_4^{2-}] concentrations were measured using a spectrophotometer instrument (cf **Figure 8.2** in **APPENDIX A**). The concentrations of CO_3^{2-} and HCO_3^{-} were determined by acid titration, which was performed in the Soil Science laboratory at UKZN, PMB Campus (cf **Figure 8.3** in **APPENDIX A**). The chemical composition of thermal springs was used to determine the types of waters present and the water quality of the stream.

4.4.2 Geothermometry

Succeeding the hydrochemistry analyses of the thermal springs, the concentration of ions such as SiO_2, K, Ca, Mg, and Na were used to estimate the GW reservoir temperatures below the surface. The Liquid-Analysis v.3 spreadsheet (Powell and Cumming, 2010) was used to calculate the equilibrium temperature in the thermal reservoirs using a variety of geothermometers (quartz, chalcedony, cristobalite, amorphous silica, Na-K, and K^2-Mg, Na-K-Ca, and Mg, K-Mg, Na-K-Ca). The equations used are shown in **Table 2.3**. Giggenbach plots were created to show the ratios between the various geothermometers and geoindicators. This was done to determine whether the Shu-Shu thermal springs have the potential to produce geothermal energy.

4.4.3 Circulation Depth

The circulation depth of the Shu-Shu thermal springs was calculated by looking at the temperature variation of the thermal waters on the surface and subsurface (Li, et al., 2021). The temperatures on the subsurface were measured in situ, while the subsurface temperatures were estimated using geothermometry equations.

Equation from (Luo, et al., 2017) was used to estimate the depth of circulation:

$$Z = \frac{Tz - To}{G} \quad \textbf{(4.1)}$$

Where:

Z- Reservoir depth- km

Tz- The average reservoir temperature calculated by the geothermometers in this project -$^{\circ}$C

To- The local annual average temperature -$^{\circ}$C (Spark, 2024)

G- The geothermal gradient - $^{\circ}$C/km (Limberger, et al., 2018)

The circulation depth is crucial in aiding the process of drilling a thermal spring.

4.4.4 Mineral saturation

Mineral saturation calculations are crucial in predicting which minerals might precipitate during the process of extracting or using the thermal waters (Ansari & Yarahmadi, 2017). To determine whether minerals in the Shu-Shu thermal springs tend to precipitate or dissolve during water-rock interactions, mineral saturation indices were estimated (Chatterjee, et al., 2017) using the GWB 11 software. In terms of an individual mineral or a group of minerals, the saturation index (SI) shows if a solution is in equilibrium with the solid phase or if it is undersaturated (dissolves) or supersaturated (precipitates) (Martínez-Florentino, et al., 2021). This equation is normally used to calculate saturation indices:

$$SI = log(\frac{IAP}{K}) \quad \textbf{(4.2)}$$

Where:

IAP- the ion activity product

K- solubility product of the minerals (Parkhurst and Appelo 1999).

4.5 Thermal Imaging with UAVs

This project used UAVs to determine the extent of the Shu-Shu thermal springs on the uThukela River. The following steps were taken:

4.5.1 Image Acquisition

The area of interest was the Shu-Shu thermal springs and the surrounding uThukela River. The images were acquired using a DJI Matrice 300 (M-300) UAV with a multispectral (blue, green, red) and Downwelling light sensor 2 (DLS-2). A thermal band was also used in this project. The production of highly accurate results most effectively depends on a high overlap between the images needed. A plan for image acquisition was designed to ensure enough overlap. The sensor was configured to capture images with a side and front overlap of 70 and 80% across the area of interest. The ground sampling distance was 100 m above the area of interest. The area was 0.18 km^2. The area was digitized on Google Earth and was saved as a Keyhole Markup Language (kml) file. The kml file was used to create a flight path to get the images of the entire area of interest. Since the GSD was 100 m, the images were captured at 0.07 m pixel resolution.

Figure 4.5: Picture of the DJI Matrice 300 UAV used to capture thermal images of the Shu-Shu springs and surrounding surface water

The highly developed UAV that was used in this project was equipped with excellent software that created an image acquisition plan based on a set of characteristics that were manually entered such as (GSD, the area of interest, and the percentage of overlap between the images). After all the parameters were uploaded on the UAV, the flight began, and the drone autonomously captured the thermal images of the thermal spring and surrounding surface waters by the chosen image acquisition strategy without the pilot intervening. The flight was arranged on the 26th of June 2024 between 10:30 am to 11 am.
The MicaSense Altum calibrated reflectance panel (CRP) was used to calibrate the instrument before and after each flight mission to account for variations in light intensity throughout the day. The Micasense Altum is a camera with 6 bands: Blue, green, red, red edge, near-infrared (NIR), and thermal infrared (LWIR).

4.5.2 UAV Image Processing

Following the image acquisition, the drone was connected to the computer through a USB cable, and images from the UAV were copied onto the computer while the drone was switched on. Pix4D fields software (version 1.8) was then used to pre-process and stitch the images together. Image alignment and georeferencing were performed to create an orthomosaic that showed the extent of Shu-Shu thermal springs. Dr. Shaeden Gokool handled the pre-processing of the UAV photos, which essentially entailed making atmospheric and radiometri c adjustments before mosaicking the corrected images to produce a single georeferenced ortho mosaic. The orthomosaic was saved in a GeoTIFF file format. To create a thermal map, the tiff images were used to generate the thermal reflectance map by creating an index to view absolute temperature. To convert the LWIR pixel values to °C, the formula:

$$Thermal_{ir} = \left(\frac{LWIR}{100}\right) - 273.15 \quad \textbf{(4.3)}$$

was used.

Where:

$Thermal_{ir}$: Surface temperature (°C)
LWIR: thermal infrared pixel value
The thermal map along with the orthomosaic were uploaded to Arc GIS for further analyses. For more details on how to process images using the software (Strecha, 2024)

CHAPTER 5: RESULTS AND DISCUSSION

5.1 Introduction

In this chapter, results obtained from the in-situ measurements, isotope, hydrochemistry, and geochemistry analyses are shown and discussed. Results obtained from the UAV are also shown and discussed.

5.2 In-situ measurements

In-situ parameters are shown in **Table 5.1** and a transect diagram showing the variation in the in-situ parameters is shown in **Figure 8.4** in **APPENDIX C**. The discharge temperatures of the Shu-Shu thermal springs range between 45°C and 50°C during the wet season and 40°C and 52°C during the dry season. Pool 7 has the highest temperature of all the concentrated thermal pools. The pH ranges from 7.2 to 7.8 during the dry season, while it fluctuates from 5 to 7.1 during the wet season and the EC ranges from 1368 to 1407 µS/cm in the dry season and measures just above 700 µS/cm in the wet season.

The surrounding surface waters have a temperature between 32-33°C in the wet season and 17-23°C in the dry season. The pH ranges from 8.1 to 8.5 during the dry season while it fluctuates from 3.8 to 7.1 during the wet season and the EC ranges from 256 to 321 µS/cm in the dry season and ranges from 155-175 µS/cm in the wet season. Compared to the surface water downstream of the thermal springs, the EC of the surface water upstream of the thermal springs is marginally lower. The same is true for pH and temperature.

The Shu-Shu thermal waters can be classified as 'Scalding' as the highest temperature is greater than 50°C (Kent, 1949). This supports work done by, Gevers (1942) and Kent (1942) that reported the surfacing temperature of the Shu-Shu thermal springs to be 52°C – 53°C and having a pH of 8.2, while a more recent investigation by Olivier et al. (2013) found the surfacing temperature to be 50°C.

The differences in the discharge temperature between the seven pools can be attributed to local conditions such as water flow velocity and characteristics of the underlying fractures (Grasby & Hutcheon, 2001). The temperature of the thermal springs indicates how deeply the water penetrates and how quickly it rises to the surface (Grasby & Hutcheon, 2001). The water

temperature of thermal springs varies seasonally. The differences in the discharge temperature of springs between wet and dry seasons are due to cooling caused by mixing between the deep thermal waters, shallow meteoric waters, and surface water from the uThukela River. This supports previous work by (Gravelet-Blondin, 2013) who stated that the Shu-Shu thermal water experience conductive cooling before emerging on the surface.

The high EC during the dry season can be attributed to water evaporation. The evaporation process during the dry season causes the concentration of ions to increase, increasing EC. This increased concentration of solutes can lead to changes in pH, making the water more acidic or alkaline, depending on the nature of the solutes (Ngabirano, et al., 2016). During the wet season, there is a dilution of the ions due to meteoric water increasing groundwater volumes, resulting in a decrease in electrical conductivity. These observations are consistent with the findings of Ngabirano et al. (2016), who reported similar seasonal variations in EC and water chemistry in thermal springs.

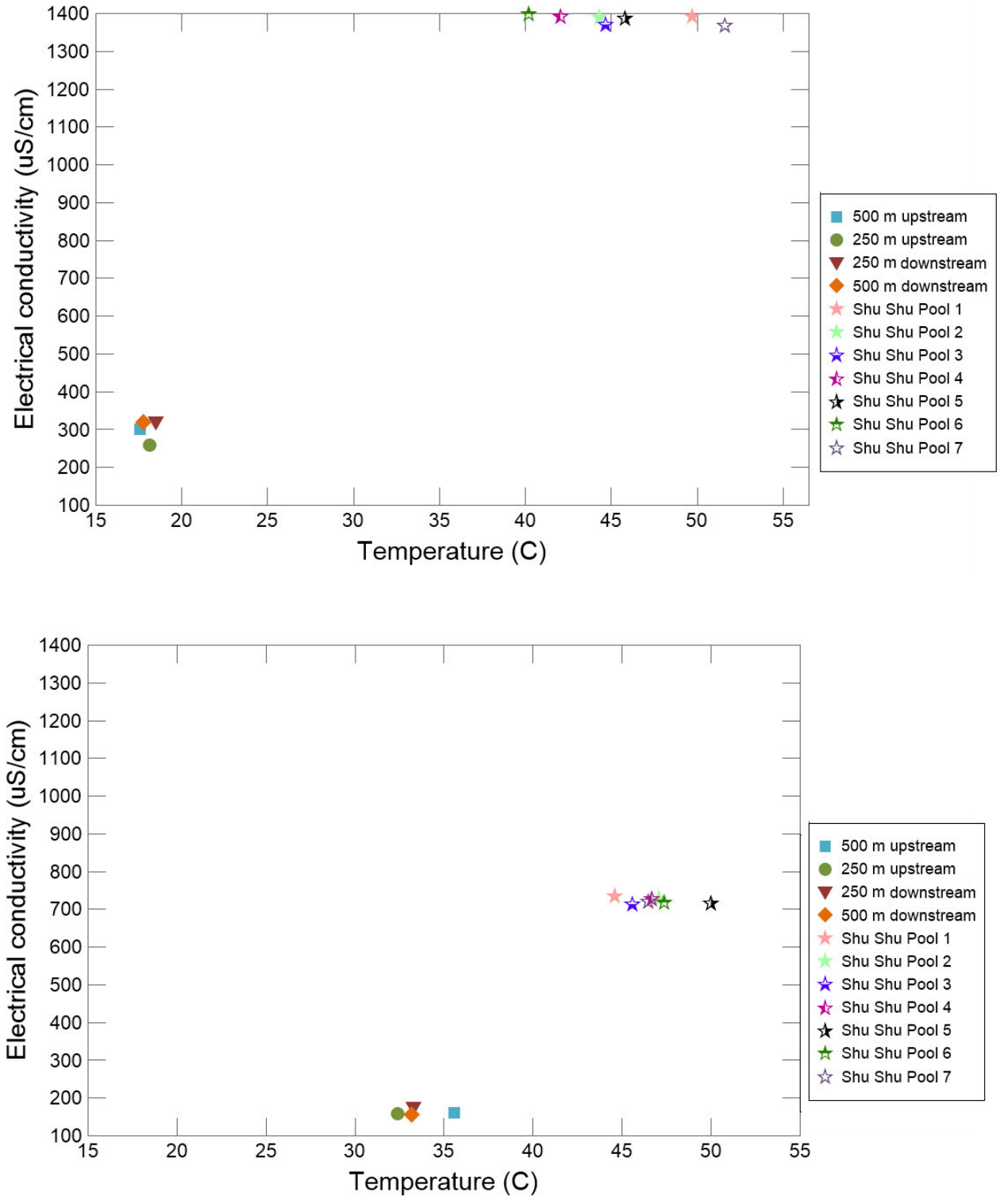

Figure 5.1: Temperature vs EC of the dry (up) and wet (down) season samples collected

Table 5.1: In-situ parameters measured from the Shu-Shu thermal springs and surrounding surface water during the wet and the dry seasons

Sampling Date	Parameter	500 m upstream	250 m upstream	Shu-Shu Pool 1	Shu-Shu Pool 2	Shu-Shu Pool 3	Shu-Shu Pool 4	Shu-Shu Pool 5	Shu-Shu Pool 6	Shu-Shu Pool 7	250 m downstream	500 m downstream
08-Dec-23	EC (µS/cm)	158	156	717	720	734	727	714	727	716	175	155
08-Dec-23	pH	3,76	7,02	6,93	6,64	6,52	6,12	6	5,95	5,15	6,13	7,1
08-Dec-23	Temp (°C)	32,6	32,40	47,4	46,5	44,6	47,1	45,6	46,7	50	33,3	33,2
07-May-24	EC (µS/cm)	202	203	344	450	1400	1395	1405	1403	1407	227	204
07-May-24	pH	6,36	6,56	6,52	6,52	6,71	6,61	6,72	6,74	6,57	7,07	6,77
07-May-24	Temp (°C)	21,4	22,1	24	25,7	44,2	44,9	41,4	42,4	51,6	23,3	22,7
26-Jun-24	EC (µS/cm)	299	256	1391	1389	1369	1392	1386	1399	1368	321	318
26-Jun-24	pH	8,50	8,12	8,15	8,1	7,41	7,28	7,69	7,86	7,59	7,66	7,5
26-Jun-24	Temp (°C)	17,59	18,15	49,75	44,32	44,7	42,06	45,82	40,23	51,62	18,51	17,8

5.3 Estimation of the Origin of the Shu-Shu thermal springs using stable isotopes

To track the origin of the thermal springs' water, $\delta^{18}O$ and $\delta^{2}H$ were analysed on water samples collected at the Shu-Shu thermal springs and surrounding surface water during the wet and dry seasons. Rainfall samples were collected from three different rainfall samplers located at Drakensberg Mountain (Mike Pass), Winterton, and Eshowe from March 2023 to July 2024. The rain samples were analysed to compare their isotopic makeup to that of the Shu-Shu thermal springs.

5.3.1 Wet season

$\delta^{18}O$ and $\delta^{2}H$ are tracers for determining some of the features of thermal springs, like the origin, the mixing with recently injected GW, and distinguishing between water-rock interaction mechanisms (Chatterjee et al., 2017). A comparison of the isotopic composition of Shu-Shu thermal springs to summer rain falling at the Highlands, Winterton, and Eshowe is shown in **Figure 5.2**. About the Shu-Shu thermal waters, the $\delta^{18}O$ values range from -3.97 to -3.13, and the $\delta^{2}H$ values range from -18 to -13.5, showing a lighter isotopic composition. The surrounding surface water near the springs' $\delta^{18}O$ values range from -1.85 to -0.37 and the $\delta^{2}H$ values range from -7.5 to 2.5, making them more enriched than the Shu-Shu thermal waters.

The difference between the Shu-Shu isotopic makeup and the surrounding SW can be attributed to the evaporation process. As evaporation occurs in SW, the water remaining behind becomes enriched in the heavier isotopes (Craig, et al., 1963; Leketa & Abiye, 2020; Diamond, 2022). Thermal springs are fed by GW, which is less exposed to direct evaporation and experiences processes like rock-water interactions (Craig, et al., 1963; Diamond, 2022; Li, et al., 2025). As the water equilibrates with the nearby rocks, this contact may cause the water's isotopic makeup to become diluted (Li, et al., 2025). GW isotopic composition is primarily influenced by the isotopic composition of the precipitation that recharges the aquifers (Salem, et al., 2022). GW can also be influenced by mixing with SW, but the overall effect is that GW tends to have a less enriched isotopic composition compared to SW (Leketa & Abiye, 2020; Salem, et al., 2022; Li, et al., 2025).

During the wet season, the Mike Pass rainfall samples $\delta^{18}O$ values range from -4.59 to -1.59 and the $\delta^{2}H$ values range from -20.9 to 11.1, showing a depletion in isotopic composition. The

Winterton rainfall samples' $\delta^{18}O$ values range from -2.77 to 0.61, and the $\delta^{2}H$ values range from -7.7 to 20.8, showing a more enriched isotopic composition. The Eshowe rainfall samples $\delta^{18}O$ values range from -3.85 to -0.69, and the $\delta^{2}H$ values range from -14.4 to 1.5, demonstrating a lighter isotopic composition than the Winterton rainfall samples.

The Shu-Shu isotopic composition displays a depletion in $\delta^{18}O$ and $\delta^{2}H$, which suggests that the spring waters' isotopic composition is more similar to the precipitation at Mike Pass. The Winterton rainfall samples are the most enriched in $\delta^{18}O$ and $\delta^{2}H$, which demonstrates the least similarities with the Shu-Shu thermal waters. The thermal springs waters showing a lighter isotopic make-up indicate that recharge occurs at higher altitudes, which means that the Shu-Shu Spring waters are recharged from the Highlands. Several reasons could be responsible for low $\delta^{18}O$ and $\delta^{2}H$: for example, the isotope effects such as the temperature effect, continental effect (Dansgaard, 1964), altitude impact, and amount effect.

The isotopic composition of precipitation gets lighter with lowering temperature, increasing latitude, increasing distance from the coast, increasing height, or increasing amount of rain during a precipitation event (Diamond & Harris, 2000; Diamond, 2022). Stable isotopes can be employed as tracers since the altitude effect causes significant composition differences. This is frequently used to mark the places where GW recharge occurs at lower-elevation thermal springs. (Blarasin et al., 2020; Diamond and Harris, 2019; Jasecko, 2019).

The Mike Pass rainfall station is located at Drakensberg Mountain at a higher altitude. Rain falling at higher elevations has less distance to travel to the ground and less chance for evaporative enrichment, in which the lighter isotopes preferentially evaporate, leading to a depletion of the isotopes (Diamond & Harris, 2000; Diamond, 2022). This implies that because thermal springs draw their water from meteoric sources, they are expected to be situated in places with moderate to high rainfall (Olivier & Jonker, 2013). However, the catchment area is not required to be physically near the thermal spring, but the catchment area needs to be higher in elevation than the spring itself (Hoffmann, 1979). Thus, it should not come as a surprise that the Shu-Shu thermal springs are situated in a low-lying region (Kent, 1952) but are recharged from the Highlands.

The isotopic composition of the rainfall samples cannot be attributed to the continental effect. The continental effect causes a decrease in stable isotope values of precipitation with increasing distance from the coast (Diamond, 2022). The results, however, show that the Winterton rainfall

samples are more enriched than the rainfall samples collected at Eshowe, but Winterton is further and further inland. The continental effect does operate at smaller, regional scales, although it is best observed at continental scales (Jasechko, 2019; Laonamsai, et al., 2021; Diamond, 2022). The isotopic composition of these rainfall samples may be due to the amount effect. Eshowe might have experienced heavier precipitation than Winterton, hence the lighter isotopic composition (Diamond, 2022).

The positive ^{18}O shift in the Shu-Shu thermal spring waters suggests that there was a rock-water interaction whereby the thermal spring waters exchange oxygen with silicate rocks before emerging to the surface (Craig, et al., 1963; Giggenbach, 1992; Diamond, 2022). The shift in ^{18}O is not great when compared to other thermal waters across the world (Diamond, 2022). That is because the rock-water interaction likely occurred over many years, causing the system to be close to the equilibrium fractionation value with the meteoric water and since the system is already at the equilibrium, there is little chance of further exchange causing further exchange to be minor (Diamond, 2022).

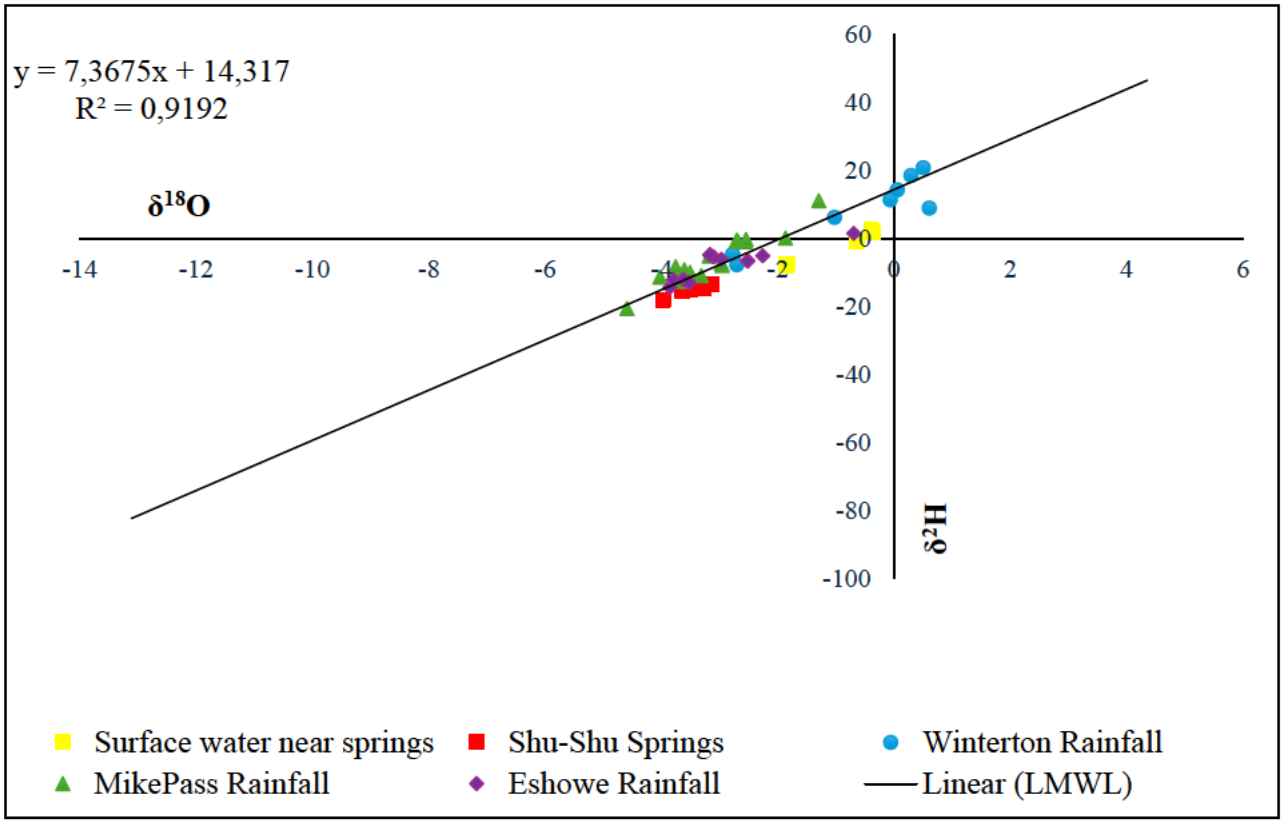

Figure 5.2: Comparison of the isotopic composition of Shu-Shu thermal springs to summer rain falling at high, intermediate, and low altitude

5.3.2 Dry season

Figure 5.3 compares the isotopic makeup of the Shu-Shu thermal springs to the rainfall samples collected from Mike Pass, Winterton, and Eshowe during the dry season in May and late June. The Local Meteoric Water Line derived from Pietermaritzburg rainfall is also shown in the Figure below. About the Shu-Shu thermal waters, in May, the $\delta^{18}O$ values range from -4.05 to -2.38, and the $\delta^{2}H$ values range from -15.6 to -7.3. In Late June, the $\delta^{18}O$ values range from -4.25 to -3.94, and the $\delta^{2}H$ values range from -16.9 to -15.5. The surrounding surface water near the springs' $\delta^{18}O$ values range from -4.5 to -2.2, and the $\delta^{2}H$ values range from -6.9 to -3.8 in early May. In late June, the $\delta^{18}O$ values range from -4.5 to -1.54, and the $\delta^{2}H$ values range from -4.5 to -2.7.

During the dry season, the Mike Pass rainfall samples $\delta^{18}O$ values range from -6.63 to -1.53 and the $\delta^{2}H$ values range from -26.4 to 8.2, showing a depletion in isotopic composition. The Eshowe rainfall samples $\delta^{18}O$ values range from -3.39 to -1.58, and the $\delta^{2}H$ values range from -3.8 to 2. The Winterton rainfall samples $\delta^{18}O$ values range from -4.31 to 0.68 and the $\delta^{2}H$ values range from -15.3 to 13.5, demonstrating a lighter isotopic composition than the Eshowe rainfall samples. Few rainfall samples from Winterton are depleted in stable isotopes than the rainfall samples from Eshowe, and that can be attributed to the continental effect (Diamond, 2022). The Shu-Shu samples still have a similar isotopic composition to the Mike Pass rainfall samples, proving that the Shu-Shu springs are recharged from the Highland. This supports the conclusion reached by Gravelet-Blondin in 2013.

According to the isotopic values, the likelihood of the oceanic origin of these thermal waters can be ruled out because $\delta^{18}O$ and $\delta^{2}H$ were not closer to 0 (Craig, 1961). There is also no presence of any significant amount of magnetic/volcanic water, which generally has $\delta^{18}O$ values ranging from +6 to +9, and the $\delta^{2}H$ values range from 40 to 80 (Giggenbach, 1992), thus proving again that the Shu-Shu thermal waters are meteoric in origin. This supports the research that has been done on the Shu-Shu thermal springs and all thermal springs in South Africa (Rindl, 1916; Kent, 1949; Ashton & Schoeman, 1986; Gevers, 1942; Kent, 1968; Hoole, 2001; Olivier, et al., 2008; Olivier, et al., 2011; Olivier & Jonker, 2013; Gravelet-Blondin, 2013).

It was observed that the isotopic composition of the Shu-Shu thermal springs was more depleted during the dry season than during the wet season. During the wet season, increased rainfall dilutes the water in the thermal springs, leading to a lower overall isotopic signature (Petersen,

et al., 2023; Letshele, et al., 2023; Li, et al., 2025). Conversely, during the dry season, evaporation concentrates the heavier isotopes in the remaining water, resulting in a higher isotopic signature (Petersen, et al., 2023; Letshele, et al., 2023; Li, et al., 2025). This is because the lighter isotopes evaporate more readily, leaving behind a larger fraction of the heavier isotopes (Diamond, 2022; Petersen, et al., 2023; Letshele, et al., 2023). Evaporation plays a key role in isotopic fractionation, as the lighter isotopes evaporate more readily than the heavier isotopes (Diamond, 2022; Letshele, et al., 2023).

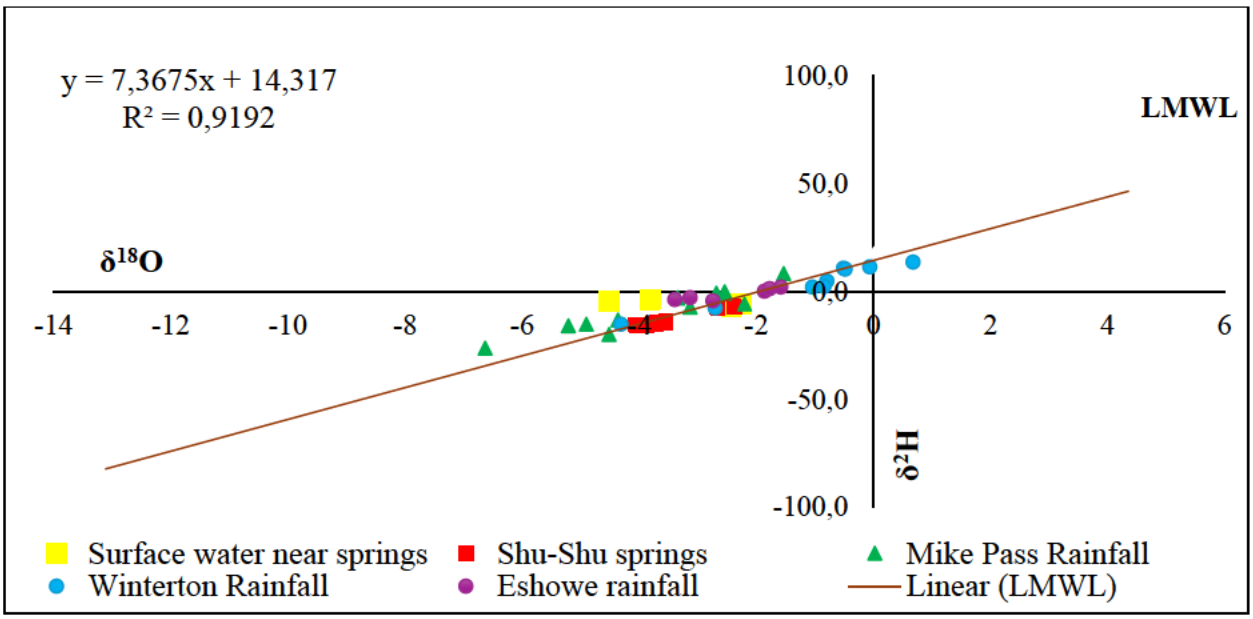

(a)

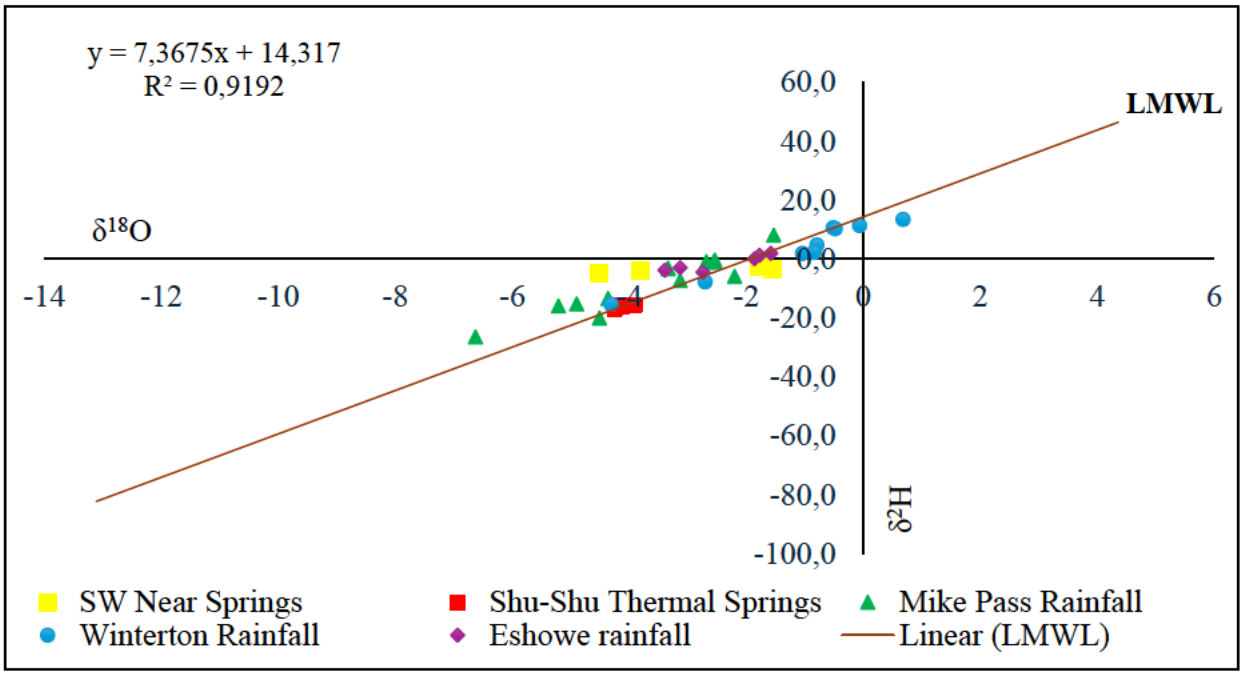

(b)

Figure 5.3: Comparison of the isotopic composition of Shu-Shu thermal springs to dry season rain falling at the Highlands, Winterton, and Eshowe. May 2024 (a) Late June 2024 (b)

5.4 Chemistry Analysis

A chemistry analysis of the Shu-Shu thermal springs and the surrounding surface water was performed. The chemical composition of thermal springs can be used to determine the types of waters present, the water quality of the stream, estimate the subsurface water temperature using geothermometry equations, and calculate the depth of circulation.

5.4.1 Hydrochemistry characterisation

The results from the hydrochemical analysis of major ions (Ca^{2+}, Mg^{2+}, Na^{+}, HCO_3^{-}, SO_4^{2-}, and Cl^{-}) are presented in **Table 5.2**. The results suggested that the Shu-Shu springs are mostly enriched with SO_4^{2-}, Na^{+} Cl^{-}, and Ca^{2+} (**Table 5.2**) in that order. These findings align with the findings by Gevers (1942) who reported that the anions Cl^{-} and SO_4^{2-} and the cations Na^{+} and Ca^{+} were the main constituents of the Shu-Shu thermal spring waters. The results further show the overall characteristics of the spring waters; the strong acids (Cl^{-} and SO_4^{2-}) are more dominant than the weak acids (HCO_3^{-}) while the alkaline (Na^{+}) is more dominant than the alkaline Earth elements (Ca^{2+} and Mg^{2+}).

The leaching of amphibolites and gneiss is responsible for most of the dissolved constituents in the Shu-Shu thermal springs, specifically plagioclase, hornblende, and biotite (Gravelet-Blondin, 2013; Gevers, 1942). The primary source of Na is albite (Na-plagioclase) which is prone to dissolving in near-neutral waters (Huang and Kiang, 1972). The relatively lower Ca levels are because anorthite (Ca-plagioclase) dissolves more quickly in acidic environments and the Shu-Shu thermal waters are usually basic (Huang and Kiang, 1972). In addition, removing Ca from GW through adsorption and/or cation exchange onto the surface of clay minerals may be responsible for this difference in Na and Ca amounts (Chae et al., 2006).

SO_4 concentrations were the highest among the ions analysed, and that was attributed to the dissolution of pyrite, which is common in the gneisses and amphibolites dominating the area (Gevers, 1942; Gravelet-Blondin, 2013). Small amounts of H_2S and CO_2 gas bubble up via the thermal waters' fault zone (Gevers, 1942), which was apparent from the gas bubbles visible on the thermal pools along with the smell. When pyrite is dispersed under reducing conditions, H_2S (and perhaps some SO_4) is formed (Gevers, 1942). This is then oxidized at shallow depths, which ultimately permits the high concentrations of SO_4 (Gevers, 1942) in the Shu-Shu thermal waters.

Table 5.2: Hydrochemical results of the Shu-Shu thermal springs and surrounding surface water

Sampling Site	Ca^{2+} (mg/L)	Mg^{2+} (mg/L)	Na^{+} (mg/L)	K^{+} (mg/L)	HCO_3^{-} (mg/L)	CO_3^{-} (mg/L)	Cl^{-} (mg/L)	SO_4^{2-} (mg/L)	Si (mg/L)	SiO2 (mg/L)	TDS (mg/L)
500 m upstream	22,1	13,1	23,3	5	30,51	0	16,3	18,8	5,37	11,49	129
250 m upstream	22	13	23,8	5	30,51	0	16,1	18,7	5,37	11,49	129
Shu-Shu Pool 1	72,8	5	239	7,85	15,25	0	150	400	26	55,62	890
Shu-Shu Pool 2	73,6	5	237	7,89	15,25	0	150	398	26	55,62	887
Shu-Shu Pool 3	72,9	5	243	7,86	15,25	0	155	411	13	27,81	910
Shu-Shu Pool 4	74,1	5	243	8,08	15,25	0	159	417	27	57,76	921
Shu-Shu Pool 5	74,5	5	225	8,28	15,25	0	161	420	25,9	55,41	909
Shu-Shu Pool 6	74,3	5	239	8,04	15,25	0	154	412	26,7	57,12	908
Shu-Shu Pool 7	73,3	5	252	7,92	15,25	0	155	408	25,3	54,12	916
250 m downstream	23	12,9	27,2	5	30,15	0	19,1	26	5,56	11,89	143
500 m downstream	22,8	13	27,2	5	30,15	0	19,2	26	5,4	11,55	143

To assess the different types of water and to understand the geochemical evolution of GW discharged at the Shu-Shu thermal springs, the milli-equivalent percentage (meq %) of key cations and anions is plotted in **Figure 5.4** and then projected into the central diamond field (Ravikumar, et al., 2015). The Piper (1944) diagram plotted using the Geochemist's Workbench version 11.0.7 (GWB 11) software shows that the hydrochemical results of the Shu-Shu thermal springs are confined to only one type: the sodium chloride (Na-Cl) type, indicating the dominance of NaCl. Numerous authors (Gevers, 1942; Kent, 1949; Olivier & Jonker, 2013) had the same conclusion.

Many thermal springs with meteoric origins are known to include NaCl (Gevers, 1942). The detected Cl levels could be partially explained by the dissolution of secondary alteration minerals like hornblende along rock fissures (Gevers, 1942). Regarding the dominant major ions in the surrounding SW, the Piper diagram demonstrated that the surrounding surface waters are confined to similar water types: mixed water type, indicating the dominance of HCO3-Na-Ca-SO4 water type. The differences in the surface water type and thermal water type indicates that the thermal springs have very little impact on the water quality of the uThukela River

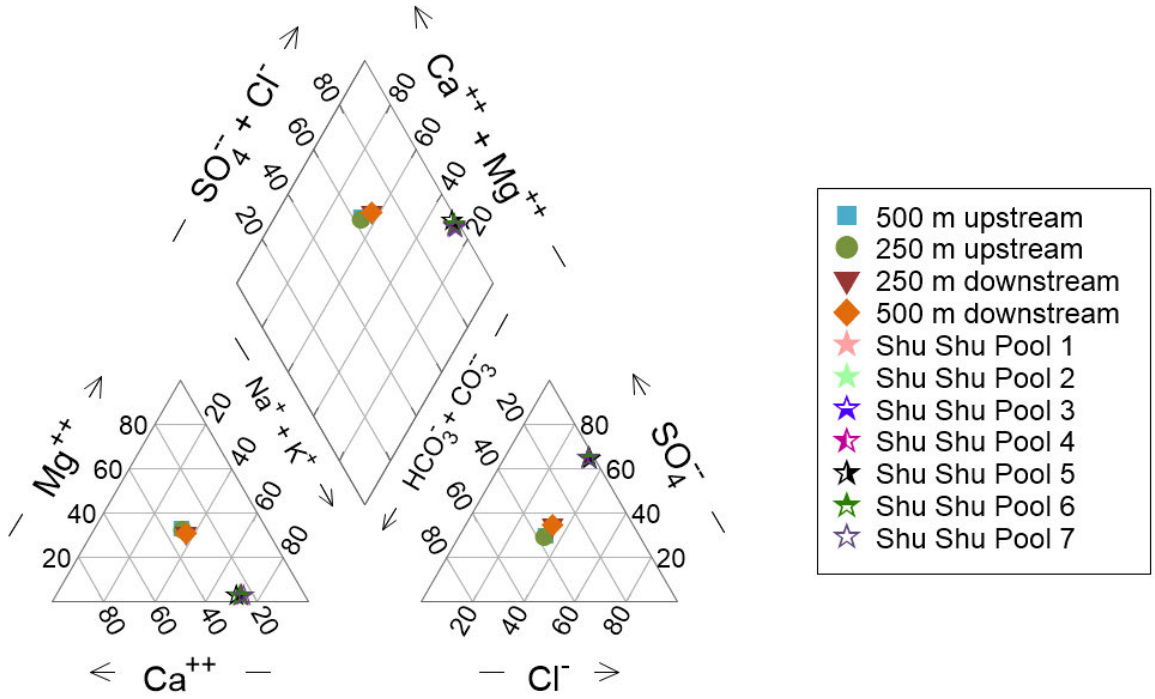

Figure 5.4: Piper diagram showing hydrochemistry results of the Shu-Shu thermal springs and surrounding surface water.

The geochemical processes leading to the Na-Cl water type are further explained using the Durov diagram to increase the reliability of the results from the Piper diagram. The results from the Piper diagram are confirmed by the Durov diagram (**Figure 5.5**). The NaCl-dominant thermal spring waters are caused by the dissolution of NaCl-dominated rocks (Gevers, 1942). A few thermal springs in Limpopo (Sagole, Tshipise, and Mphephu) are of a similar type, and the NaCl was linked to the underlying geology originating from gneissic rocks (Durowoju, et al., 2019). NaCl water types are typical of marine and deep groundwaters, which are influenced by the dissolution of halite/rock salt (Durowoju, et al., 2019). Despite having multiple pools, the Shu-Shu thermal springs have a uniform water type. Gevers (1942) and Kent (1949) claimed that most of the components dissolved in the Shu-Shu thermal springs originate from the dissolution of different minerals in the gneisses and amphibolite that the hot waters flow through to the surface.

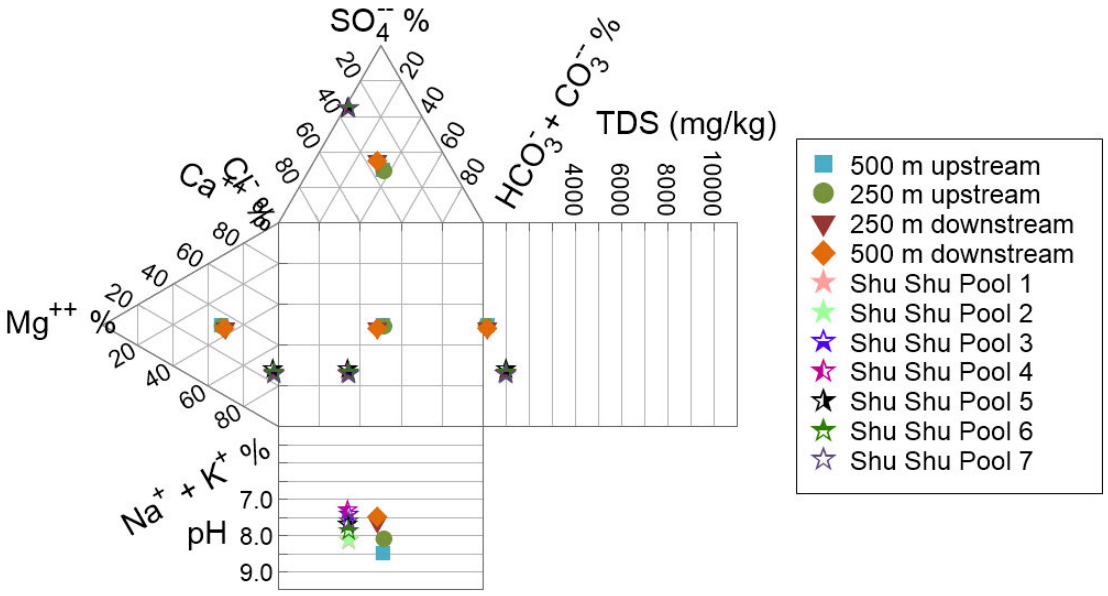

Figure 5.5: Durov diagram showing hydrochemistry results of the Shu-Shu thermal springs and surrounding surface water.

The Gibbs plot **(Figure 5.6)** offers crucial information on the mechanisms governing the chemistry of GW systems (Marandia & Shand, 2018). Gibbs diagrams were created using the corresponding ratios of Cl/ (Cl+ HCO_3) and Na/(Na+Ca) vs TDS. The Gibbs diagram is frequently used to identify hydrogeochemical evolution, which includes precipitation, rock weathering, and evaporation–crystallization processes (Marandia & Shand, 2018).

All the Shu-Shu water samples and surrounding surface-water samples lie in the rock-weathering process dominance area. Several chemical interactions occur with the rocks when GW moves from recharge to discharge zones (Ashton & Schoeman, 1986). The temporal and spatial variations of these chemical reactions depend on geological formations, residency time, and the chemical makeup of the original waters (Durowoju, et al., 2019). The Gibbs diagram indicates that the main hydrochemical process is water-rock interaction. This supports the conclusion reached by (Gevers, 1942; Huang & Kiang, 1972; Olivier & Jonker, 2013; Gravelet-Blondin, 2013) which stated that the water-rock interaction processes brought on by the chemical weathering of the rock-forming minerals primarily regulate the chemistry of the Shu-Shu thermal springs,

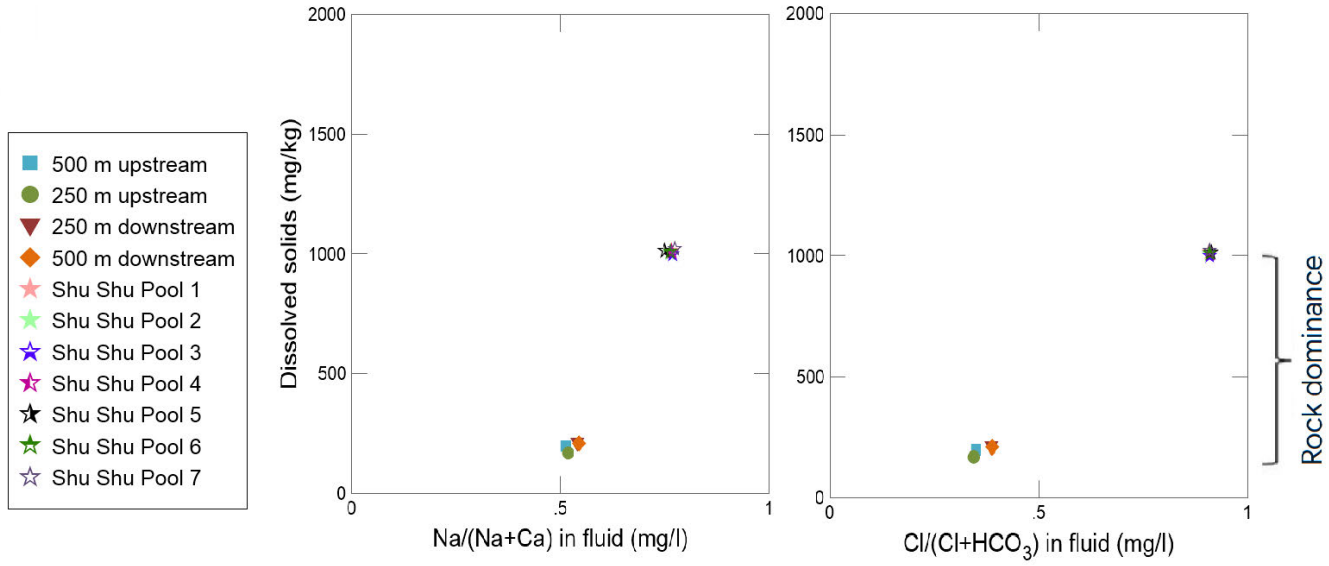

Figure 5.6: Gibbs diagram showing the mechanisms controlling the chemistry of the Shu-Shu thermal springs

Plotting (Ca+Mg) against (HCO_3+SO_4) is another method for identifying geochemical processes (Datta & Tyagi, 1996; Lakshmanan, et al., 2003). By differentiating between carbonate and silicate weathering controlling factors, it illustrates the distribution of thermal water between silicate and carbonate weathering processes. The distribution of the water samples plots below the 1:1 line which indicates that they are in the silicate weathering field. Additionally, it is important to consider the influence of anthropogenic activities on the geochemical signatures, as urbanization and agricultural practices can significantly alter the natural processes (Smith et al., 2010; Johnson & Lee, 2015). These factors can lead to variations in the concentrations of major ions, further complicating the interpretation of geochemical data. Furthermore, the role of climate change in altering precipitation patterns and temperature can also impact the geochemical processes, as noted by Chen et al. (2018), who found that shifts in climate can exacerbate the effects of human activities on water chemistry. Understanding these interactions is crucial for accurate assessments of water quality and resource management (Mason et al., 2021).

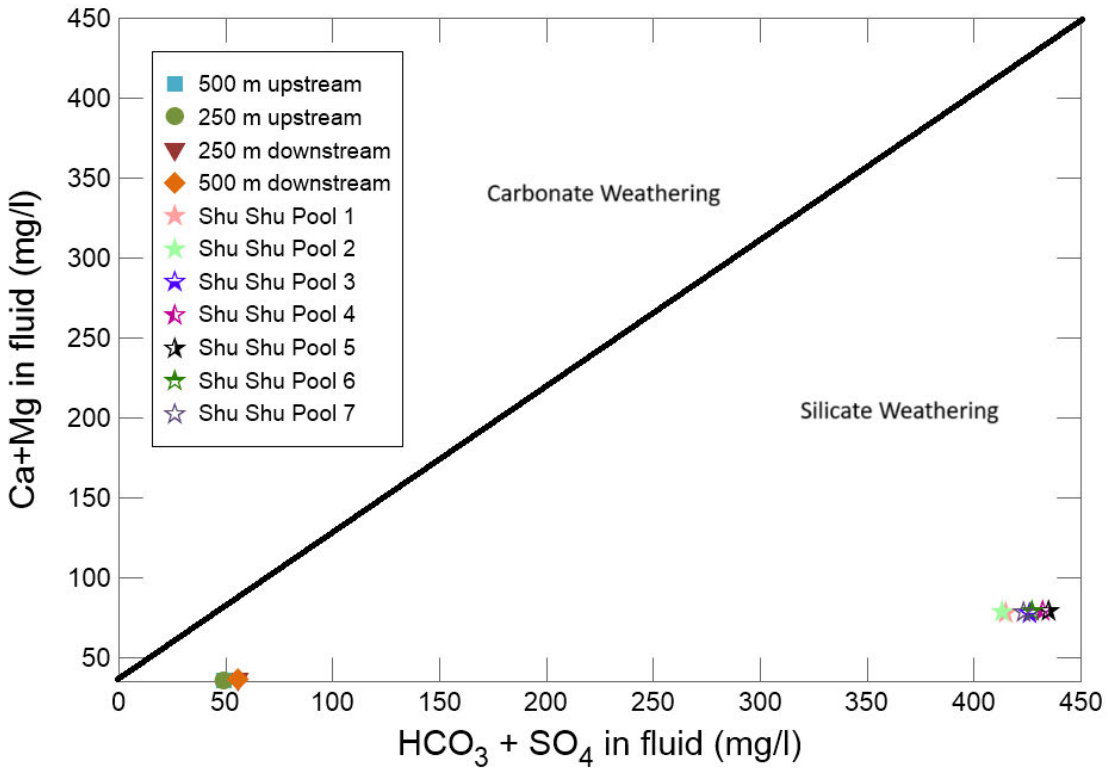

Figure 5.7: Plot of (Ca+Mg) vs (HCO_3+SO_4) for the Shu-Shu thermal springs and surrounding surface water

The concentration of Na–Cl in thermal springs is influenced by various geological and hydrological factors. The Shu-Shu thermal springs are created when GW is heated by the Earth's geothermal energy and rises to the surface. As the water moves through silicate weathering rocks, it absorbs minerals and salts, which contribute to its chemical makeup. Sodium and chloride are among the most prevalent elements in the Shu-Shu thermal springs, as well as in many other thermal springs. Their presence is associated with the interaction between rocks and water, as well as the dissolution of sodium chloride-containing rocks, such as halite or rock salt. The heated water dissolves these minerals and transports them to the surface. Various diagrams illustrating the relationship between several hydrochemical indices and chloride are presented in **Figure 8.5** in **APPENDIX C**, further demonstrating the interaction between rocks and water and the process of ion exchange.

5.4.2 Estimation of subsurface temperatures using Geothermometry

Solute geothermometers determine a thermal system's temperature by measuring changes in element concentrations in thermal springs as a function of temperature (Asnin, et al., 2022). Full equilibration and no-mixing are two assumptions that geothermometers are predicated on, and these assumptions don't always hold (Fournier, 1977; Nicholson, 1993). The Silica and ratio-based geothermometers were used to estimate the subsurface reservoir temperatures of the Shu-Shu thermal springs.

5.4.2.1 The Silica-cation geothermometer

The silica geothermometer uses the solubility of siliceous minerals (quartz, chalcedony, and amorphous silica), which is regulated by temperature and pressure, to determine the value of the last equilibrium temperature (Karingithi, 2009; Martínez-Florentino, et al., 2021). The basic reaction for silica dissolution is:

$SiO_2(qtz) + 2H_2O = H_4SiO_4$ **(5.1)**

The estimated reservoir temperatures using the Silica geothermometer equations (cf **Table 2.3**) are shown in **Table 5.3**.

Table 5.3: Estimated reservoir temperatures using the Silica geothermometer equations

Sample Name	Amorphous Silica	Chalcedony conductive	Quartz conductive	Quartz adiabatic
Shu-Shu Pool 1	-10	77	107	107
Shu-Shu Pool 2	-10	77	107	107
Shu-Shu Pool 3	-35	45	77	80
Shu-Shu Pool 4	-8	79	109	108
Shu-Shu Pool 5	-10	77	107	107
Shu-Shu Pool 6	-9	79	108	108
Shu-Shu Pool 7	-11	76	106	106

The relationship between Log (K^2/Mg) and the SiO_2 geothermometer is illustrated in **Figure 5.8**. Pool 3 of the Shu-Shu thermal springs, whose geothermometer readings fall between 76 and 80°C exhibits a quartz equilibrium. The rest of the pools show an equilibrium with chalcedony minerals. All the pools except Pool 3 present an equilibrium with chalcedony, making it possible to estimate a temperature between 76 and 79°C using the Chalcedony geothermometers.

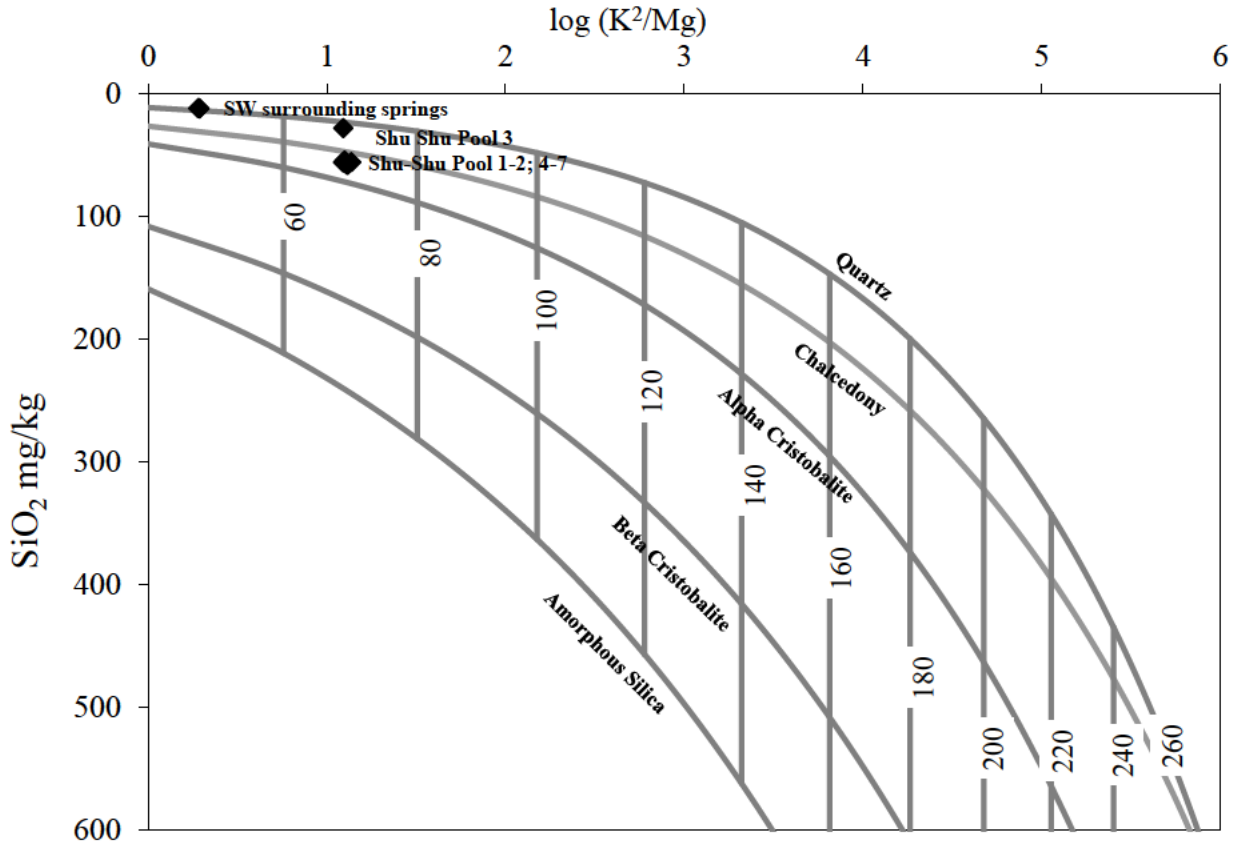

Figure 5.8: SiO_2 vs Log ($(K^+)^2/(Mg^{2+})$) geoindicator diagram (Giggenbach and Goguel, 1989) for the Shu-Shu thermal water samples.

5.4.2.2 The cation ratio-based geothermometer

The estimated reservoir temperature calculated using the cation ratio-based geothermometers (Na-K, K-Mg, Ca-Mg, Na-K-Ca, Na-K-Ca Mg-corrected) are shown in the table below. These geothermometers are less affected by secondary processes such as dilution as compared to the Silica geothermometers with a single component (Martínez-Florentino, et al., 2021).

Table 5.4: Reservoir Temperatures estimated using the cation ratio-based geothermometer equations (°C)

Sample Name	Na/K (Fournier, 1979)	Na/K (Truesdell, 1976)	Na/K (Giggenbach, 1988)	Na/K (Tonani, 1980)	Na/K (Nieva & Nieva, 1987)	Na/K (Tonani, 1980)	K/Mg (Giggenbach, 1988)	Na-K-Ca (Fournier & Truesdell, 1973)	Na-K-Ca Mg corrected
Shu-Shu Pool 1	137	92	157	117	126	104	70	72	72
Shu-Shu Pool 2	138	93	158	118	126	104	70	72	72
Shu-Shu Pool 3	136	91	156	116	125	103	70	72	72
Shu-Shu Pool 4	138	93	157	118	126	104	70	73	73
Shu-Shu Pool 5	144	100	163	126	132	111	71	73	73
Shu-Shu Pool 6	139	94	158	119	127	105	70	72	72
Shu-Shu Pool 7	134	89	154	114	123	101	70	73	73

The ratio-based geothermometers cannot be used if the samples are not in equilibrium as re-equilibrium could result by combining thermal and freshly infiltrated water (Martínez-Florentino, et al., 2021). The ratio-based geothermometers consider cationic exchange processes (where feldspar and clay are present) if an equilibrium is maintained (Martínez-Florentino, et al., 2021). To evaluate the thermal water samples' degree of equilibration, the Na/K and K^2/Mg geothermometers can also be used along with the Na-K-Mg (Giggenbach, 1988) diagram (Martínez-Florentino, et al., 2021).

Triangular diagrams are presented as effective resources for understanding geothermal geochemistry (Chenaker, et al., 2018). The Na–K–Mg ternary diagram (Giggenbach, 1988) is used to identify the various types of water that originate in deep reservoirs and assess the equilibrium status between water and minerals such as feldspars and clay (Chenaker, et al., 2018). In the ternary diagram (Wen, et al., 2012), waters can be classified into three groups: fully equilibrated, partially equilibrated, and immature (Chenaker, et al., 2018). For a cation ratio-based geothermometer to be used, the water must be equilibrated or partially equilibrated (Chenaker, et al., 2018). As shown in **Figure 5.9**, all samples plot far from the total equilibrium line meaning that the application of these cation ratio-based geothermometers is not feasible (Chenaker, et al., 2018). All the thermal water samples are in the field of immature water suggesting none of these waters have attained full equilibrium with their associated host rocks (Giggenbach, 1988). This indicates that conductive cooling or the mixing of warmer waters with colder ones may be the primary processes responsible for the reduction in temperature of the Shu-Shu thermal waters (Giggenbach, 1988).

The 10K/(10K-Na) vs 10Mg/(10Mg+Ca) plot in **Figure 8.6** in **APPENDIX C** reaches the same conclusion. All samples plot above the equilibrium line, which shows that the Na and K concentrations are not controlled by the temperature-dependent equilibrium of alkali feldspars (Giggenbach, 1988). This lack of attainment of equilibrium is further demonstrated by the overestimation of subsurface temperature attained from using various Na–K geothermometers. Conversely, the temperatures derived from the Na–K–Ca geothermometer, the Mg-corrected Na–K–Ca, and the K–Mg geothermometer are deemed unreliable, as they tend to slightly underestimate the subsurface temperature of the springs, and the magnesium levels in the Shu-Shu are low (**Table 5.2**). Based on the discussion above, it can be concluded that silica geothermometers (quartz-conductive and chalcedony-conductive) provide more reliable reservoir temperatures compared to the cationic ratio-based geothermometers.

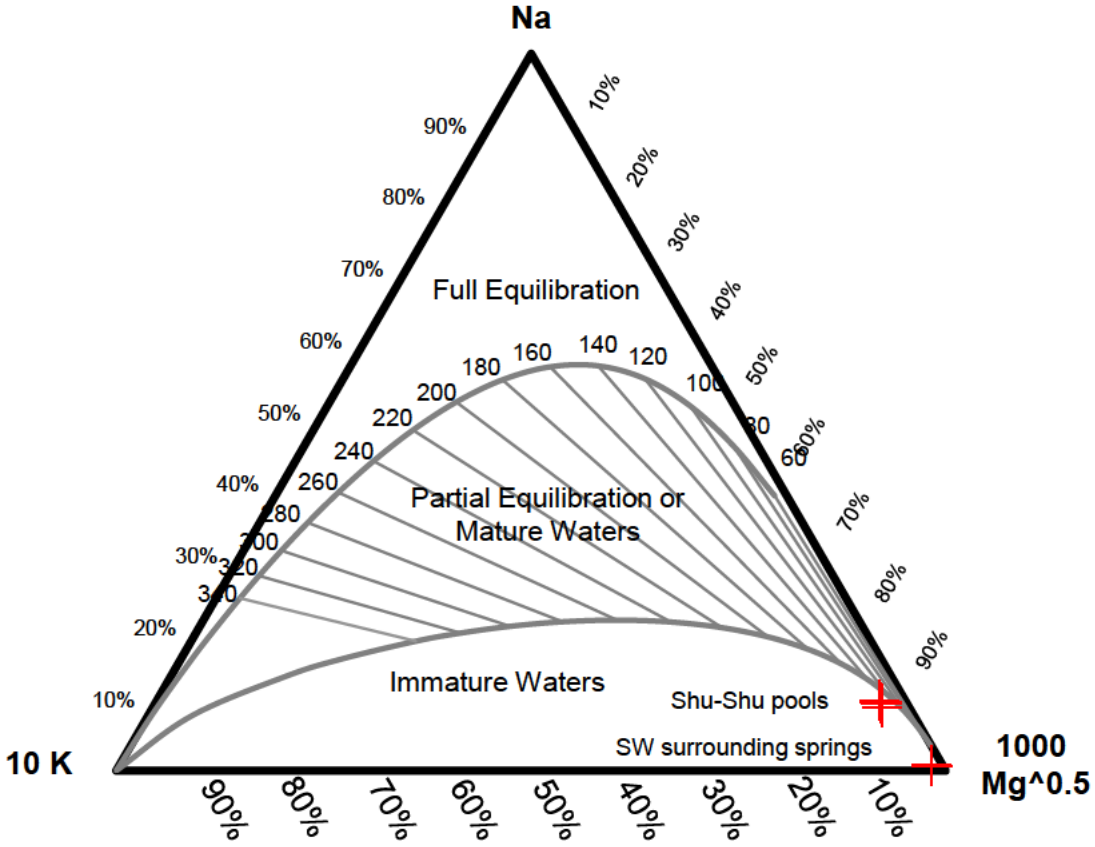

Figure 5.9: K-Mg-Na geoindicator diagram (Giggenbach, 1988) for thermal water and surrounding SW samples. Ion concentration data reported in mg/L

Based on estimated subsurface temperatures (<100 °C), the Shu-Shu thermal springs can be classified as having a low-enthalpy energy potential. The Shu-Shu thermal springs are not suitable for producing electricity as the subsurface temperature is less than 170 °C (Narsilio, et al., 2014). However, the springs are suitable for only direct use applications, for example, heating applications like greenhouses, homes, and fisheries. Additionally, it is important to note that low-enthalpy geothermal resources can also be utilised for aquaculture, which can enhance fish growth rates and improve sustainability in fisheries (Lund et al., 2010). Furthermore, the integration of these thermal springs into district heating systems could provide a more efficient energy solution for local communities (Lund & Freeston, 2010).

5.4.3 Estimation of the depth of circulation

The depth at which GW needs to circulate for reheating differs by region, depending on the geothermal gradient. This gradient is influenced by factors such as the age and thickness of the Earth's crust, as well as the level of volcanic activity nearby (Diamond, 2022). Generally, there is a notable difference between the relatively low geothermal gradients of about 10 to 30 °C/km found in tectonically stable areas and the much higher geothermal gradients present in volcanically active regions, where boiling water and steam can occur just tens to hundreds of meters below the surface (Diamond, 2022).

Equation 4.1 was used to estimate the circulation depth of the Shu-Shu thermal springs. The estimated circulation depths of the thermal springs are shown in **Table 5.5** below. The estimated subsurface temperatures that were applied to the equation are those that showed equilibration according to the Giggenbach and Goguel (1989) diagram, which are the quartz (conductive) and chalcedony (Conductive) geothermometers. The local annual average temperature used was 17.5 °C (Spark, 2024)

Silica geothermometers including the quartz, the chalcedony, and the cation ratio-based geothermometers, are commonly used to estimate reservoir temperature (Giggenbach, 1988; Fournier & Truesdell, 1973; Fournier & Potter, 1979; Tonani, 1980; Fouillac & Michard, 1981; Fournier & Potter, 1982; Arnorsson, 1983; Chiodini, et al., 1995). The various chemical geothermometers consistently provide dissimilar reservoir temperatures due to intricate geological conditions (Li, et al., 2021). The Shu-Shu thermal water samples did not reach partial or full equilibrium in this study, indicating that the cation ratio-based geothermometers were unsuitable for estimating the reservoir temperature (Fouillac & Michard, 1981; Fournier & Potter, 1982; Arnorsson, 1983; Chiodini, et al., 1995). In addition to that, the water temperatures were low, and no steam loss was observed. This is why the quartz (conductive) and chalcedony (conductive) geothermometers; with no steam loss were used to estimate the depth of circulation (Tonani, 1980; Zheng & Guo, 1996; Li, et al., 2021)

The calculated circulation depth is estimated to range from 1.83 km to 1.95 km. A positive correlation exists between the circulation depth and the thermal springs' reservoir temperature. There is a significant temperature differential between the thermal springs and reservoir waters, as the deeper a spring's circulation, the longer its circulation path may be, and the larger the opportunity and proportion of the cold-water mixture. As previously mentioned, the Shu-Shu

springs have a low energy potential. In thermal springs with high geothermal potential, circulation depths can range from approximately 2 to 5 km, or even deeper, depending on the geothermal gradient and heat flow (Dhansay, et al., 2017). The Shu-Shu springs don't meet the criterion; hence, they are classified as having low-enthalpy energy potential.

Table 5.5: The depth of circulation estimated using Equation (5.2) and reservoir temperatures estimated using the Quartz (conductive) and Chalcedony (conductive) geothermometers

Sample Name	Discharge Temperature (°C)	SiO2 (mg/L)	Reservoir Temperature (°C)	Circulation Depth (km)
Shu-Shu Pool 1	49,75	55,62	77	1,86
Shu-Shu Pool 2	44,32	55,62	77	1,86
Shu-Shu Pool 3	44,7	27,81	77	1,95
Shu-Shu Pool 4	42,06	57,76	79	1,92
Shu-Shu Pool 5	45,82	55,41	77	1,86
Shu-Shu Pool 6	40,23	57,12	79	1,92
Shu-Shu Pool 7	51,62	54,12	76	1,83

5.4.4 Mineral Saturation of the Shu-Shu springs

To determine which minerals tend to precipitate or dissolve during water-rock interactions, mineral saturation indices were estimated (Chatterjee, et al., 2017). The results of the calculated saturation indices (SI) of minerals for the Shu-Shu thermal springs water samples at the measured discharge temperature are shown in **Figure 5.10** below. The water is undersaturated with respect to that specific mineral if the SI is less than zero and oversaturated with respect to that individual mineral phase if the SI is greater than zero. A SI equal to zero means that thermal equilibrium exists with the solid phase of the specific mineral (Diamond, 2022).

The mineral saturation calculations performed using the GWB software indicate that all the thermal waters are supersaturated with respect to quartz, tridymite, chalcedony, and cristobalite (**Figure 5.10**) and undersaturated with respect to amorphous silica, anhydrite, gypsum, bassanite, and halite, among others (cf **Table 8.4** in **APPENDIX C**). This geochemical behaviour closely resembles that of the El Tatio geothermal field in northern Chile, where thermal waters also exhibit oversaturation of quartz, tridymite, cristobalite, and chalcedony. The similarity suggests that the Shu-Shu Springs, although meteoric in origin, undergo physicochemical processes comparable to those in high-enthalpy volcanic systems. Similarly, the Tuzla geothermal site in Turkey also exhibits oversaturation of both quartz and chalcedony (Tonkul et al., 2025).

The silicate mineral gets easily dissolved in deep geothermal reservoirs due to high temperatures (Guo, et al., 2015). As the fluid moves upward, the solubility decreases because of the decreasing temperature, pressure, and the mixing with cold water (Chatterjee, et al., 2017). This then results in the oversaturation of some of the silica minerals (cf **Figure 8.7** in **APPENDIX C**) such as quartz, tridymite, chalcedony, and cristobalite (Michard, 1990; Guo, et al., 2015; Chatterjee, et al., 2017). According to Tonkul, et al. (2025), the supersaturation of chalcedony and quartz is due to the effects of degassing and temperature fluctuations. At temperatures below 100°C, these minerals become saturated in geothermal fluids (Tonkul, et al., 2025). However, changes in temperature and the process of degassing can result in oversaturation (Tonkul, et al., 2025). The oversaturation of silica minerals can directly lead to silica scaling, a major challenge in geothermal energy production (Zarrouk, et al., 2014). This could hinder the generation of geothermal energy from the Shu-Shu springs.

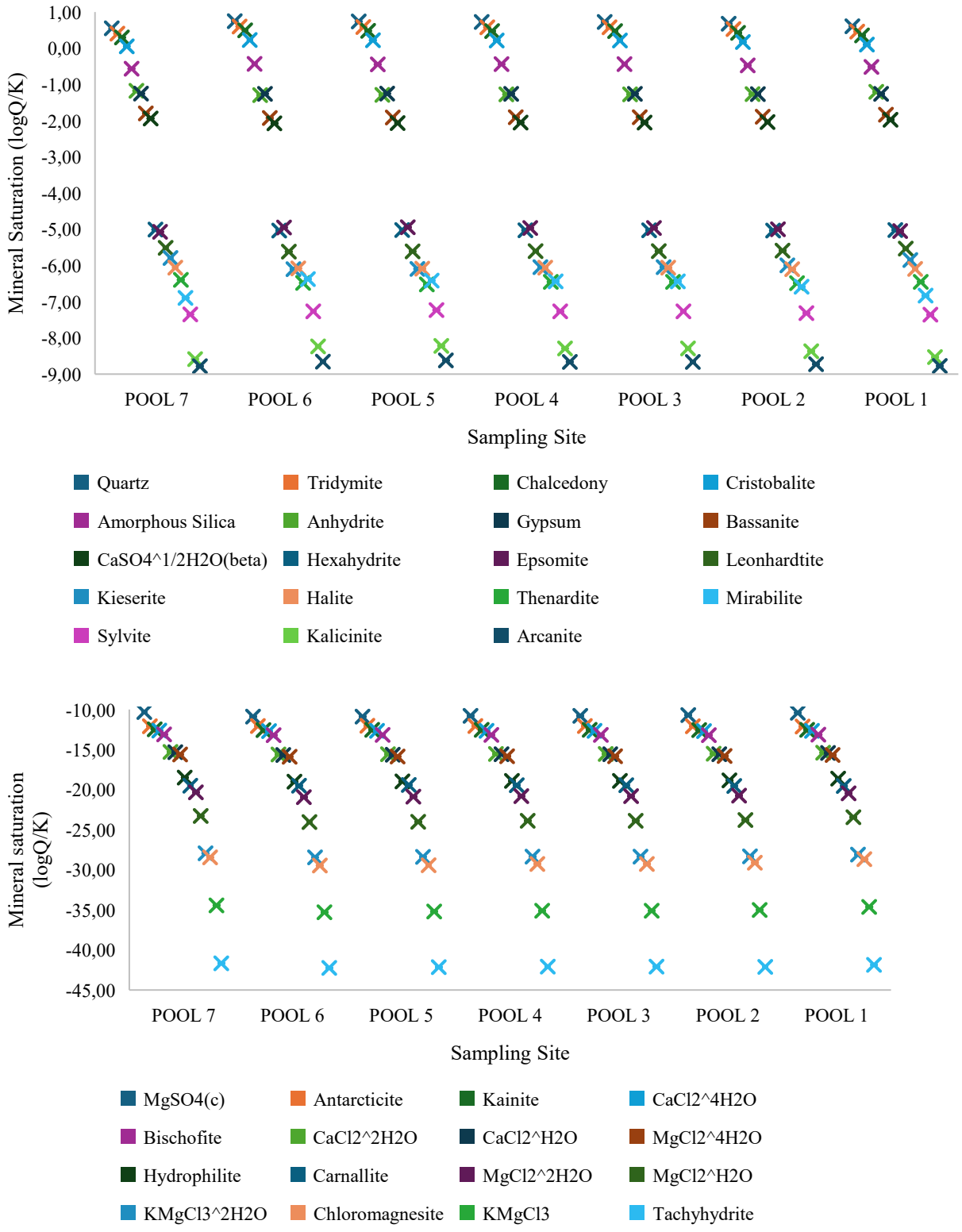

Figure 5.10: Saturation indices values of Shu-Shu thermal water samples with respect to minerals.

5.5 Shu-Shu thermal springs investigated using UAV

A drone was flown over the study area during the dry season to examine the extent of the Shu-Shu thermal springs and the geological features that govern the formation of the springs.

5.5.1 Geological control of the occurrence

The orthomosaic that was generated from the Pix4D field software is shown in **Figure 5.11**. The Shu-Shu Springs are situated on an island in the middle of the uThukela River. The change in the direction of the river near the spring is evident in underlying geological features such as fractures, and dykes. Most of the South African thermal springs are somewhat related to fault structures (Petersen & Parsons, 2001; Lin, et al., 2015). There are 11 thermal springs in the Western and Eastern Cape provinces that are related to the regional faults known as the Worcester and Cango-Baviaankoof faults. Thermal springs situated in the Limpopo province are related to the Melinda and Klein Tshipise faults (Lin, et al., 2015). In addition, the Groenkloof fountain in Pretoria which occurs at the Malmani/Pretoria Group shale contact, is also strongly affected by a northeast striking fault (Lin, et al., 2015).

The Shu-Shu springs are situated at the Namaqua-Natal Belt, which is known as the zone of metamorphic rocks on the southern edge of the Kaapvaal Craton (Nyabeze, et al., 2013). A fault line striking at N 63° E governs the formation of the Shu-Shu springs (Gevers, 1942). The Shu-Shu fault line is a breccia consisting of amphibolites and gneisses among other metamorphic rocks (Gevers, 1942). A Geographical study (Carranza & Maseko, 2024) has shown that intersections of lineaments that trend ENE and WNW influence thermal spring occurrences in eastern South Africa on a regional scale, and the Shu-Shu are located on the eastern part of South Africa.

The movement of warm GW from the subsurface to the surface is regulated by these structural lineament junctions (Carranza & Maseko, 2024). The understanding that these various regions are defined by distinct tectonic domains supports the geographical investigations' findings about the diverse paths controlling the movement of heated GW for the formation of thermal springs in the eastern part of South Africa (Carranza & Maseko, 2024).

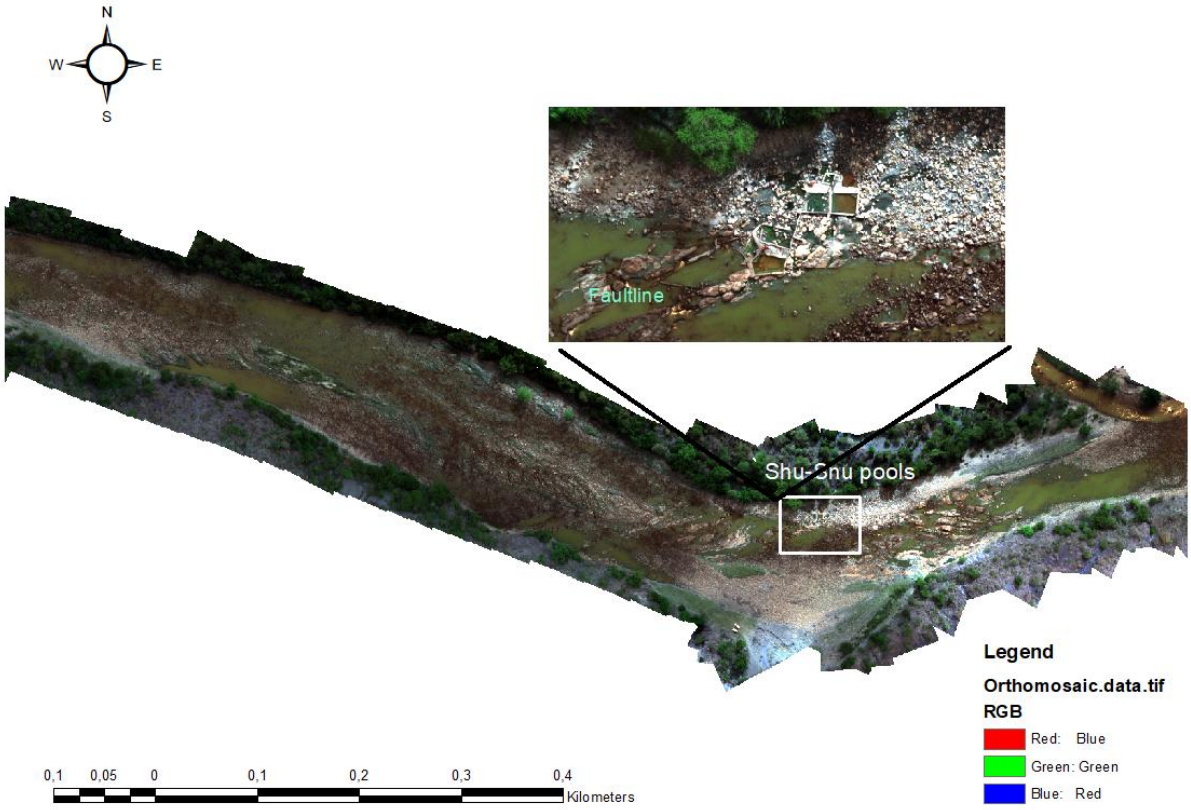

Figure 5.11: Orthomosaic map of the study area produced from pix4D fields

5.5.2 Extent of the discharge zone and Volume of water

The project's objectives included investigating the extent of the Shu-Shu Springs. A thermal map illustrating the Shu-Shu Springs and the surrounding surface water is presented in **Figure 5.12**. To calibrate the surface water temperature of the springs and the adjacent uThukela River, **Equation (4.3)** was employed. Utilizing the Identify feature in ArcGIS, it was found that the hottest waters were located in pool 7, registering a temperature of 41°C, which is 10°C lower than the in-situ temperature recorded. The orange colour on the map signifies the highest surface temperatures, while blue indicates the lowest. The location of the Shu-Shu Springs is also depicted in **Figure 5.12.** Notably, the orange patches extend further eastward and align at an angle of 63° between north and east, coinciding with the fault line that governs the formation of the Shu-Shu Springs.

The extent of discharge is not only confined to the 7 concentrated pools that make up the main visible springs. There are discharge zones situated East of the concentrated pools, which extend to approximately 120 m from the concentrated visible pools. The area of the discharge zone is approximately 3100 m^2. The discharge zones are not easily visible to the naked eye, which leads to the conclusion that the Shu-Shu springs have a low flow rate. The flow from the Shu-Shu springs is so minimal that it has never been documented in any scientific literature. This strongly suggests that the metamorphic basement rocks governing the spring system have inherently low hydraulic conductivity and that groundwater circulation is highly restricted. Moreover, the oversaturation of silica minerals within the geothermal fluids can result in silica scaling and deposition within fractures, progressively decreasing the permeability of the rocks and contributing further to restricted flow (Duku et al., 2022).

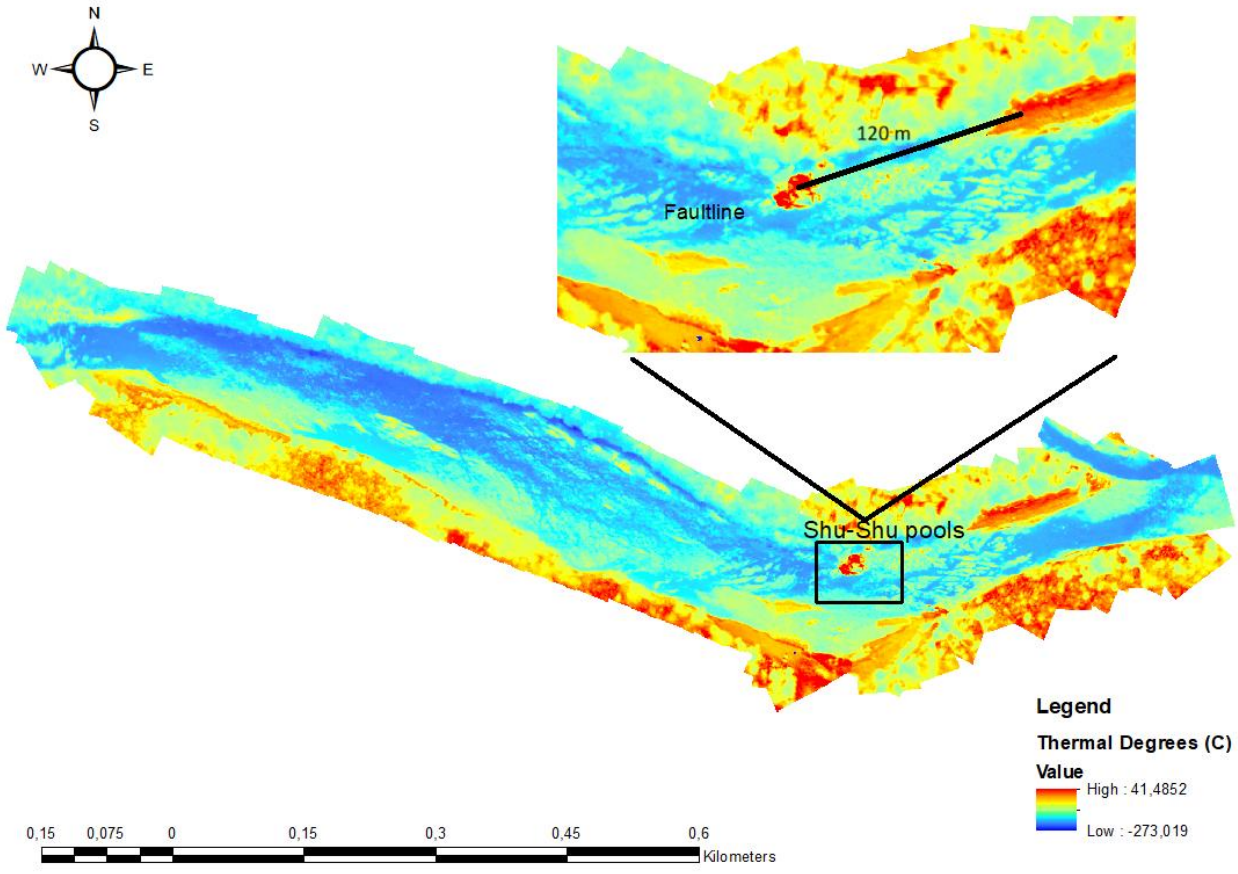

Figure 5.12: Thermal map of the study area produced from pix4D fields

In contrast to geothermal systems in other countries, where active fault zones commonly consist of poorly cemented, unconsolidated, or brecciated fault-core materials that act as high-permeability conduits, South Africa's tectonic framework presents a different picture (Andreoli et al., 1996). Neotectonic activity is limited in the region, as shown by the absence of recent terrace development, low-magnitude planation surfaces, and limited evidence of young crustal movements (Andreoli et al., 1996). As such, it would be misleading to assume that groundwater flow within South African fault zones is primarily controlled by abundant fractures or high-porosity fault cores, as is often the case elsewhere (Lin et al., 2015). Instead, the majority of South African fault zones are lithified, cemented, and metamorphosed, and therefore tend to act as aquicludes that impede groundwater flow (Xu et al., 2009; Lin et al., 2015).

Nevertheless, localised weathering and hydrothermal alteration can enhance fracture permeability along some fault planes, creating narrow conduits for groundwater circulation (Gevers, 1942; Fronzi et al., 2021). In the case of the Shu-Shu springs, the controlling fault has experienced only limited weathering and alteration, which reduces permeability and restricts groundwater flow. As a result, the system has not developed into a high-discharge spring. This is reflected in the small discharge and low flow rates (Lin et al., 2015).

Seasonal rainfall also influences the springs: during the dry season, evaporation concentrates solutes and reduces flow, while in the wet season, recharge dilutes the waters, but discharge remains low because of the rocks' limited permeability (Charlesworth & Matthews, 1981; Gravelet-Blondin, 2013). Collectively, these factors explain why the Shu-Shu springs discharge is both limited in extent and minimal in volume, despite the clear structural control of the governing fault line.

CHAPTER 6: CONCLUSIONS

This chapter summarises the aims and objectives of the study and the various approaches used to establish them. It also provides a summary of the results and contributions made, along with recommendations for future research.

6.1 The aims and objectives and summary of the approach

Exploring thermal systems and addressing the lack of research on South African thermal springs and their connection to SW/GW interaction was the main aim of this project. The objectives included determining the origin, extent, and depth of the Shu-Shu thermal springs along with their effects on the water quality of the uThukela River.

The origin of the Shu-Shu springs was determined using stable isotope analyses, whereby the isotope composition of the springs was compared to the isotope composition of rainfall samples collected from Eshowe, Winterton, and Drakensberg Mountain. The extent of the Shu-Shu springs was determined using UAVs and Pix4D Fields software. The depth of circulation was calculated using equation **5.2**, and hydrochemistry analyses were performed on the water samples to assess the thermal springs' impact on the water quality of the surrounding surface water of the uThukela River.

6.2 Summary of Findings

The isotope and chemical data suggested that the waters from Shu-Shu thermal springs are almost entirely recharged by rainwater, which originates at higher altitudes in Drakensberg Mountain. The water heats up through deep water circulation and travels to the surface through faults and fractures within the uThukela catchment. The surface waters surrounding the springs are more enriched in isotopic composition, and that is attributed to evaporation. The waters are mainly Na-Cl type, which are characterised by rock-water interaction and the dissolution of minerals from gneiss and amphibolites. The saturation index calculation showed that the Shu-Shu springs are supersaturated concerning four minerals that are polymorphs of silica, such as quartz, tridymite, chalcedony, and cristobalite, but amorphous silica was undersaturated. Other minerals that were undersaturated included gypsum and halite, amongst others.

The discharge temperatures range from 45 °C to 52 °C between the wet and dry seasons. The Shu-Shu thermal springs present an equilibrium with chalcedony and quartz. The Silica (Chalcedony and Quartz) geothermometers predict a geothermal reservoir temperature of 76°C-80°C with an estimated depth of water penetration of 1.83-1.95 km, characterising the springs as having low-enthalpy energy potential. The ratio-based geothermometers cannot be used to approximate the reservoir temperature as the Shu-Shu waters have not reached full nor partial equilibrium. In addition, the ratio-based equations tend to overestimate the reservoir temperature. The Shu-Shu thermal waters experience conductive cooling and mixing with meteoric/surface water, which leads to a decrease in temperature

The orthomosaic and thermal maps that were developed from the stitched images from the UAV show that the Shu-Shu formation is governed by geological structures such as faults and dykes. The Faultline is evident from the visible breccia that strikes 63° between North and East. The common rocks near the springs are metamorphic rocks, which have a low hydraulic conductivity, which limits the potential of the springs to produce geothermal energy. Leading to the conclusion that geothermal energy potential will not be a matter of slightly high subsurface temperature, but the permeability of the rocks.

6.3 Future Possibilities and Recommendations

More thermal springs need to be explored, particularly those found in the Free State, as there is a lack of studies in that area. Thermal springs such as the Western Cape's Blandvlei and Limpopo's Siloam should be investigated for the production of geothermal energy as they are the hottest thermal springs in South Africa. Recommendations also include exploring other thermal springs in South Africa that have high hydraulic conductivity to produce geothermal energy. Even though subsurface temperatures may be slightly high, nothing can be done if the springs have low discharge. Extensive geophysics and drilling are also recommended to get a better understanding of the subsurface characteristics of the thermal springs.

CHAPTER 7: REFERENCES

Abbey, A. et al., 2024. Tracing short-lived hydrothermal circulation systems and water–rock interactions around small-scale intrusions. *Geochimica et Cosmochimica Acta,* Volume 366, pp. 113-127.

Abubakar Jumare, I., Bhandari, R. & Zerga, A., 2019. Environmental life cycle assessment of grid-integrated hybrid renewable energy systems in Northern Nigeria. *Sustainability,* 11(21), p. 5889.

Abubakar, A., Hashim, M. & Pour, A., 2019. Remote sensing satellite imagery for prospecting geothermal systems in an aseismic geologic setting: Yankari Park, Nigeria. *International Journal of Applied Earth Observation and Geoinformation,* Volume 80, pp. 157-172.

Adebayo, T. et al., 2021. Dominance of fossil fuels in Japan's national energy mix and implications for environmental sustainability. *International Journal of Environmental Research and Public Health,* 18(14), p. 7347.

Andreoli, M., Doucoure, M. & Van Bever Donker, J., 1996. Neotectonics of Southern Africa – a review. *Africa Geoscience Review,* 3(1), pp. 1-16.

Ansari, M. & Yarahmadi, S., 2017. Hydrochemistry and Mineral Saturation of Thermal Spring in Ramsar Area, North of Iran. *International Journal of Advanced Biotechnology and Research (IJBR),* 8(3), pp. 1667-1676.

Arnorsson, S., 1983. Chemical equilibria in Icelandic geothermal systems—implications for chemical geothermometry investigations. *Geothermics,* 12(2-3), pp. 119-128.

Ashton, P. & Schoeman, F., 1986. Southern African thermal springs. *The Naturalist,* 30(1), pp. 32-34.

Asnin, S. et al., 2022. Identification of water–rock interaction of surface thermal water in Songwe medium temperature geothermal area, Tanzania. *Environmental Earth Sciences,* 81(21), p. 513.

Bahati, G., Natukunda, J. & Tuhumwire, J., 2003. *Geothermal energy in Uganda, country update.* Reykjavik, s.n.

Barbier, E., 2002. Geothermal energy technology and current status: an overview. Renewable and sustainable energy reviews. 6(1-2), pp. 3-65.

Bond, G., 1946. *A geochemical survey of the underground water supplies of the Union of South Africa: with particular reference to their utilisation in power,* Pretoria: Gorvenment Printer.

Bozdağ, A., 2016. Hydrogeochemical and isotopic characteristics of Kavak (Seydişehir-Konya) geothermal field. *Turkey. Journal of African Earth Sciences,* Volume 121, pp. 72-83.

Carranza, E. & Maseko, R., 2024. Regional- to district-scale controls on thermal springs occurrence in South Africa: Insights from investigations of their spatial distribution and their spatial relationships with geological features. *Geothermics,* 117(3), p. 102866.

Chai, Y. et al., 2021. Conversion relationship between groundwater and surface water in the Taizi River Basin in China based on geochemical and isotopic characteristics. *Environmental Science and Pollution Research,* 28(16), pp. 20045-20057.

Charlesworth, E. & Matthews, P., 1981. *Archaean granulites along the southern margin of the Kaapvaal craton in eastern South Africa.* Johannesburg, IAEA, pp. 34-35.

Chatterjee, S. et al., 2017. Isotope–geochemical characterization and geothermometrical modeling of Uttarakhand geothermal field, India. *Environmental Earth Sciences,* Volume 76, pp. 1-21.

Chenaker, H., Houha, B. & Vincent, V., 2018. Hydrogeochemistry and geothermometry of thermal water from north-eastern Algeria. *Geothermics,* Volume 75, pp. 137-145.

Chen, X., Smith, J., & Lee, A. 2018. The impact of climate change on water chemistry. *Journal of Environmental Science*, 45(3), pp. 123-135.

Chen, W., Liu, J. & Li, J., 2019. Classification of UAV and bird target in low-altitude airspace with surveillance radar data. *The Aeronautical Journal,* 123(1260), pp. 191-211.

Chiodini, G., Frondini, F. & Marini, L., 1995. Theoretical geothermometers and pCO2 indicators for aqueous solutions coming from hydrothermal systems of medium-low

temperature hosted in carbonate-evaporite rocks. Application to the thermal springs of the Etruscan Swell. Italy. *Applied Geochemistry,* Volume 10, pp. 337-346.

Craig, H., 1961. Isotopic variations in meteoric waters. *Science,* 133(3465), pp. 1702-1703.

Craig, H., Gordon, L. & Horibe, Y., 1963. Isotopic exchange effects in the evaporation of water: 1. Low-temperature experimental results. *Journal of Geophysical Research,* 68(17), pp. 5079-5087.

Darling, W., Edmunds, W. & Smedley, P., 1997. Isotopic evidence for palaeowaters in the British Isles. *Applied Geochemistry,* 12(6), pp. 813-829.

Datta, P. & Tyagi, S., 1996. Major ion chemistry of groundwater in Delhi area: chemical weathering processes and groundwater flow regime. *Journal geological society of India,* 47(2), pp. 179-188.

Dhansay, T. et al., 2017. South Africa's geothermal energy hotspots inferred from subsurface temperature and geology. *South African Journal of Science,* 113(11-12), pp. 1-7.

Diamond, R., 2022. *Stable Isotope Hydrology.* 1st ed. Guelph: The Groundwater Project.

Diamond, R. & Harris, C., 2000. Oxygen and hydrogen isotope geochemistry of thermal springs of the Western Cape, South Africa: Recharge at high altitude? *Journal of African Earth Sciences,* 31(3), pp. 467-481.

DiPippo, R., 1999. *Small geothermal power plants: design, performance and economics,* Dartmouth: GHC Bulletin.

Di Pippo, R. (2012). *Geothermal power plants: Principles, applications, case studies and environmental impact* (3rd ed.). Elsevier.

Duku, E., Ongarora, B. & Tanui, P., 2022. Effect of Boiling and Cooling of Geothermal Fluids on Precipitation of Secondary Minerals: A Case Study of Olkaria Fields, Kenya. *Journal of Geoscience and Environment Protection,* 10(9), pp. 251-270.

Durowoju, O., Butler, M., Ekosse, G. & Odiyo, J., 2019. Hydrochemical processes and isotopic study of geothermal springs within Soutpansberg, Limpopo Province, South Africa. *Applied Sciences,* 9(8), p. 1688.

Ellis, AJ. & Mahon, WAJ., 1977. *Chemistry and Geothermal Systems*. Academic Press.

Favier, A. et al., 2021. Characterization of an exhumed high-temperature hydrothermal system and its application for deep geothermal exploration: An example from Terre-de-Haut Island

(Guadeloupe archipelago, Lesser Antilles volcanic arc). *Journal of Volcanology and Geothermal Research,* Volume 418, pp. 107-256.

Fouillac, C. & Michard, G., 1981. Sodium/lithium ratio in water applied to geothermometry of geothermal reservoirs. *Geothermics,* 10(1), pp. 55-70.

Fournier, R., 1977. Chemical geothermometers and mixing models for geothermal systems. *Geothermics,* 5(1-4), pp. 41-50.

Fournier, R., 1979. A revised equation for the Na/K geothermometer. *GRC Transactions.,* Volume 3.

Fournier, R. & Potter, R., 1979. Magnesium correction to the Na-K-Ca chemical geothermometer. *Geochimica et Cosmochimica Acta,* 43(9), pp. 1543-1550.

Fournier, R. & Potter, R., 1982. A revised and expanded silica (quartz) geothermometer. *Bulletin of Geothermal Resources Council,* Volume 11, pp. 3-12.

Fournier, R. & Potter, R., 1982. A revised and expanded silica (quartz) geothermometer. *Bulletin of Geothermal Resources Council,* Volume 11, pp. 3-12.

Fournier, R. & Truesdell, A., 1973. An empirical Na-K-Ca geothermometer for natural waters. *Geochimica et Cosmochimica acta,* 37(5), pp. 1255-1275.

Fronzi, D. et al., 2021. The role of faults in groundwater circulation before and after seismic events: Insights from tracers, water isotopes and geochemistry. *Water*, *13*(11), p.1499

Garcia-Valles, M. et al., 2008. Mineralogical characterization of silica sinters from the El Tatio geothermal field, Chile. *American Mineralogist,* 93(8-9), pp. 1373-1383.

Gemici, Ü. & Filiz, Ş., 2001. Hydrochemistry of the Çeşme geothermal area in western Turkey. *Journal of Volcanology and Geothermal research,* 110(1-2), pp. 171-187.

Gevers, T., 1942. The hot springs in the Tugela River Near Kranskop, Natal. *South African Journal of Geology,* 45(01), pp. 65-74.

Giggenbach, W., 1988. Geothermal solute equilibria. derivation of Na-K-Mg-Ca geoindicators. *Geochimica et cosmochimica acta,* 52(12), pp. 2749-2765.

Giggenbach, W., 1989. Collection and analysis of geothermal and volcanic water and gas discharges. *Chem. Div. DSIR Report,* pp. 2401-2481.

Giggenbach, W., 1992. Isotopic shifts in waters from geothermal and volcanic systems along convergent plate boundaries and their origin. *Earth and planetary science letters,* 113(4), pp. 495-510.

Glaser, B. et al., 2018. Mapping surface-saturation dynamics with thermal infrared imagery. *Hydrology and Earth System Sciences,* 22(11), pp. 5987-6003.

Grasby, S. & Hutcheon, I., 2001. Controls on the distribution of thermal springs in the southern Canadian Cordillera. *Canadian Journal of Earth Sciences,* Volume 38, pp. 427-440.

Gravelet-Blondin, K., 2013. *A geological and hydrogeological study of the Shu Shu thermal springs, KwaZulu-Natal,* Durban, South Africa: University of KwaZulu-Natal.

Guo, Q. et al., 2015. Natural attenuation of geothermal arsenic from Yangbajain power plant discharge in the Zangbo River, Tibet, China. *Applied Geochemistry,* Volume 62, pp. 164-170.

Gupta, H. & Roy, S., 2006. *Geothermal energy: an alternative resource for the 21st century.* s.l.:Elsevier.

Gutiérrez-Negrín, L., 2024. Evolution of worldwide geothermal power 2020–2023. *Geothermal Energy,* 12(1), p. 14.

Han, D. et al., 2010. Evaluation of groundwater hydrochemical characteristics and mixing behavior in the Daying and Qicun geothermal systems, Xinzhou Basin. *Journal of Volcanology and Geothermal Re,* 189(1-2), pp. 92-104.

Hanna, 1996. *Hanna Instruments Worldwide.* [Online] Available at: https://images.app.goo.gl/ArocFjb21vz37dJ9A [Accessed 01 March 2024].

Hartnady, C. & Jones, M., 2007. *Geothermal studies of the Table Mountain Group aquifer systems,* Cape Town: Water Research Commission.

Hayashi, M., 2004. Temperature-electrical conductivity relation of water for environmental monitoring and geophysical data inversion. *Environmental monitoring and assessment,* Volume 96, pp. 119-128

Henley, R., Truesdell, A., Barton, P. & Whitney, J., 1984. Fluid-mineral equilibria in hydrothermal systems. *Society of Economic Geologists,* Volume 1.

Hoffmann, J., 1979. *The chemical composition of hot springs in South and Southwest Africa,* Cape Town: National Institute for Water Research.

Hoole, R., 2001. *The Development of Lilani Hot Spring: An Analysis of Socio-Economic and Environmental Impacts,* Pietermaritzburg: Unpublished M.Sc. Dissertation, University of Natal.

Huang, W. & Kiang, W., 1972. Laboratory dissolution of plagioclase feldspars in water and organic acids at room temperature. *American Mineralogist: Journal of Earth and Planetary Materials,* 57(11-12), pp. 1849-1859.

Huttrer, G., 2001. The status of world geothermal power generation 1995–2000. *Geothermics,* 30(1), pp. 1-27.

Jasechko, S., 2019. Global isotope hydrogeology—Review. *Reviews of Geophysics,* 57(3), pp. 835-965.

Johnson, L., & Lee, A. 2015. Urbanization and its effects on geochemical signatures. *Environmental Research Letters*, 10(2), pp. 234-245.

Karingithi, C., 2009. *Chemical Geotermometers for Geothermal Exploration. Short Course IV on Exploration for Geothermal Tesources, organized by UNUGTP, KenGen and GDC, Kenya.,* Naivasha: s.n.

Kebede, S., 2013. *Groundwater in Ethiopia.* Berlin/Heidelberg: Springer.

Kebede, S., 2024. *Isotope chemistry* [Interview] (28 October 2024).

Kent, L., 1949. The thermal waters of the Union of South Africa and SouthWest Africa. *South African Journal of Geology,* 52(1), pp. 231-264.

Kent, L., 1968. The thermal waters in the Republic of South Africa.

Kharaka, Y. & Mariner, R., 1989. *Chemical geothermometers and their application to formation waters from sedimentary basins. In Thermal history of sedimentary basins: methods and case histories.* New York, Springer.

Kim, E., Nam, S., Koo, J. & Hwang, T., 2021. Hybrid approach of unmanned aerial vehicle and unmanned surface vehicle for assessment of chlorophyll-a imagery using spectral indices in stream, South Korea. *Water,* 13(14), p. 1930.

Kottek, M. et al., 2006. World map of the Köppen-Geiger climate classification updated. *Meteorologische Zeitschrift,* 15(3), pp. 259-263.

Lakshmanan, E., Kannan, R. & Kumar, M., 2003. Major ion chemistry and identification of hydrogeochemical processes of ground water in a part of Kancheepuram district, Tamil Nadu, India. *Environmental geosciences,* 10(4), pp. 157-166.

LaMoreaux, P. & Tanner, J., 2001. *Springs and bottled waters of the world: ancient history, source, occurrence, quality and use.* Eds ed. Berlin: Springer Science.

Laonamsai, J. et al., 2021. Spatial and temporal distributions of stable isotopes in precipitation over Thailand. *Hydrological processes,* 35(1), p. 18 pages.

Leketa, K. & Abiye, T., 2020. Investigating stable isotope effects and moisture trajectories for rainfall events in Johannesburg, South Africa. *Water SA,* 46(3), pp. 429-437.

Letshele, K. et al., 2023. Stable hydrogen and oxygen isotopes reveal aperiodic non-river evaporative solute enrichment in the solute cycling of rivers in arid watersheds. *Science of the Total Environment,* Volume 856, p. 159133.

Li, C. et al., 2021. Hydrogeochemical Characteristics of Hot Springs and Their Short-Term Seismic Precursor Anomalies along the Xiaojiang Fault Zone, Southeast Tibet Plateau. *Water,* 13(19), p. 2638.

Li, J. et al., 2025. Investigating Groundwater–Surface Water Interactions and Transformations in a Typical Dry–Hot Valley Through Environmental Isotopes Analysis. *Water,* 17(6), p. 775.

Limberger, J. et al., 2018. Geothermal energy in deep aquifers: A global assessment of the resource base for direct heat utilization. *Renewable and Sustainable Energy Reviews,* Volume 82, pp. 961-975.

Lin, C. & Lai, Y., 2018. UAV path prediction for CD&R to manned aircraft in a confined airspace for cooperative mission. *International Journal of Aerospace Engineering,* 2018(1), p. 8759836.

Lin, L. et al., 2015. *Impact of fault structures on the occurrence of groundwater in fractured rock aquifers,* Pretoria, WRC Report, (2053/1), p.14.: Water Research Commission.

Lloyd, W. & Heathcote, A., 1985. *Natural Inorganic Hydrochemistry in Relation to Groundwater, an Introduction,* Oxford: Clarendon Press.

Lonergan, A. & Cange, J., 1994. *Cation and Anion Analysis: Application s to Enhance and Expedite Site-Level Hydrogeological Investigations: Proceedings of the 1994 Focus Conference on Eastern Regional Ground Water Issues, NGWA. pp. 619-630.* s.l., s.n.

Lund, JW. & Freeston., D.H. 2001. World-wide direct uses of geothermal energy 2000. *Geothermics*, *30*(1), pp. 29-68.

Lund, JW., Freeston, DH. & Boyd, TL., 2011. Direct utilization of geothermal energy 2010 worldwide review. *Geothermics*, *40*(3), pp.159-180.

Luo, L. et al., 2017. Determining the recharge sources and circulation depth of thermal waters in Xianyang geothermal field in Guanzhong Basin: The controlling role of Weibei Faul. *Geothermics,* Volume 69, pp. 55-64.

Marandia, A. & Shand, P., 2018. Groundwater chemistry and the Gibbs Diagram. *Applied Geochemistry,* Volume 97, pp. 209-212.

Martínez-Florentino, T., Esteller-Alberich, M., Exp´osito, J. & Domínguez-Mariani, E., 2021. Hydrogeochemistry and geothermometry of thermal springs in the eastern Trans-Mexican Volcanic Belt. *Geothermics,* Volume 96, pp. 1-18.

Martin, J. & Croukamp, L., 2021. Exploration into the potential for a low-enthalpy geothermal power plant in Cape fold belt. *Geothermics,* Volume 89.

Mason, R., Smith, J., & Johnson, L. 2021. Water quality assessments and resource management. *Water Resources Management,* 35(4), pp. 567-580.

Mazor, E. & Verhagen, B., 1983. Dissolved ions, stable and radioactive isotopes and noble gases in thermal waters of South Africa. *Journal of Hydrology,* 63(3-4), pp. 315-329.

Michard, G., 1990. Behaviour of major elements and some trace elements (Li, Rb, Cs, Sr, Fe, Mn, W, F) in deep hot waters from granitic areas. *Chemical Geology,* 89(1-2), pp. 117-134.

Narsilio, G., Bidarmaghz, A. & Colls, S., 2014. *Geothermal energy: introducing an emerging technology. In: Proceedings of International Conference on Advances in Civil Engineering for Sustainable Development.* Melbourne, s.n.

Ngabirano, H., Byamugisha, D. & Ntambi, E., 2016. Effects of Seasonal Variations in Physical Parameters on Quality of Gravity Flow Water in Kyanamira Sub-County, Kabale District, Uganda. *Journal of Water Resource and Protection,* Volume 8, pp. 1297-1309.

Nicholson, K., 1993. Geothermal Sysystems. In: *Geothermal Fluids: Chemistry and Exploration Techniques.* Berlin: Springer, pp. 1-18.

Nieva, D. & Nieva, R., 1987. Developments in geothermal energy in Mexico—part twelve. A cationic geothermometer for prospecting of geothermal resources. *Heat recovery systems and CHP,* 7(3), pp. 243-258.

Nyabeze, P. & Gwavava, O., 2013. *Determination of depth models for the vadose zone and shallow groundwater aquifer at Siloam hot spring in Limpopo province of South Africa: results from modelling of electromagnetic and electrical resistivity data,* Pretoria: Unpublished Report: Counsil for Geoscience.

Nyabeze, P. et al., 2013. The geological and biological hot spring scene in South Africa. In: J. Olivier & C. Jonker, eds. *Optimal Utilisation of Thermal Springs in South Africa.* Pretoria: Water Research Commision, pp. 15-35.

Olivier, J. & Jonker, N., 2013. *Optimal utilisation of thermal springs in South Africa,* Pretoria: Water Research Commission.

Olivier, J., Van Niekerk, H. & Van der Walt, I., 2008. Physical and chemical characteristics of thermal springs in the Waterberg area in Limpopo Province, South Africa. *Water SA,* 34(2), pp. 163-174.

Olivier, J., Venter, J. & Jonker, C., 2011. Thermal and chemical characteristics of hot water springs in the northern part of the Limpopo Province, South Africa. *Water SA,* 37(4), pp. 427-436.

Omenda, P., Mangi, P., Ofwona, C. & Mwangi, M., 2020. *Country update report for Kenya 2015-2019. In Proceedings of world geothermal congress.* Iceland, Proceedings World Geothermal Congress 2020+1.

Petersen, K. & Parsons, R. (., 2001. *A synthesis of the hydrogeology of the Table Mountain Group – Formation of a Research Strategy,* Pretoria: Water Research Commision.

Petersen, R. et al., 2023. The use of stable isotopes to identify surface water–groundwater interaction in the Kruger National Park, South Africa. *Water SA,* 49(2), pp. 96-102.

Petraccia, L. et al., 2006. Water, mineral waters and health. *Clinical nutrition,* 25(3), pp. 377-385.

Piper, A., 1944. A graphic procedure in the geochemical interpretation of water-analyses. *Eos, Transactions American Geophysical Union,* Volume 9, pp. 914-928.

Press, F. & Siever, R., 1986. *Earth.* Eds ed. Boston: Macmillan.

Ravikumar, S., Agrahari, A. & Singh, S., 2015. Mapping the intellectual structure of scientometrics: A co-word analysis of the journal Scientometrics (2005–2010). *Scientometrics,* Volume 102, pp. 929-955.

Rimstidt, J. & Barnes, H., 1980. The kinetics of silica-water reactions. *Geochima et Cosmochimica Acta,* Volume 44, p. 1683–1699.

Rindl, M., 1916. Medicinal springs of South Africa. *South African Journal of Science,* 13(1916), pp. 528-552.

Salem, Z. et al., 2022. Oxygen and hydrogen stable isotopes as recharge indicators, Central Nile Delta Quaternary aquifer, Egypt. *Journal of King Saud University-Science,* 34(3), p. 101834.

Sedano-Cibrián, J. et al., 2022. Thermal water prospection with UAV, low-cost sensors and GIS. Application to the Case of La Hermida. *Sensors,* 22(18), p. 6756.

Smith, J. 2010. Anthropogenic activities and geochemical processes. *Geochemistry International,* 48(1), pp. 45-60.

Spark, W., 2024. *Cedar Lake Ventures, Inc.* [Online] Available at: https://weatherspark.com/y/96787/Average-Weather-in-Nkandla-KwaZulu-Natal-South-Africa-Year-Round [Accessed 14 November 2024].

Strecha, C., 2024. *Pix4D.* [Online] Available at: https://support.pix4d.com/hc/en-us/articles/360000173463

Tarcan, G., 2005. Mineral saturation and scaling tendencies of waters discharged from wells (> 150 °C) in geothermal areas of Turkey. *Journal of Volcanology and Geothermal Research,* 142(3-4), pp. 263-286.

Tonami, F., 1970. Geochemical methods of exploration for geothermal energy. *Geothermics,* Volume 2, pp. 492-515.

Tonani, F., 1980. *Some Remarks on the Application of Geochemical Techniques in Geothermal Exploration.* Strasbourg, s.n.

Tonkul, S. et al., 2025. Effect of degassing on scaling in hypersaline system: Tuzla geothermal field, Turkey. *Geotherm Energy,* 13(1), p. 5.

Truesdell, A., 1976. *Summary of section III-geochemical techniques in exploration.* San Fransisco, s.n.

Tshibalo, A., Olivier, J. & Nyabeze, P., 2015. *South Africa Geothermal Country Update (2010-2014).* s.l., Proceedings World.

Tshibalo, A., Olivier, J. & Venter, J., 2010. *South Africa Geothermal Country Update (2005-2009).* Bali, In Conference proceedings of the World Geothermal Congress.

Vélez-Nicolás, M. et al., 2021. Applications of unmanned aerial systems (UASs) in hydrology: A review. *Remote Sensing,* 13(7), p. 1359.

Wan, M. et al., 2021. Total variation-based interframe infrared patch-image model for small target detection. *IEEE Geoscience and Remote Sensing Letters,* Volume 19, pp. 1-5.

Wen, Y., Wang, N. & Hu, Z., 2012. Hydrochemistry of geothermal water in Tianshui and adjacent area, Gansu province, China. *Environmental Earth Science,* Volume 67, pp. 1281-1290.

Xu, Y., Lin, L. & Jia, H., 2009. Groundwater flow conceptualization and storage determination of the Table Mountain Group (TMG) Aquifers. *Water Research Commission. Report*, 1419(1).

You, Y. et al., 2021. Applicability of Difference in Oxygen-18 and Deuterium of Water Sources and Isotopic Hydrograph Separation in a Bamboo Catchment during Different Rainfall Types. *Water,* 13(24), pp.3531.

Zarrouk, S., Woodhurst, B. & Morris, C., 2014. Silica scaling in geothermal heat exchangers and its impact on pressure drop and performance: Wairakei binary plant, New Zealand. *Geothermics,* Volume 51, pp. 445-459.

Zheng, X. & Guo, J., 1996. Silica geothermal temperature scale and its related problems. *Ground Water,* Volume 18, pp. 85-88.

CHAPTER 8: APPENDIX A

Figure 8.1 shows the concentrated pools that make up the Shu-Shu thermal springs. **Figure 8.2** shows a typical spectrophotometer that is used to analyse chemical parameters. **Figure 8.3** shows glass beakers that were used in the soil science laboratory for the titration.

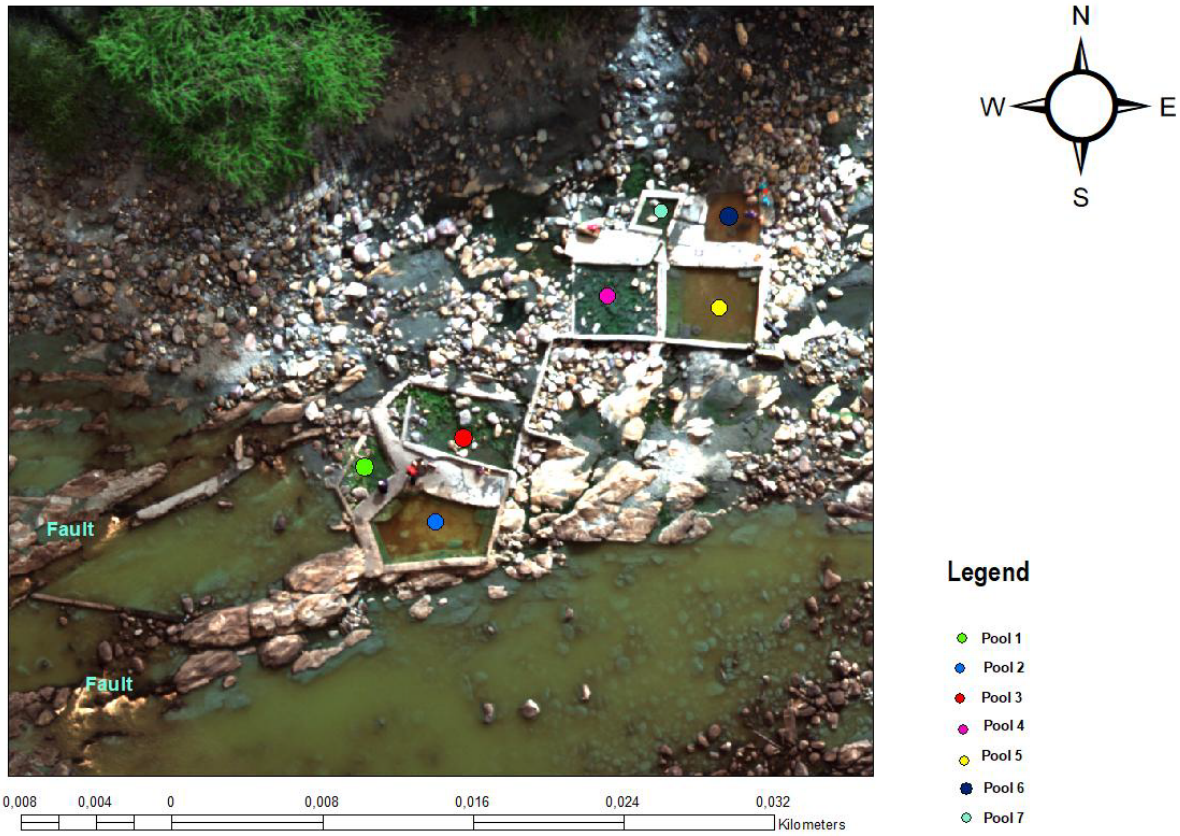

Figure 8.1: The seven concentrated pools that make up the Shu-Shu thermal springs

Figure 8.2: A typical spectrophotometer instrument seen in a lab (Source: Wikipedia Commons)

Figure 8.3: Glass beakers that were used in the soil science labolatory during the process of titration

CHAPTER 8: APPENDIX B

Table 8.1: Isotope values of the Shu-Shu thermal springs water samples and surrounding surface waters

Sampling Date				23-Dec-23		07-May-24		26-Jun-24	
Latitude (S)	Longitude (E)	Elevation (m)	Sampling spot	δ^2H ‰	$\delta^{18}O$ ‰	δ^2H ‰	$\delta^{18}O$ ‰	δ^2H ‰	$\delta^{18}O$ ‰
-28,858139	31,006856	222	500 m upstream	-1	-0,64	-6,9	-2,43	-3,4	-1,54
-28,859144	31,009083	219	250 m upstream	1,8	-0,37	-5,7	-2,26	-2,7	-1,78
-28,860189	31,010708	210	Shu-Shu Pool 1	-14,5	-3,43	-7,3	-2,38	15,5	-4,13
-28,860056	31,010911	210	Shu-Shu Pool 2	-15,3	-3,64	-7,5	-2,66	-15,6	-4,17
-28,859889	31,011214	210	Shu-Shu Pool 3	-13,5	-3,13	-15,5	-3,88	-16,9	-4,25
-28,859806	31,011600	210	Shu-Shu Pool 4	-14,6	-3,27	-15,4	-3,78	-15,5	-3,94
-28,859750	31,011800	210	Shu-Shu Pool 5	-15,1	-3,5	-14,2	-3,55	-16,0	-4,13
-28,859711	31,012042	210	Shu-Shu Pool 6	-14,8	-3,33	-14,8	-3,71	-15,5	-3,91
-28,859936	31,012189	210	Shu-Shu Pool 7	-18	-3,97	-15,6	-4,05	-15,5	-4,16
-28,859728	31,013425	210	250 m downstream	-7,5	-1,84	-6,9	-2,43	-3,8	-3,8
-28,859439	31,014997	210	500 m downstream	2,5	-0,39	-5,7	-2,26	-4,5	-4,5

Table 8.2: Isotope data from the samples collected from the comparable rainfall stations during the wet season

MikePass			Eshowe			Winterton		
Sampling Date	**$\delta^{18}O$ ‰**	**$\delta^{2}H$ ‰**	**Sampling Date**	**$\delta^{18}O$ ‰**	**$\delta^{2}H$ ‰**	**Sampling Date**	**$\delta^{18}O$ ‰**	**$\delta^{2}H$ ‰**
14-Dec-22	-3,74	-11,5	08-Dec-23	-3,85	-14,4	20-Nov-23	0,61	8,9
24-Jan-23	-3,6	-9,2	08-Dec-23	-3,79	-12,2	12-Jan-24	-2,77	-4,6
28-Sep-23	-2,95	-7,9	08-Dec-23	-3,62	-12,1	23-Jan-24	-1,02	6,2
25-Oct-23	-4,59	-20,6	08-Dec-23	-3,52	-13	25-Jan-24	0,06	14,3
09-Nov-23	-4,02	-11,4	26-Dec-23	-0,69	1,5	22-Feb-24	0,51	20,8
09-Nov-23	-3,31	-10,9	16-Jan-24	-2,51	-6,6	27-Feb-24	0,3	18,5
25-Nov-23	-1,86	0,1	16-Jan-24	-2,25	-5,1			
12-Dec-23	-3,74	-11,2	16-Jan-24	-2,51	-6,6			
12-Dec-23	-3,68	-12,6	20-Feb-24	-3,16	-4,8			
12-Dec-23	-3,73	-9,9	20-Feb-24	-2,96	-6,1			
12-Dec-23	-3,75	-8,3	20-Feb-24	-3,1	-5,4			
14-Dec-23	-2,7	-0,6	20-Feb-24	-3,16	-4,8			
14-Dec-23	-2,7	-0,6						
25-Jan-24	-3,5	-10						
25-Jan-24	-3,17	-5,2						
25-Jan-24	-2,96	-7,4						
29-Feb-24	-1,29	11,1						

Table 8.3: Isotope data from the samples collected from the comparable rainfall stations during the dry season

Mike Pass			Winterton			Eshowe		
Sampling Date	**$\delta^{18}O$ ‰**	**$\delta^{2}H$ ‰**	**Sampling Date**	**$\delta^{18}O$ ‰**	**$\delta^{2}H$ ‰**	**Sampling Date**	**$\delta^{18}O$ ‰**	**$\delta^{2}H$ ‰**
28-Mar-23	-2,55	-1	06-Mar-23	-2,7	-7,7	29-Jun-23	-1,86	0,1
28-Mar-23	-2,68	-0,9	16-Mar-23	-0,06	11,4	29-Jun-23	-1,77	1,3
28-Mar-23	-2,54	-0,3	11-Apr-23	-0,79	4,8	29-Jun-23	-1,58	2
25-Apr-23	-2,2	-5,9	15-May-23	0,68	13,5	26-Jun-24	-2,74	-4,4
22-May-23	-5,21	-15,9	01-Jun-23	-0,84	2,3	31-Jul-24	-3,13	-2,9
29-Jun-23	-1,53	8,2	11-Jun-23	-1,04	2	31-Jul-24	-3,39	-3,8
23-Jul-23	-4,9	-15,2	09-May-24	-4,31	-15,3			
03-Apr-24	-4,36	-13,3	04-Jun-24	-0,51	10,7			
23-Apr-24	-4,51	-20	24-Jun-24	-0,48	10,3			
23-Apr-24	-6,63	-26,4						
31-May-24	-3,13	-7,3						
24-Jun-24	-3,34	-3,1						
24-Jun-24	-3,34	-3,1						

CHAPTER 8: APPENDIX C

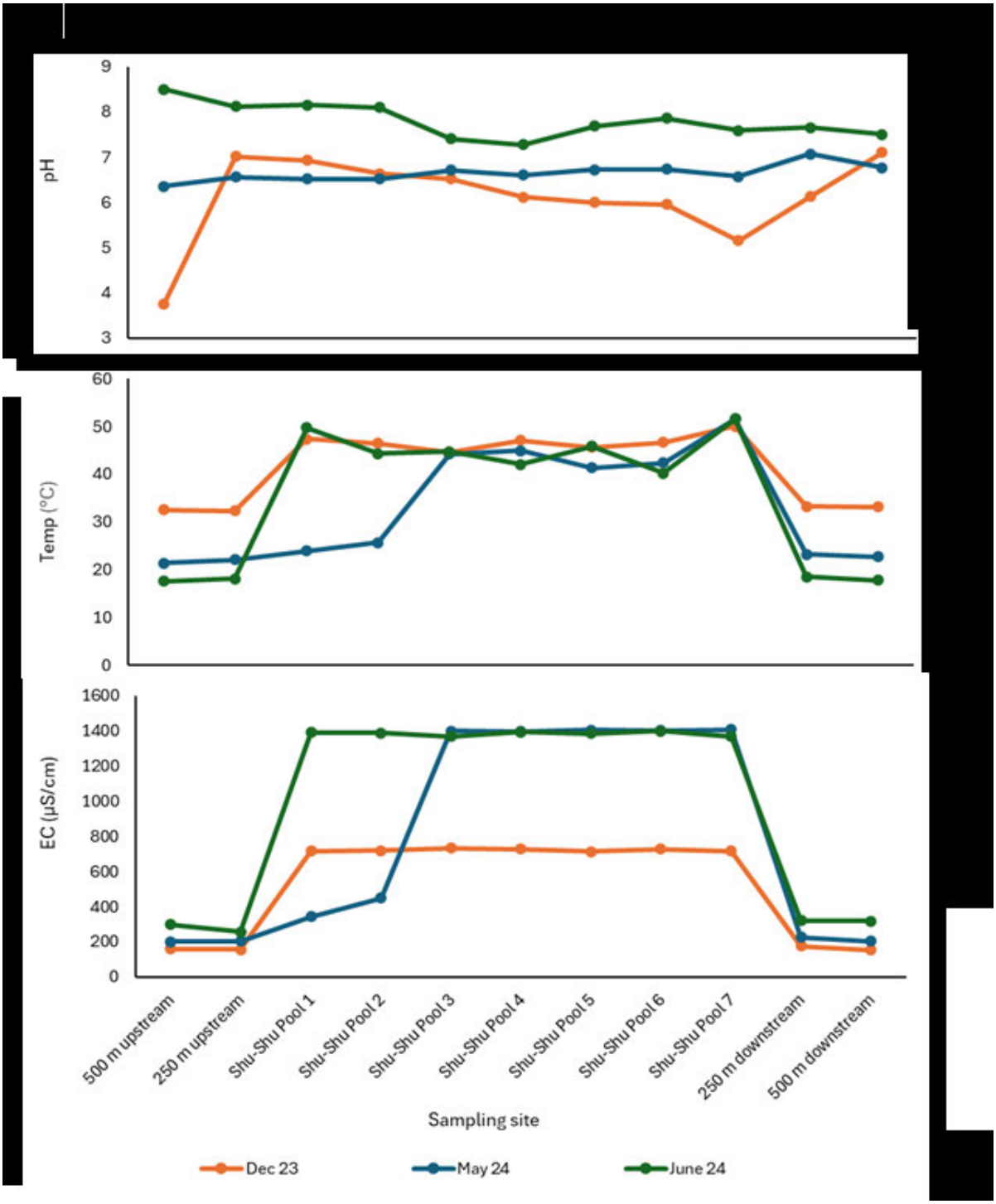

Figure 8.4: Temp, EC, and pH variations along Shu-Shu springs transect across seasons

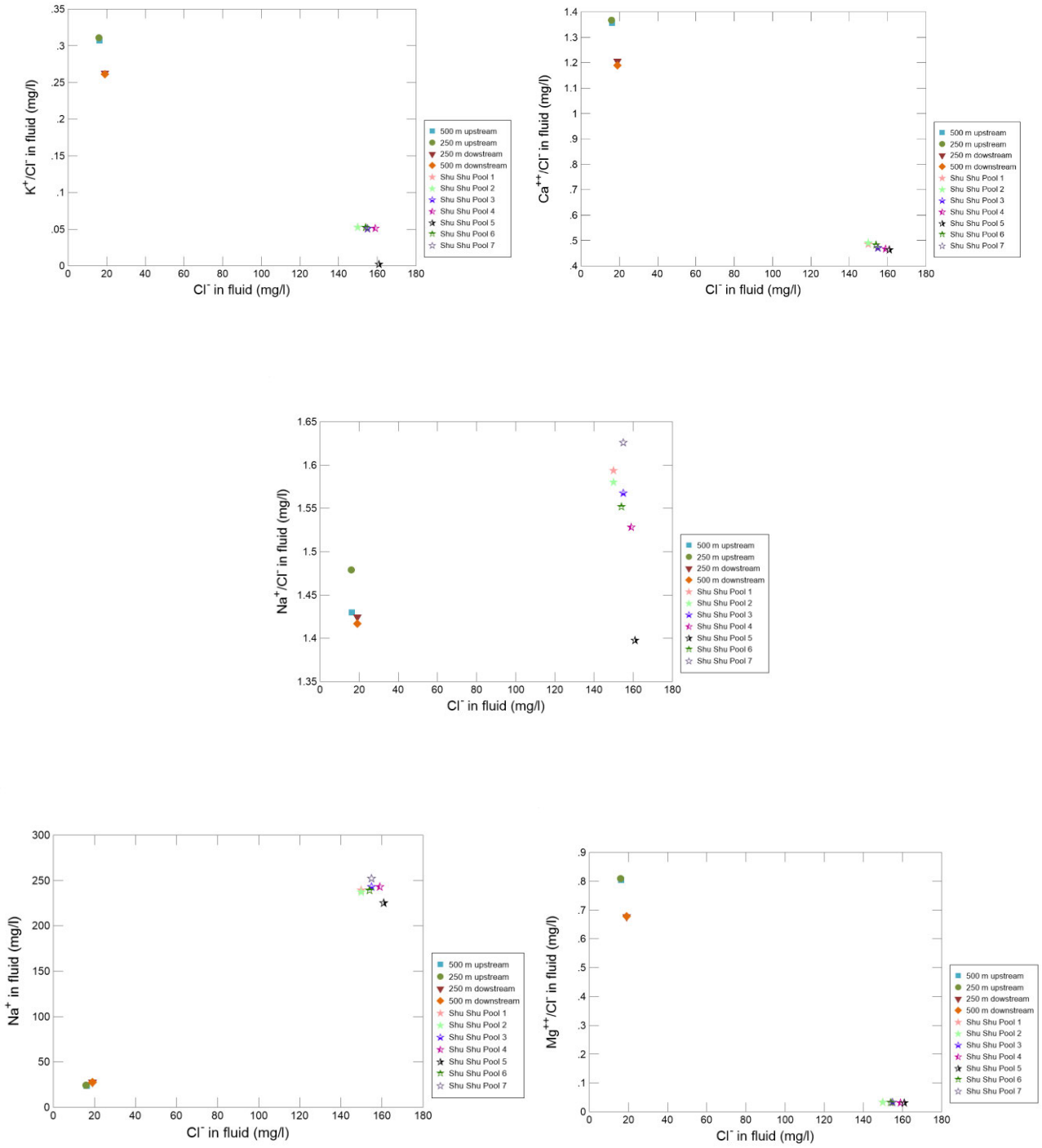

Figure 8.5: Relationship among various hydrochemical indices versus Cl^- for thermal waters. Ranges for rock weathering, ion exchange, and typical values in groundwater (Cl^-)

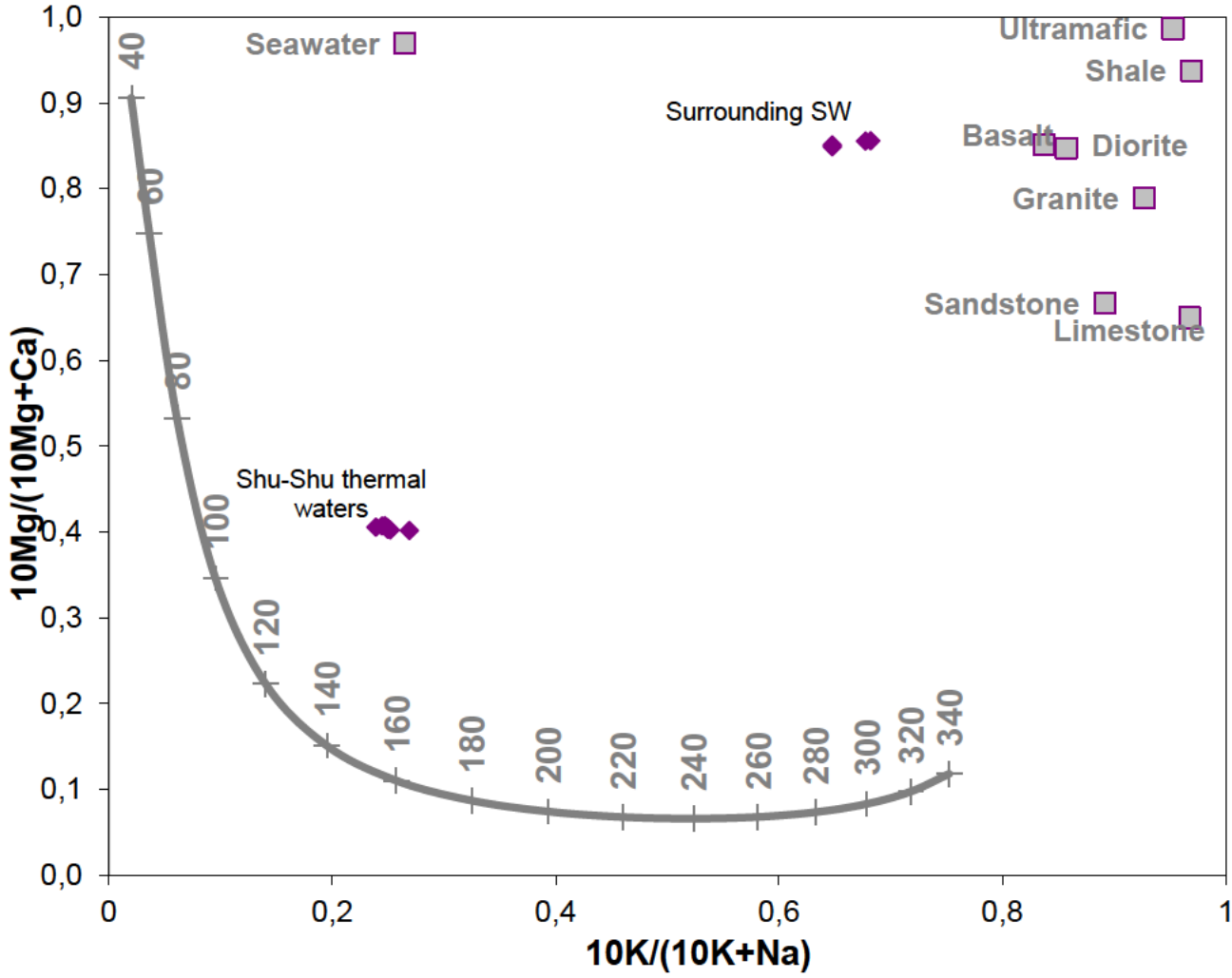

Figure 8.6: 10Mg/(10Mg+Ca) versus 10K/(10K+Na) binary diagram to check the suitability of applying ratio-based cation geothermometers

Table 8.4: Saturation indices of the Shu-Shu water samples calculated using the GWB 11 software

Mineral saturation states log Q/K	POOL 7	POOL 6	POOL 5	POOL 4	POOL 3	POOL 2	POOL 1
Quartz	0,55	0,75	0,74	0,73	0,73	0,68	0,61
Tridymite	0,40	0,60	0,58	0,58	0,58	0,53	0,46
Chalcedony	0,30	0,49	0,48	0,47	0,47	0,43	0,35
Cristobalite	0,05	0,23	0,22	0,21	0,21	0,17	0,11
Amorphous silica	-0,56	-0,43	-0,45	-0,44	-0,44	-0,48	-0,52
Anhydrite	-1,18	-1,30	-1,29	-1,28	-1,27	-1,26	-1,21
Gypsum	-1,25	-1,26	-1,26	-1,26	-1,26	-1,27	-1,26
Bassanite	-1,80	-1,92	-1,92	-1,90	-1,90	-1,89	-1,83
$CaSO_4.½H_2O$ (beta)	-1,94	-2,07	-2,07	-2,05	-2,05	-2,04	-1,97
Hexahydrite	-5,01	-5,03	-5,03	-5,03	-5,03	-5,03	-5,02
Epsomite	-5,07	-4,95	-4,94	-4,97	-4,97	-5,00	-5,05
Leonhardtite	-5,52	-5,62	-5,61	-5,60	-5,60	-5,59	-5,54
Kieserite	-5,79	-6,10	-6,09	-6,05	-6,05	-6,00	-5,85
Halite	-6,06	-6,08	-6,09	-6,06	-6,06	-6,10	-6,10
Thenardite	-6,40	-6,48	-6,52	-6,46	-6,46	-6,49	-6,46
Mirabilite	-6,89	-6,37	-6,42	-6,44	-6,44	-6,59	-6,84
Sylvite	-7,36	-7,27	-7,24	-7,27	-7,27	-7,32	-7,36
Kalicinite	-8,59	-8,24	-8,23	-8,29	-8,29	-8,37	-8,53
Arcanite	-8,78	-8,66	-8,62	-8,67	-8,67	-8,73	-8,78
$MgSO_4$(c)	-10,31	-10,88	-10,88	-10,79	-10,79	-10,69	-10,43
Antarcticite	-12,10	-12,07	-12,03	-12,05	-12,05	-12,10	-12,12
Kainite	-12,49	-12,59	-12,55	-12,55	-12,55	-12,58	-12,53
$CaCl_2.4H_2O$	-12,63	-12,71	-12,67	-12,67	-12,67	-12,70	-12,67
Bischofite	-13,11	-13,22	-13,18	-13,18	-13,17	-13,20	-13,15
$CaCl_2.2H_2O$	-15,31	-15,61	-15,57	-15,54	-15,54	-15,53	-15,40
$CaCl_2.H_2O$	-15,33	-15,67	-15,64	-15,60	-15,60	-15,57	-15,42
$MgCl_2.4H_2O$	-15,61	-15,90	-15,87	-15,83	-15,83	-15,82	-15,69
Hydrophilite	-18,51	-19,03	-18,99	-18,92	-18,92	-18,86	-18,63

Carnallite	-19,52	-19,51	-19,44	-19,47	-19,47	-19,55	-19,56
$MgCl_2.2H_2O$	-20,34	-20,93	-20,89	-20,82	-20,81	-20,74	-20,48
$MgCl_2.H_2O$	-23,29	-24,05	-24,01	-23,91	-23,90	-23,80	-23,46
KMgCl3.2H2O	-27,96	-28,47	-28,40	-28,35	-28,35	-28,33	-28,10
Chloromagnesite	-28,47	-29,47	-29,43	-29,29	-29,29	-29,14	-28,68
$KMgCl_3$	-34,44	-35,30	-35,23	-35,13	-35,12	-35,03	-34,64
Tachyhydrite	-41,69	-42,26	-42,15	-42,11	-42,10	-42,13	-41,87

Figure 8.7: Images of mineral (Silica) precipitation on the surface near the Shu-Shu springs